Steel fibre reinforced concrete and CFRP laminate strips for high effective flexural strengthening of RC slabs

Everaldo Bonaldo
Joaquim O. Barros, Paulo B. Lourenço

Report 05-DEC/E-14

The present research has been carried out under the financial support of FCT, under PhD grant number SFRH / BD / 11232 / 2002

Date: October 2005
No. of pages: 103

Keywords: flexural strengthening, reinforced concrete slabs, CFRP laminate, thin-bonded overlay, steel fibre reinforced concrete.

Escola de
Engenharia

Departamento de
Engenharia Civil

Universidade
do Minho

Azurém, 4800-085 Guimarães - Tel. +351 253 510 200 - Fax +351 253 510 217 - E-mail secG@civil.uminho.pt

Contents

Summary

The use of composites materials is a remarkable strengthening technique for increasing and upgrading the flexural load carrying capacity of reinforced concrete (RC) members. The Near Surface Mounted (NSM) strengthening technique consists in applying carbon fiber-reinforced polymer (CFRP) laminate strips into slits opened on the concrete cover of the elements to be strengthened. A normal cold cured epoxy based adhesive is used to bond the CFRP laminate strips to concrete.

Laboratory tests have shown that the NSM technique is an adequate strengthening strategy to increase the flexural resistance of RC slabs. However, in RC slabs of low or medium concrete strength, the increment of the flexural resistance that NSM can provide is limited by the maximum permissible compressive strain in the compressed part of the slab, in order to avoid concrete crushing or unadvisable damage. This restriction reduces the efficiency of the strengthening, being questionable the use of the NSM technique in these cases.

A new layer of concrete bonded, by an epoxy compound, to the existing concrete at the compressed region is suitable to overcome this limitation. Since a thin layer (three to five centimetres) is enough for the aforementioned purpose, the volumetric contraction due to shrinkage and thermal effects can induce uncontrolled cracking in the concrete of this layer. Adding steel fibres to concrete, the post cracking residual stress can be increased in order to prevent the formation of uncontrolled crack patterns.

In the present work, the combined strengthening strategy, a SFRC overlay and NSM CFRP laminate strips, was applied to increase, significantly, the flexural resistance of RC slabs. Experimental results of four-point bending tests, carried out in concrete slabs strips unstrengthened and strengthened, are presented and analysed.

1 Introduction

In the following a brief background of the hybrid strengthening system is presented, as well as the objectives and scope of the present work.

Brief Background

The Near-Surface Mounted (NSM) strengthening technique has been used in the recent years, with remarkable efficiency, to increase the flexural strength (NANI, 2000; FIB, 2001; CAROLIN, 2003; BARROS & FORTES, 2005; KOTYNIA, 2005) and shear resistance (DE LORENZIS & NANNI, 2001a/2001b; BARROS & DIAS, 2003) of reinforced concrete elements. The NSM technique involves the embedment of CFRP bars - of circular, square or rectangular cross-section - into grooves opened on the concrete surface. The CFRP bars are bonded to concrete using an epoxy-based adhesive (see ***Figure 1.1***). A simple procedure is used to open the grooves for NSM strengthening: a concrete saw moves on supporting rails which are fastened to the bottom surface of the element (see ***Figure 1.2***). Entire cleanness of the sawing task is totally guaranteed attaching a receptacle for the dust powder to the concrete saw machine.

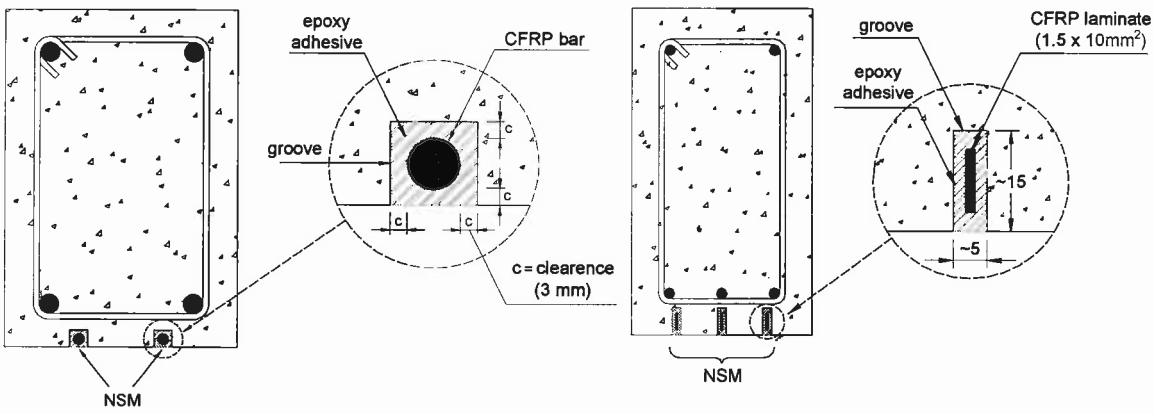

(a) (b)

Figure 1.1 *- Details of the NSM technique for the flexural strengthening of RC beams: (a) CFRP bars of circular cross-section, and (b) CFRP bars of rectangular cross-section [(a) ALKHRDAJI & NANNI, 1999 and CAROLIN, 2001 and 2003, (b) BARROS & FORTES, 2005 and KOTYNIA, 2005].*

When compared to the Externally Bonded Reinforcement (EBR) technique, the NSM technique assures a higher anchoring capacity to the FRP reinforcing material (see ***Figures 1.3 - 1.5***). In consequence, a high tensile stress can be mobilized in the CFRP, as long as the member load carrying capacity is not limited by a premature failure mode (BLASCHKO & ZILCH, 1999; FIB, 2001; CAROLIN, 2003).

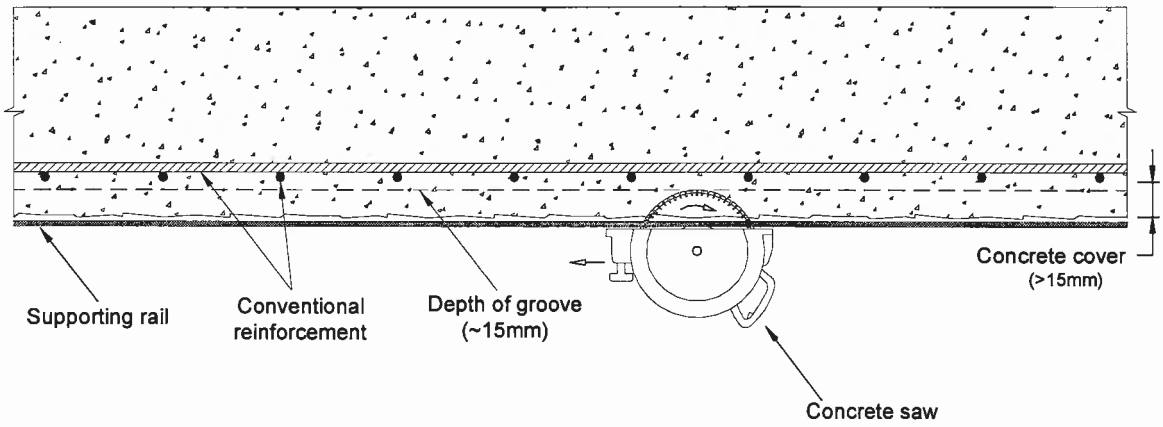

Figure 1.2 *- Making the grooves for NSM technique [adapted from TÅLJSTEN & CAROLIN, 2001; CAROLIN, 2001; CAROLIN, 2003].*

For RC slabs of low or medium concrete strength, the increment of the flexural resistance that NSM can provide might be limited by the maximum allowable compression strain in the most compressed concrete fibre. This drawback can be overcome adding a concrete layer in the compression zone of the existent slab (BARROS & SENA-CRUZ, 2001).

To attain the desired structural performance (e.g. full composite action), the new concrete overlay and the existent concrete slab should behave monolithically. A sound bond between the new layer and the existing concrete slab can be guaranteed if a proper epoxy compound is used (BONALDO, BARROS & LOURENÇO, 2004).

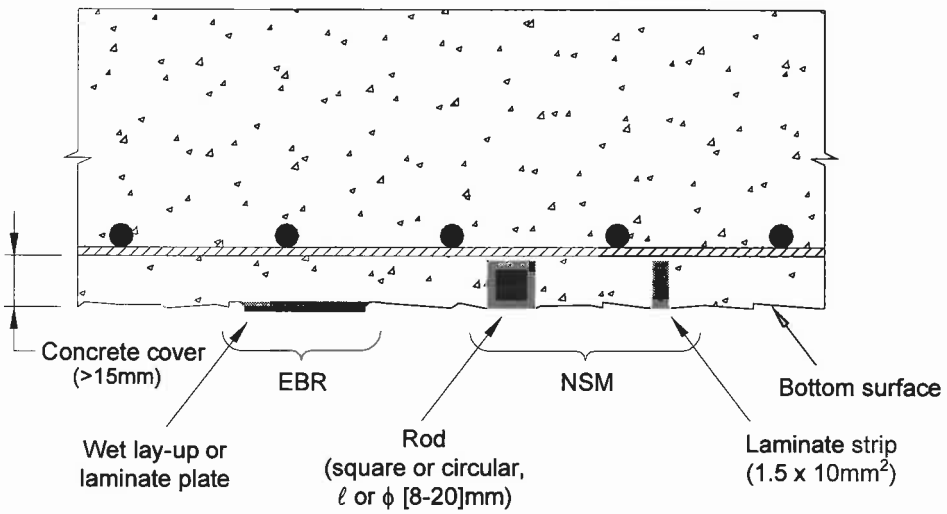

Figure 1.3 *- Strengthening techniques: externally bonded reinforcement, EBR, and near surface mounted, NSM [adapted from TÅLJSTEN & CAROLIN, 2001; CAROLIN, 2001; CAROLIN, 2003].*

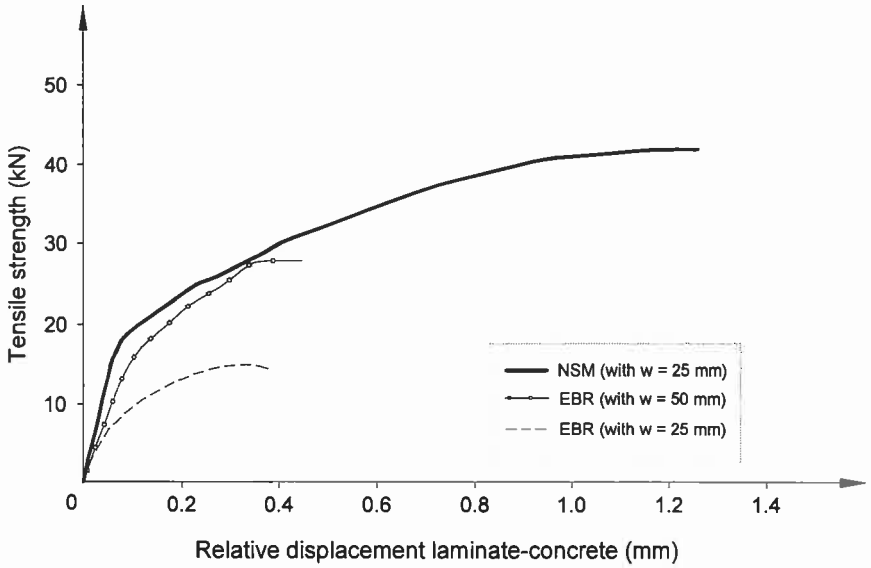

Figure 1.4 *- Strength-slip relationships for NSM e EBR (bond length 250 mm, refer to Figure 1.5). [BLASCHKO & ZILCH, 1999]*

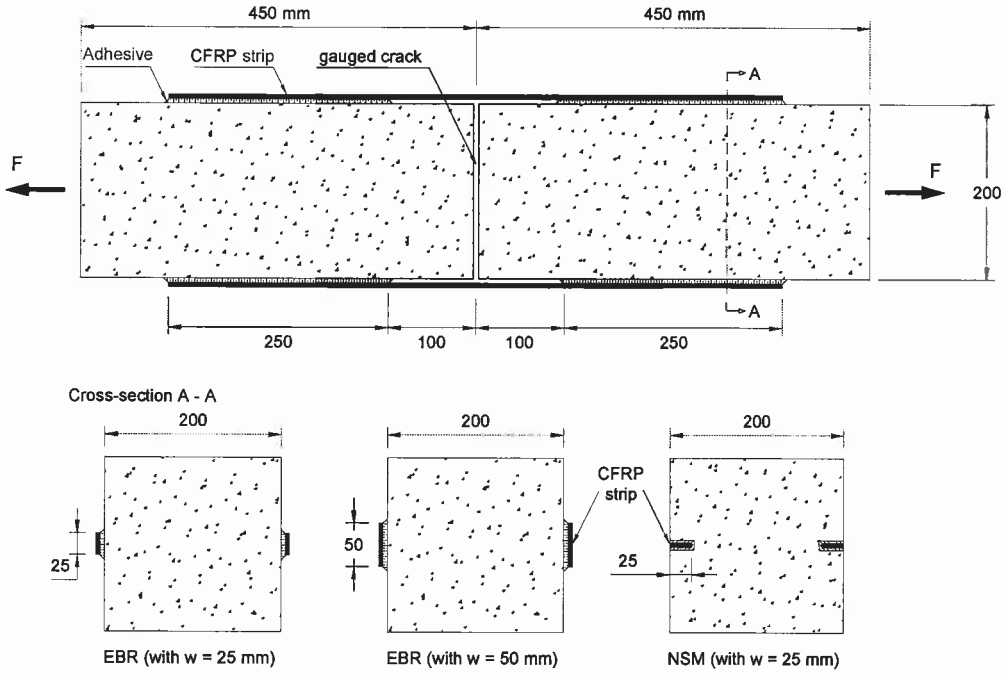

Figure 1.5 *- Geometry of the double-shear specimen for the bond tests carried out by BLASCHKO & ZILCH, 1999.*

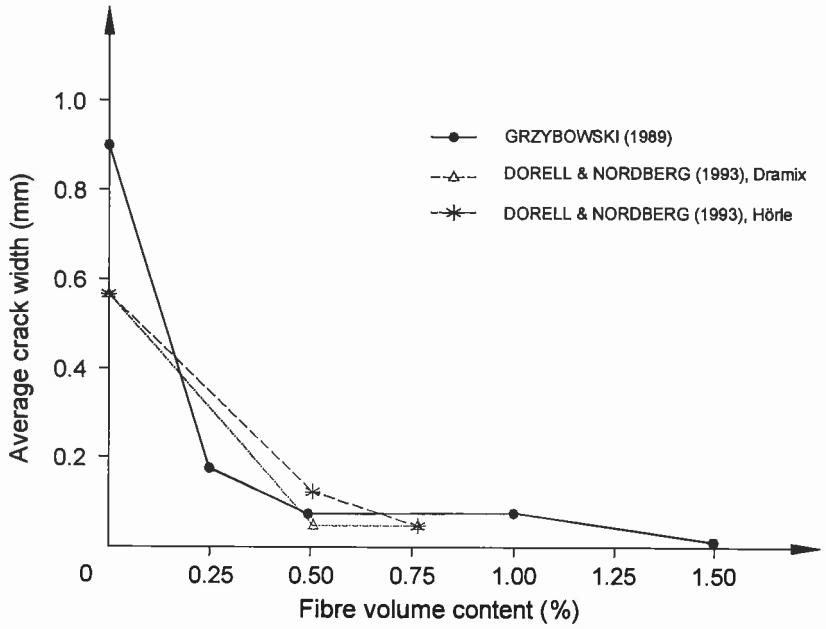

Figure 1.6 *- Beneficial effects of steel fibres on reducing average crack widths reported in literature.*
[GRZYBOWSKI, 1989; GRZYBOWSKI & SHAH, 1990 and DORELL & NORDBERG, 1993]

Since a thin concrete layer is enough for the aforementioned purpose, the restrained shrinkage and the temperature variation can induce uncontrolled cracking in the concrete of this layer. Adding discrete fibres to concrete, such as steel fibres, the crack widths resulting from drying restrained shrinkage can be substantially reduced (refer to ***Figure 1.6***). Even addition of a small amount of fibres (as small as 0.25 percent by volume) gives significant reductions of crack widths. Moreover, the post cracking residual tensile strength can be increased (BARROS et al, 2004), in order to prevent the formation of uncontrolled crack patterns. ***Figure 1.7*** shows the influence of the steel fibre addition on the concrete tensile stress-strain behaviour. While plain concrete has a very stress-strain slope decay after cracking, which is typical of brittle materials, composite SFRC is able to withstand large strain restraining the cracks.

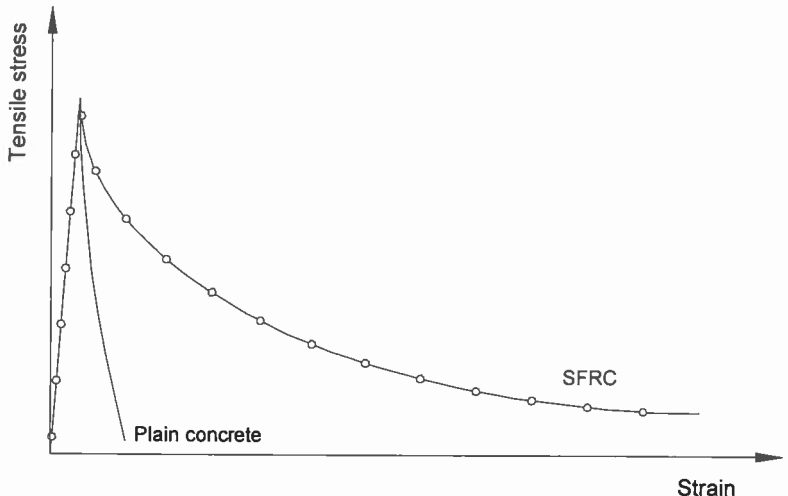

Figure 1.7 *- Sketch of steel fibre influence on the concrete tensile stress-strain behaviour.*
[FISCHER & LI, 2003]

The influence of the fibre content on the concrete compressive stress-strain behaviour is presented in ***Figure 1.8***. In the plain concrete, the post-peak strength decrease abruptly after peak load, while a significant residual strength is retained in the softening phase of the fibrous concrete. This residual strength increases with the fibre content, which means that increasing the fibre content results in a tougher material. This material benefit can be used to avoid concrete crushing in the strengthening of RC slabs.

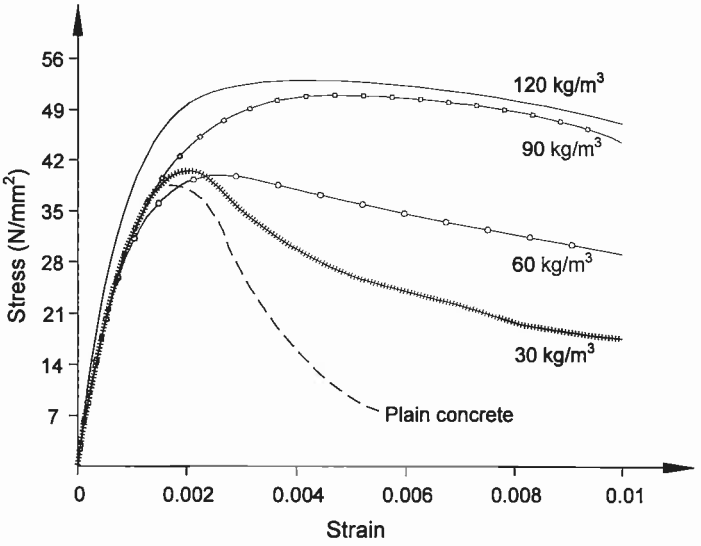

Figure 1.8 - *Steel fibre influence on the concrete compressive stress-strain behaviour, registered in specimens reinforced with Dramix 50/50 [BALAGURU, 1992].*

BARROS & SENA-CRUZ (2001) has advanced a strengthening strategy, combining SFRC and CFRP materials. To increase, for a certain level, the flexural resistance of a RC slab, these authors have studied three strengthening alternatives. One solution is composed by CFRP laminates, but the tensile stress that can be installed in the CFRP laminates was limited by the concrete compressive strain. Adding a thin layer of SFRC to the slab compression zone, this restriction was overcome and the ultimate flexural capacity was increased of about 45%. The moment-curvature relationship, obtained by the numerical analysis, is depicted in ***Figure 1.9*** for the three studied situations: slab strengthened with a thin layer of SFRC, slab strengthened with CFRP, and slab strengthened with CFRP and overlaid with a thin layer of SFRC. This figure also includes the moment-curvature of the unstrengthened slab.

In this report, a strengthening strategy for increasing the load carrying capacity of RC slabs, firstly engineered by (BARROS & SENA-CRUZ, 2001), was experimentally investigated. This strategy consists on applying CFRP laminates in the tensile bottom slab surface, according to the NSM technique, and bonding, with appropriate epoxy-based adhesive, a SFRC layer in the compression top slab surface (see ***Figure 1.10***). To asses the efficacy of the NSM strengthening technique for increasing the flexural

resistance of slabs strips failing in bending, four point bending tests with RC slab strips were carried out in displacement control.

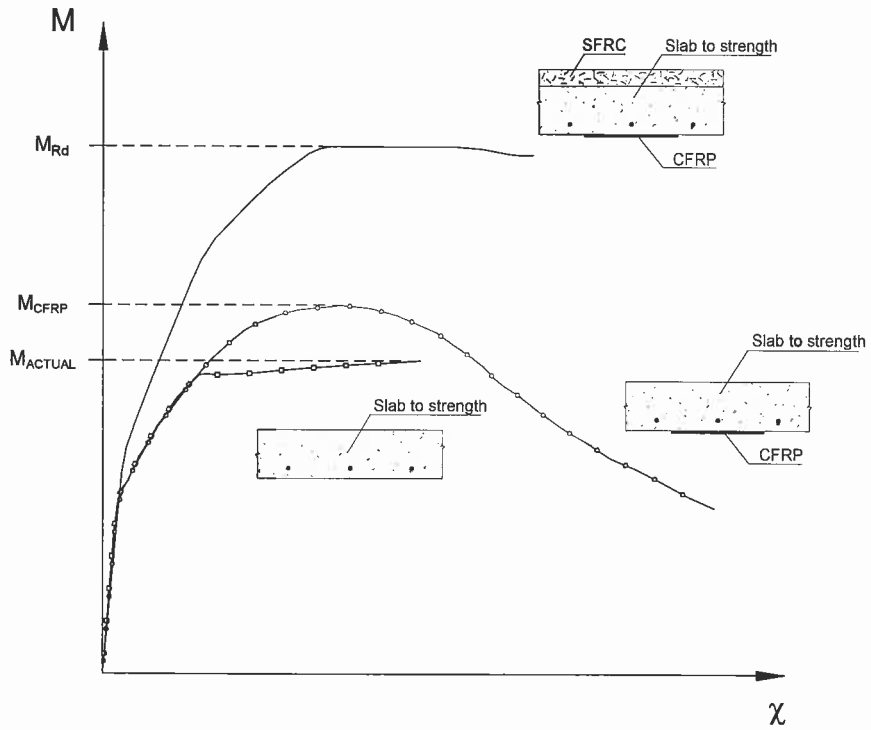

***Figure 1.9** - Moment-curvature relationships from the numerical analysis [adapted from BARROS & CRUZ, 2001].*

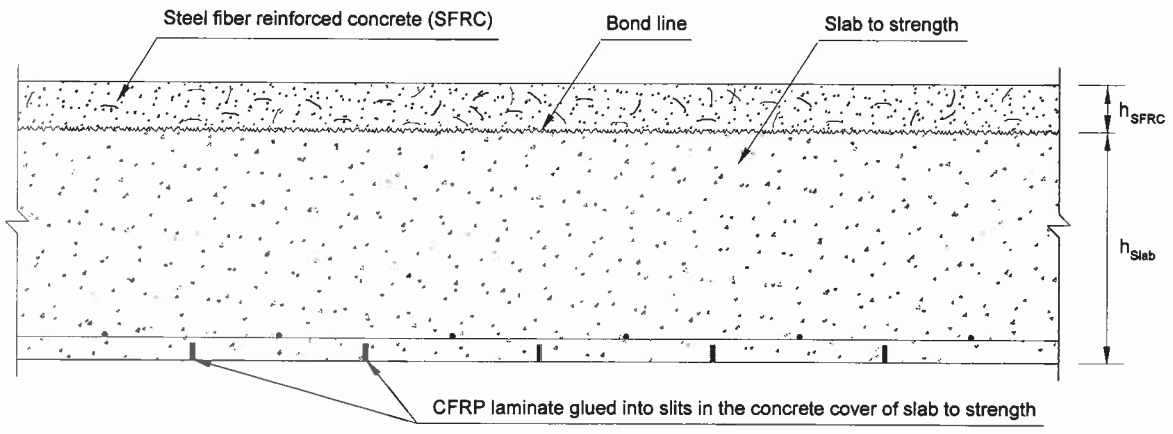

***Figure 1.10** - The hybrid strengthening technique for concrete slabs.*

Objectives and Scope

The present study has the following objectives:

- Evaluate the strengthening efficacy of the NSM technique for RC slabs;

- Evaluate the structural performance of the hybrid strengthening technique: CFRP laminates and SFRC overlay for RC slabs.

The experimental program is composed by eight slab strips: two control slabs, three NSM CFRP strengthened slabs, and three slabs strengthened with NSM CFRP and a SFRC overlay, simultaneously.

2 Experimental Program

The following sections detail the test specimens, test configuration, measuring devices, and test program.

Specimen and Test Configuration

To asses the efficacy of the hybrid strengthening technique for the increase of flexural load carrying capacity of RC slabs, the slab strip specimens represented in ***Figure 2.1*** were used. The test set up and the cross section dimensions of the tested slab strip specimens are also illustrated in ***Figure 2.1***.

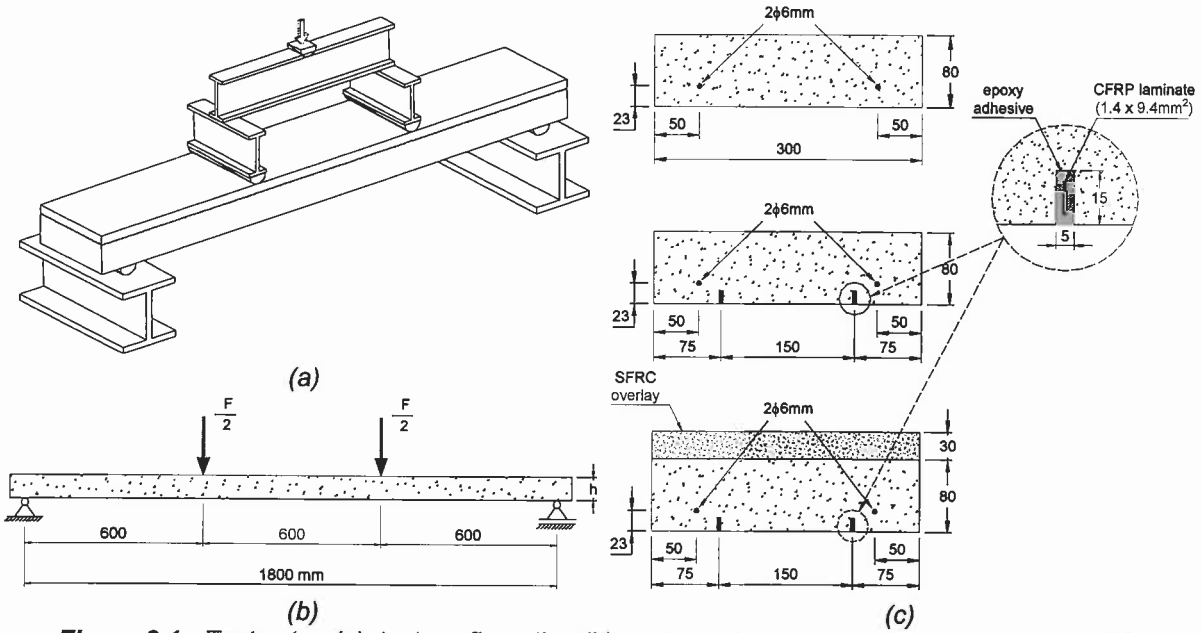

Figure 2.1 - *Test setup (a), test configuration (b), and specimens cross-section dimensions (c).*

The number of CFRP laminate strips applied in each RC slab was evaluated in order to increase 50% the service load (assumed equal to the load producing a mid-span displacement of $\ell/250$ = 1800 mm/250 = 7.2 mm).

Measuring Devices

To measure the deflection of the slab strip, five displacement transducers (LVDT 61472, LVDT 19906, LVDT 3558, LVDT 3468 and LVDT 63796) were applied (see ***Figure 2.2***). The LVDT 3558, positioned at the slab strip mid-span was also used to control the test at 20 μm/s up to the deflection of 49 mm. After this deflection, the

actuator internal LVDT was used to control the test at 25 μm/s displacement rate. The applied force (F) was measured using a load cell (±200 kN and accuracy of 0.5%) placed between the loading steel frame and the actuator of 600 kN load capacity. One strain gauge was installed at each steel bar (SG1 and SG2), at the mid span position, to measure the strain in the steel reinforcements, see ***Figure 2.2***. Five strain gauges were installed at one CFRP laminate (SG3, SG4, SG5, SG6 and SG7) for evaluating the strain variation along the laminate. One or two strain gages (SG8 or SG8 and SG9) were also bonded on the top concrete surface to determine the maximum concrete compression strain. In this experimental program FLA-3-11, BFLA-5-3 and PFL-30-11 strain gauges from TML (TML, 2004) were used, in steel bars, CFRP laminates and concrete, respectively.

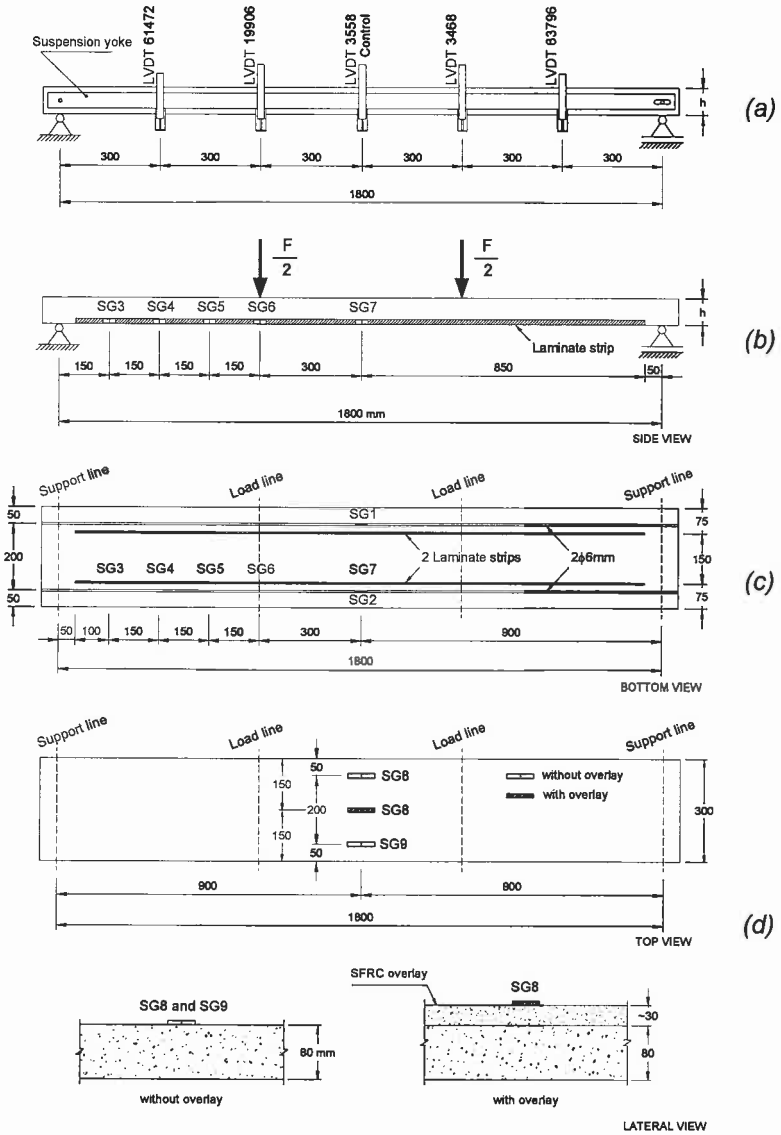

Figure 2.2 *- Arrangement of displacement transducers and strain gauges: displacement transducers (a), position of the strain gauges at the CFRP laminate - side view (b), lay-out of the strain gauges at the steel bars and at the CFRP laminate - bottom view (c), and strain gauges at the concrete slab top surface - top and lateral view (d).*

The main technical characteristics of the used displacement transducers are included in ***Table 2.1***.

Table 2.1 - *Technical characteristics of the LVDTs, extracted from technical datasheet (RDP, 1995).*

LVDT	Linear Range (mm)	Linearity (%)
61472	±12.5	±0.04
19906	±25	±0.07
3558	±25	±0.08
3468	±25	±0.08
63796	±12.5	±0.04

Figure 2.3 shows the full arrangement of the bending test set up, while ***Figure 2.4*** includes a photo of a specimen being tested. A servo-controlled test machine was used in the experimental program.

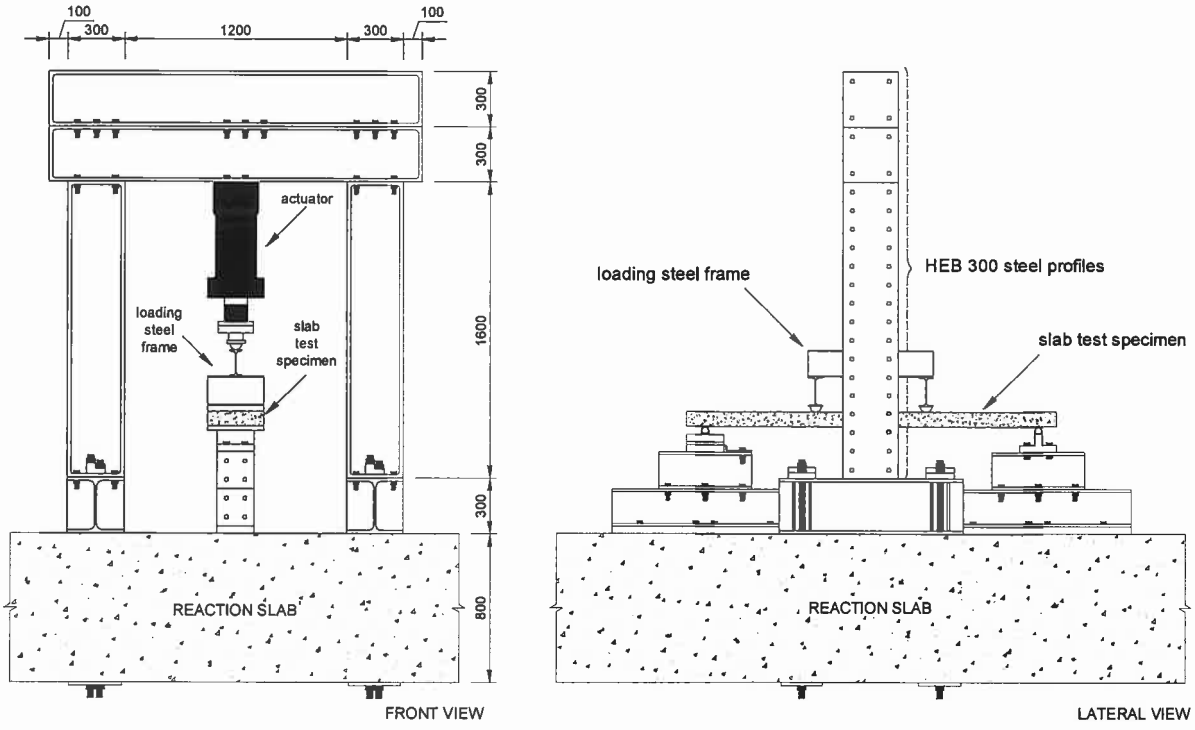

Figure 2.3 - *Layout of the four-point bending test (dimensions in millimetres).*

Test Program

In the present experimental program the influence of the CFRP laminate strengthening and the SFRC overlay strengthening on the flexural behaviour of reinforced concrete slabs is analyzed. For this purpose, unstrengthened (control), strengthened with CFRP laminates, and simultaneously strengthened with CFRP

laminates and SFRC overlay specimens (***Figure 2.1****(c)*) were tested under monotonic loading.

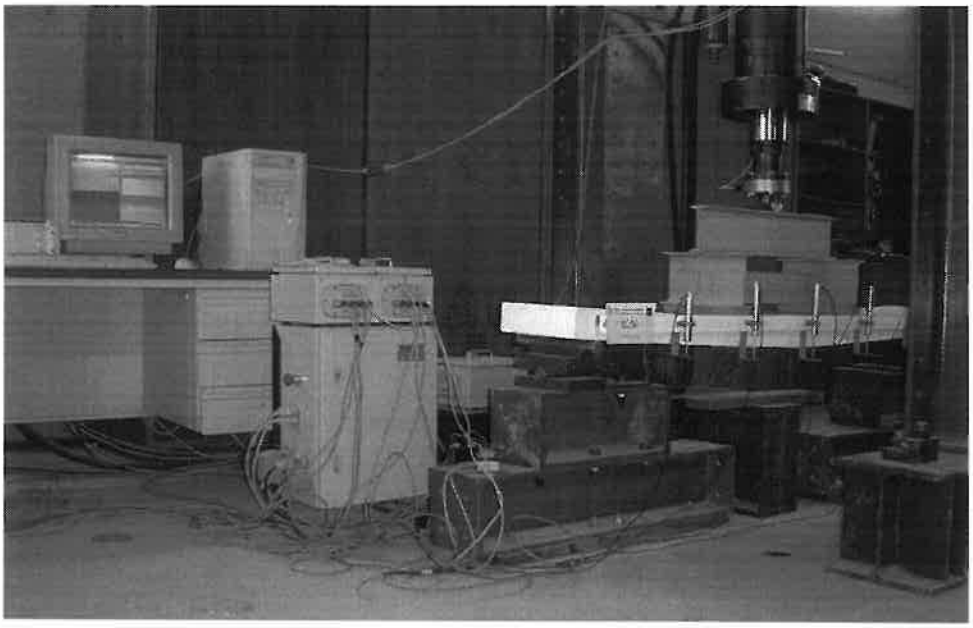

Figure 2.4 *- The SL06 specimen being tested.*

3 Materials Characterization

The following sections detail the various materials used in the present experimental program.

Concrete Slab and Concrete Overlay

A laboratory trial phase was developed at the Laboratory of the Structural Division of the University of Minho aiming to establish the following compressive strength grades (CEB-FIP Model Code, 1993): C40/50 for the concrete slab strips; C40/50 and C45/55 for the SFRC overlay.

For the purpose of defining the mix properties, a *Faury* mix design method was used, see e.g. COUTINHO (1988), using aggregates available in the Northern Region of Portugal (Minho). Details about the physical properties of the aggregates are given in **Annex A**. In **Annex B** the sieve analyses of the aggregates and the information about maximum aggregate size are included. Hooked ends DRAMIX® RC-80/60-BN steel fibres were used to reinforce the concrete overlay. This fibre has a length (ℓ_f) of 60 mm, a diameter (d_f) of 0.75 mm, an aspect-ratio (ℓ_f / d_f) of 80 and a yield strength of about 1100 N/mm^2 (DRAMIX, 1998). Previous work revealed that this fibre has high performance since significant increase in the ultimate load carrying capacity of the structural concrete elements was obtained (BARROS & FIGUEIRAS, 1998).

Fibres were charged into the mix as the last concrete component. While concrete was being mixed, the steel fibre tablets were gradually and continuously charged into the mix at the same location, for all batches. This procedure was used in an attempt of assuring similar fibre dispersion conditions.

The concrete mix proportions and the main properties of the ordinary concrete (substrate) and SFRC overlay are shown in ***Table 3.1***. Here, W/B is the water-to-binder ratio (Portland cement for the plain concrete and Portland cement plus fly ash for the SFRC). The percentage of RHEOBUILD®1000 superplasticizer refers to the weight of cement plus fly ash. More details regarding the compressive strength of the conceived concretes can be found in **Annex C**.

The flexural behaviour of the concretes was also characterized, carrying out three-point bending tests on notched beams, according to RILEM (1985) for ordinary concrete, and following the recommendations of to RILEM (2000, 2002) for SFRC. More details about the bending tests are described in **Annex D**.

Table 3.1 *- Mix proportions and main properties of the ordinary concrete and SFRC.*

Components	Mix designation									
	SL01	**SL02**	**SL03**	**SL04**	**SL05**	**SL06**	**SL07**	**SL08**	**O1**	**02**
Cement I 42.5 R (kg/m^3)	300								300	350
Fly ash[a] (kg/m^3)	-								30	35
Fine river sand (kg/m^3)	346								288	198
Coarse river sand (kg/m^3)	568								598	662
Fine aggregate 4/11 (kg/m^3)	426								410	394
Coarse aggregate 11/16 (kg/m^3)	542								511	552
Superplasticizer (%)	2.5								2.5	2.5
Steel fibre (kg/m^3)	-								30	30
W/B ratio	0.47	0.46	0.45	0.51	0.45	0.44	0.45	0.45	0.43	0.36
Slump[b] (mm)	220	185	210	215	180	180	175	165	225[c] 210[d]	220[c] 190[d]
fc_{28d}[e] (MPa)	39.0	43.0	42.0	27.0	47.0	47.0	48.0	50.0	-	-
fc[f] (MPa)	45.5	48.0	43.0	32.5	49.5	49.0	48.0	49.0	39.0	53.0

[a] obtained from thermoelectric source
[b] Slump determined according to ASTM C143 (1998)
[c] Slump before adding the steel fibres
[d] Slump after adding the steel fibres
[e] Value of 1 cylinder specimen (150 mm x 300 mm)
[f] Average value of 3 cylinder specimens (150 mm x 300 mm) at the daytime of the slab test

It can be noticed that the target concrete strength classes were satisfactorily achieved. However, during the production of the concrete mixes, water contents higher than the target value was added, mainly to the SL04 mix. In the O1 concrete mix, the moisture of the aggregates used in the mix calculations, did not reflect the real values. Therefore, some dispersion of the compressive strength, fc, was obtained in the ordinary concrete and a significant difference of fc was registered in the two SFRC mixes.

Table 3.2 includes the individual ($f_{ct,fl}$) and average ($f_{ctm,fl}$) values of flexural tensile strength, individual ($f_{ct,ax}$) and average ($f_{ctm,ax}$) values of axial tensile strength, and the individual (G_f) and average (G_{fm}) values of the fracture energy for the plain concrete

mixes. In the SL04 concrete mix, with a higher water-to-cement ratio, the flexural tensile strength, axial tensile strength and fracture energy were slightly lower compared to the other concrete mixes. ***Figure 3.1*** shows the load versus displacement curves for each plain concrete mix obtained from flexural tests. Each curve is the average of the lad-displacement relationship recorded in the three specimens of each mix.

Table 3.3 includes the values of the equivalent flexural tensile strength parameters (RILEM, 2000 and 2002) and the flexural modulus of elasticity for the SFRC mixes. ***Figure 3.2*** shows the average load versus displacement curve for each SFRC mix obtained from flexural tests. Each curve is the average of the lad-displacement relationship recorded in, at least, three specimens of each mix.

Table 3.2 - *Flexural tensile strength, axial tensile strength and fracture energy of ordinary concrete.*

Plain concrete mix	Age at testing (days)	Beam	$f_{ct,fl}$ (N/mm^2)	$f_{ctm,fl}$ (N/mm^2)	$f_{ct,ax}$ (N/mm^2)	$f_{ctm,ax}$ (N/mm^2)	G_f (N/m)	G_{fm} (N/m)
SL01	138	1	5.01	4.98 (*0.07*) [*1.43%*]	2.77	2.75 (*0.04*) [*1.51%*]	206	200 (*8.12*) [*4.06%*]
		2	5.02		2.77		203	
		3	4.89		2.70		191	
SL02	131	1	6.02	5.86 (*0.40*) [*6.76%*]	3.32	3.24 (*0.21*) [*6.45%*]	208	189 (*21.47*) [*11.35%*]
		2	5.41		3.00		166	
		3	6.16		3.40		193	
SL03	126	1	6.34	5.92 (*0.42*) [*7.15%*]	3.50	3.27 (*0.24*) [*7.22%*]	216	211.44 (*6.06*) [*2.87%*]
		2	5.92		3.27		214	
		3	5.50		3.03		204	
SL04	106	1	4.60	4.73 (*0.59*) [*12.42%*]	2.53	2.61 (*0.32*) [*12.26%*]	180	189 (*22.02*) [*11.63%*]
		2	5.37		2.96		215	
		3	4.22		2.33		174	
SL05	112	1	5.53	5.59 (*0.45*) [*8.14%*]	3.07	3.10 (*0.25*) [*7.99%*]	206	204.18 (*5.62*) [*2.75%*]
		2	5.17		2.86		209	
		3	6.07		3.36		198	
SL06	112	1	6.20	6.10 (*0.12*) [*1.99%*]	3.42	3.37 (*0.07*) [*1.95%*]	223	213 (*20.93*) [*9.81%*]
		2	5.96		3.30		189	
		3	6.14		3.39		228	
SL07	83	1	6.07	6.01 (*0.08*) [*1.31%*]	3.35	3.32 (*0.04*) [*1.35%*]	200	233 (*46.11*) [*19.79%*]
		2	5.96		3.29		266	
SL08	103	1	6.01	5.80 (*0.28*) [*4.86%*]	3.32	3.21 (*0.15*) [*4.72%*]	192	199 (*20.86*) [*10.48%*]
		2	5.91		3.27		223	
		3	5.48		3.04		183	

(*value*) Standard deviation
[*value*] Coefficient of Variation (COV) = (Standard deviation/Average) x 100

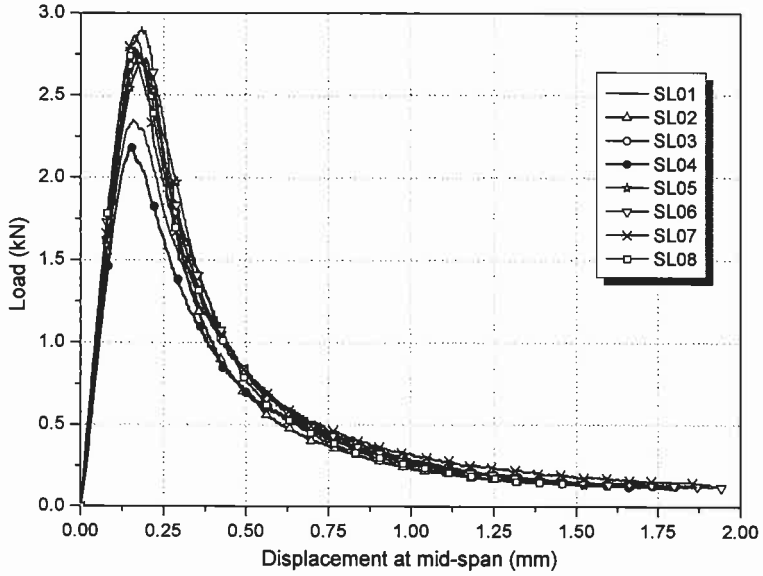

Figure 3.1 *- Load versus displacement curve for each plain concrete mix.*

Table 3.3 *- Equivalent flexural tensile strength parameters and flexural modulus of elasticity of SFRC.*

SFRC mix	Age at testing (days)	Beam	$f_{eq,2}$ (N/mm^2)	$f_{eqm,2}$ (N/mm^2)	$f_{eq,3}$ (N/mm^2)	$f_{eqm,3}$ (N/mm^2)	E_{cf} (kN/mm^2)	E_{cfm} (kN/mm^2)
O1	68	1	3.184	5.000 (*1.634*)	3.110	4.831 (*1.500*)	35.04	30.14 (*4.26*)
		2	5.466		5.518		27.28	
		3	6.351		5.864		28.11	
O2	54	1	3.800	4.116 (*0.479*)	3.809	3.862 (*0.583*)	34.65	32.32 (*3.18*)
		2	3.669		3.125		34.73	
		3	4.716		4.540		27.96	
		4	4.280		3.976		31.94	

(*value*) Standard deviation

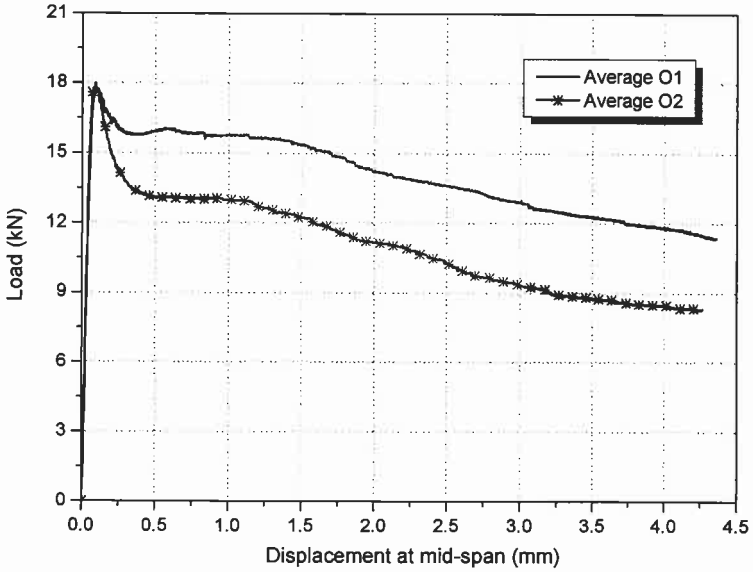

Figure 3.2 *- Load versus displacement curve for the SFRC O1 and O2 mixes.*

Overlay Bond Product

Epoxy resin is widely used as the bond product for most materials used in construction, such as concrete, masonry units, wood, glass, and metals. Since epoxy-based bond products used in the present experimental program are unaffected by moisture, they are appropriated to bond fresh to hardened concrete. Bonding fresh concrete overlay to an existing concrete slab is an example of such application (ACI 503R-93).

An epoxy resin-based bond agent with a Trademark of Sikadur®32N (see ***Figure 3.3***), supplied by Sika® Portugal, was selected to bond fresh SFRC overlay to hardened reinforced concrete slab. This resin was composed by two components (A and B), and was available in packages of 1.2 kg (0.8 kg component A and 0.4 kg component B). Some information about the bond product is summarized in ***Table 3.4***.

Figure 3.3 *- Bond product packaging, 1.2 kg unit.*

In a previous study, the selected bond coat provided excellent performance in bonding fresh SFRC to hardened concrete substrate (BONALDO et al, 2004).

Table 3.4 *- Main properties of the product, extracted from commercial datasheet (SIKA, 2002).*

Properties				
Specific gravity	**Bond strength**	**Mechanical resistance**	***Pot life*[a] and open time[b] at 20 C**	**Mixing ratio**
Approximated 1.4 kg/l	to concrete: 2.5 - 3.0 N/mm^2 (concrete failure) to steel: 18 - 20 N/mm^2	Compressive strength: ~60 - 70 N/mm^2 Tensile strength: ~18 - 20 N/mm^2 Flexural strength: ~30 - 35 N/mm^2	Approximated 20 min, and Approximated 3 h	Comp. A: 2 parts by weight Comp. B: 1 parts by weight

[a] The maximum time between final mixing and application during which a resin or adhesive remains usable (COMYN, 1997). Also known as *working life* or *usable life*.

[b] The open time starts when the adhesive has been applied to the parts to be joined, and it represents the time limit during which the joint has to be closed (MAYS & HUTCHINSON, 1992).

Mechanical properties of the overlay bond coating adhesive

To access the tensile mechanical properties of the hardened epoxy resin, seven tensile tests in machined specimens (see ***Figure 3.4***) were carried out according to ISO 527-2 (1993). A testing machine Instron 4505 with 150 mm distance between grips (see ***Figure 3.5***) was used. A test speed of 1 mm/min, as is required for this type of material, was selected for all the tests. The tensile test results are displayed in ***Table 3.5***, and the specimens before and after testing are shown in ***Figure 3.6***. The recorded stress-strain curves are depicted in ***Figure 3.7***. The strain was measured from the displacements recorded in the displacement transducer of the actuator.

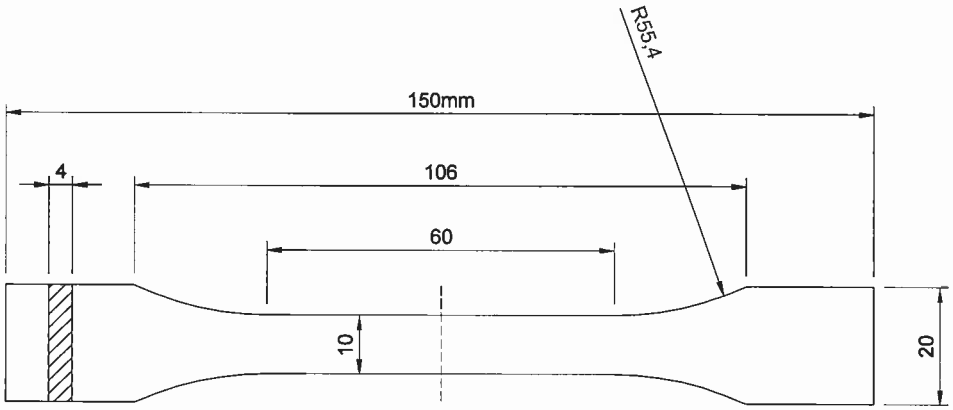

Figure 3.4 *- Shape and dimensions of the test specimens (type 1B - ISO 527-2, 1993).*

The bond coating adhesive was applied onto dry and clean sandblasted concrete surface, i.e., free from surface contaminants such as dust, laitance, oil or grease, following the manufacturer specifications. A bond coating dosage of 0.90 kg/m^2 was adopted (BONALDO et al, 2004).

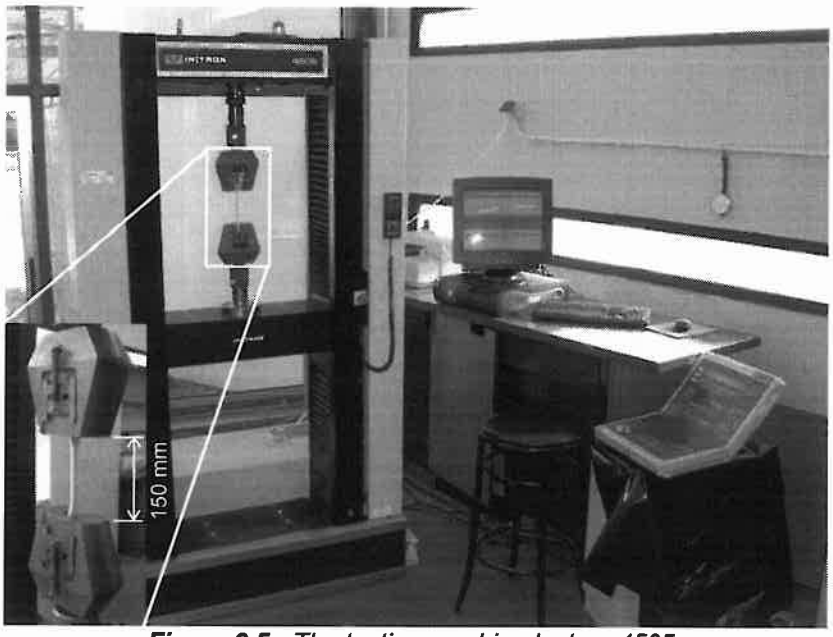

Figure 3.5 *- The testing machine Instron 4505.*

Table 3.5 *- Results of the tension tests on the overlay bond coating adhesive specimens.*

Specimen	Ultimate tensile stress (N/mm^2)	Ultimate tensile strain (‰)	Modulus of elasticity[a] (kN/mm^2)
1	28.79	11.63	3.67
2	26.39	9.82	3.76
3	24.04	9.51	3.51
4	27.92	10.87	3.75
5	25.93	10.76	3.56
6	25.96	10.81	3.54
7	26.86	11.80	3.59
Average	26.56	10.74	3.62
Std.Dev.	1.53 (5.76%)	0.85 (7.89%)	0.10 (2.78%)

[a] *Tensile Modulus of Elasticity* calculated from the stress-strain data using a linear regression procedure applied over the strain range 0-1.80 ‰

(*value*) Coefficient of Variation (COV) = (Standard deviation/Average) x 100

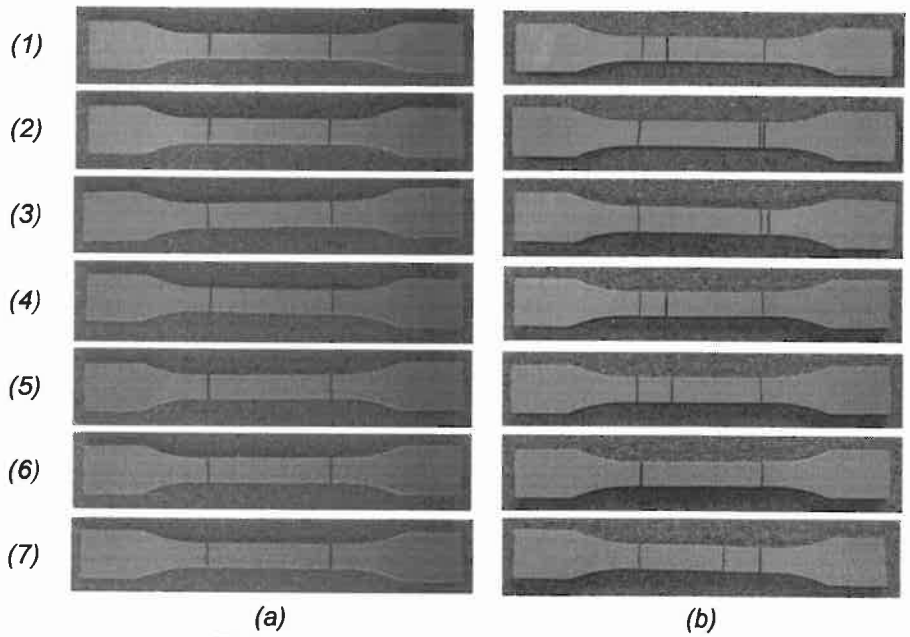

Figure 3.6 *- Test specimens before testing (a) and, after testing (b).*

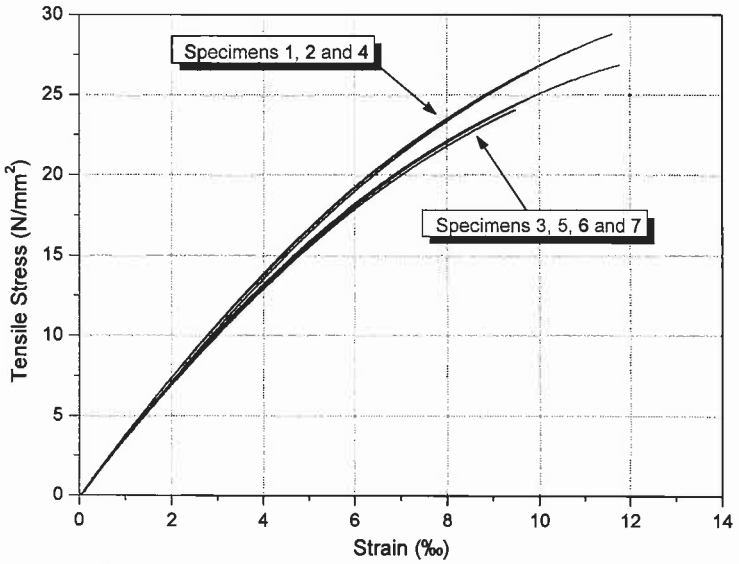

Figure 3.7 *- Tensile stress-strain curves for the Sikadur®32N epoxy resin.*

CFRP-Concrete Bond Product

A low viscosity epoxy based adhesive with a Trademark of MBrace®Resin 220, supplied by Bettor MBT® Portugal, was used to bond the prefabricated CFRP laminates to the concrete, into the grooves. The epoxy resin adhesive two component, resin and activator, are provided in 5 kg unit packaging (see ***Figure 3.8***). According to the supplier, the epoxy adhesive has the properties indicated in ***Table 3.6***.

Table 3.6 *- Main properties of the MBrace®Resin 220, extracted from datasheet (BETTOR MBT, 2005).*

Properties			
Density (at 20 °C)	**Mechanical resistance**	***Pot life,* open time and hardening** (at 20 °C)	**Mixing ratio**
1.7 kg/l	Tensile strength: > 2.5 N/mm² (concrete failure) Shear strength: > 1.8 N/mm² (concrete failure)	Minimum 3 min, ≈ 60 min, ≈ 3 days	Comp. I: 3.805 parts by weight Comp. II: 1.195 parts by weight

Figure 3.8 *- CFRP bond product packaging, 5 kg unit.*

Mechanical properties of the CFRP-concrete bond product

Uniaxial tensile tests were performed on moulded specimens to determine the tensile behavior of the epoxy adhesive used for bonding the CFRP laminate to concrete. The tests followed the procedures outlined in ISO 527-2 (1993). The shape and dimensions of test specimens are shown in ***Figure 3.9***. Due to the low viscosity of the epoxy resin and to avoid the presence of voids, specimens of reduced dimensions have been adopted and moulded under some pressure. The moulding steps of the test specimens are shown in ***Figure 3.10***.

A testing machine Instron 4505 (see ***Figure 3.5***) was used and a test speed of 1 mm/min selected for all the tests, complying with the procedures outlined by ISO 527-2 (1993). The tensile test results are included in ***Table 3.7*** and represented in ***Figure 3.11***.

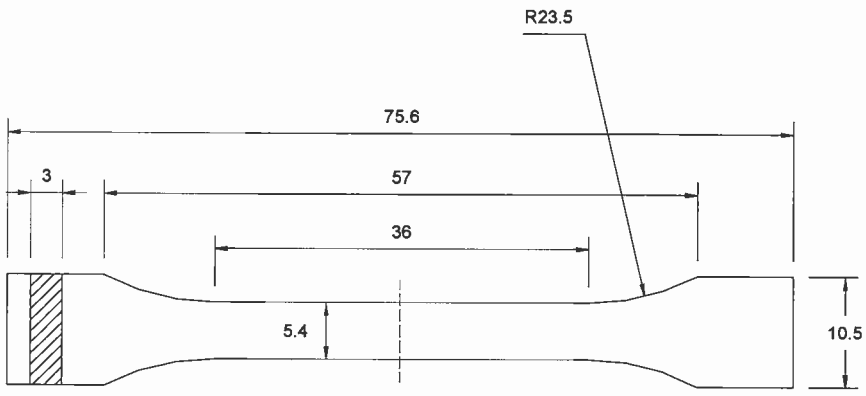

Figure 3.9 *- Shape and dimensions of the test specimen (dimensions in millimeters).*

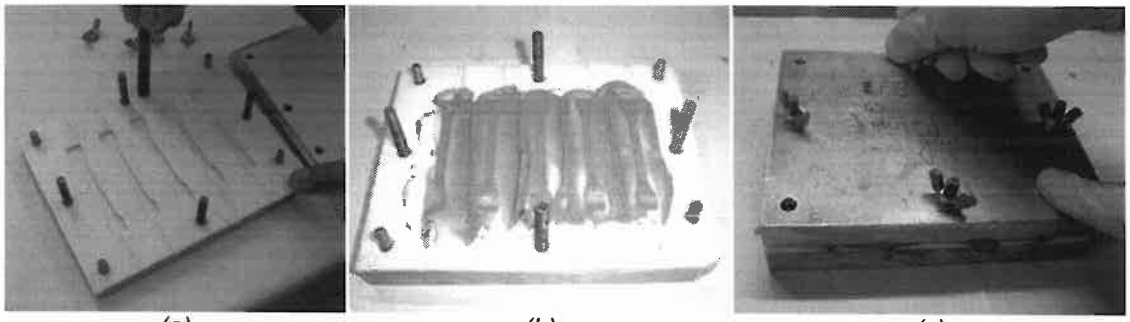

(a) (b) (c)

Figure 3.10 *- Preparation of the test specimens: (a) test specimen mould, (b) resin casting, and (c) applying pressure.*

Table 3.7 *- Results of the MBrace®Resin 220 tensile tests.*

Specimen	Ultimate tensile stress (N/mm^2)	Ultimate tensile strain (‰)	Modulus of elasticity[a] (kN/mm^2)
1	32.75	4.62	7.530
2	38.38	5.72	7.341
3	33.49	4.62	7.646
4	27.91	3.93	7.448
5	30.66	4.45	7.496
6	35.40	4.60	8.230
7	34.60	5.71	7.025
8	32.39	5.29	7.188
9	31.64	4.58	7.352
Average	33.03	4.83	7.473
Std.Dev.	2.81 *(8.52%)*	0.57 *(11.80%)*	0.320 *(4.28%)*

[a] *Tensile Modulus of Elasticity*, calculated from the stress-strain data using a linear regression procedure over the strain range 0-2.20 ‰

(*value*) Coefficient of Variation (COV) = (Standard deviation/Average) x 100

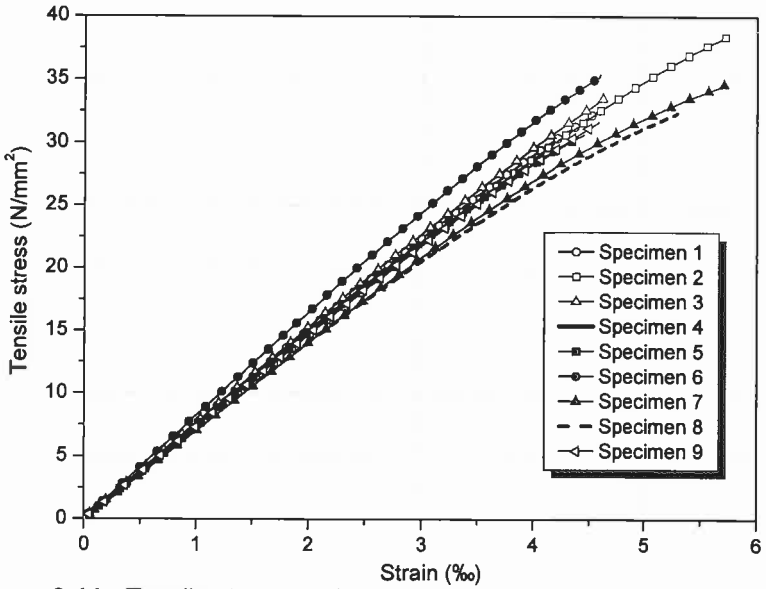

Figure 3.11 *- Tensile stress-strain curves for the MBrace®Resin 220 resin.*

CFRP Laminate

The CFRP laminate was provided in a roll and was produced by S&P® Clever Reinforcement Company (S&P, 2004) and distributed by Bettor MBT® Portugal (BETTOR MBT, 2004), see ***Figure 3.12***. The laminate had the trademark *MBrace Laminado LM* (BETTOR MBT, 2003), and was composed by unidirectional carbon fibres, agglutinated by an epoxy adhesive. According to the supplier, the *MBrace Laminado LM* has the main properties included in ***Table 3.8***.

Twenty measurements of the thickness and the width were carried out to determine the dimensions of the cross-section of the CFRP laminate strip. A thickness of 1.411±0.013 mm and a width of 9.372±0.038 mm were obtained.

To determine the tensile mechanical properties of the CFRP laminate, four tensile tests in coupon specimens (see ***Figure 3.13***) were carried out according to ISO 527-5 (1993) and ASTM 3039 (1993). A testing machine Instron 4208 with 150 mm distance between grips and gauge length of 50 mm (see ***Figure 3.14***) was used. A displacement rate of 2 mm/min was selected for all the tests. The failure tensile stress, failure tensile strain and modulus of elasticity are listed in ***Table 3.9***. The CFRP laminate tensile stress-strain curves are shown in ***Figure 3.15***.

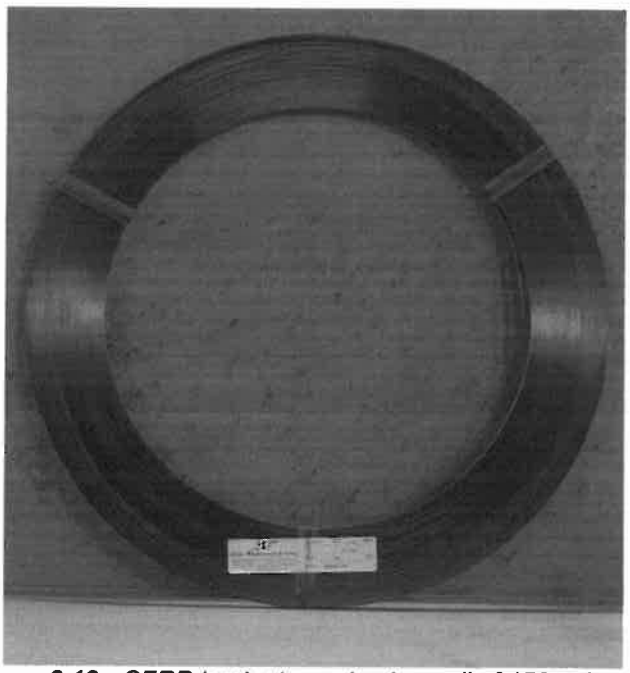

Figure 3.12 - *CFRP laminate packaging, roll of 150 m length.*

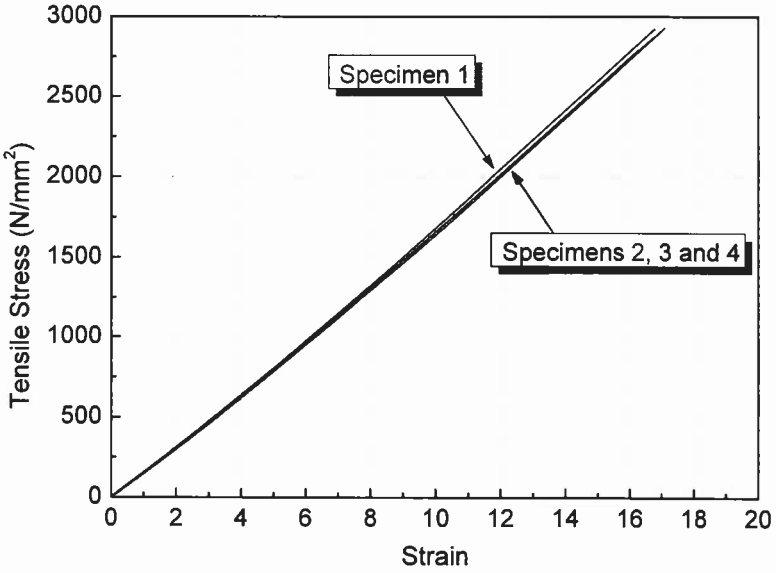

Figure 3.15 *- CFRP laminate tensile stress-strain curves.*

Table 3.9 *- Results of the CFRP laminate tensile tests.*

Specimen	Ultimate tensile stress (N/mm^2)	Ultimate tensile strain (‰)	Modulus of elasticity[a] (kN/mm^2)	Modulus of elasticity[b] (kN/mm^2)
1	2922.10	18.84	155.080	167.740
2	2927.42	19.11	153.150	164.300
3	2876.15	18.12	158.690	165.230
4	2790.86	17.72	157.540	164.820
Average	2879.13	18.45	156.100	165.500
Std. Dev.	63.19 (*2.19%*)	0.64 (*3.49%*)	2.48 (*1.59%*)	1.53 (*0.92%*)

[a] According to ISO 527-1 and ISO 527-5 (1997)
[b] *Tensile Chord Modulus of Elasticity*, according to ACI (2002) and ASTM 3039 (1993)
(*value*) Coefficient of Variation (COV) = (Standard deviation/Average) x 100

The ultimate tensile strain in ***Table 3.9*** was evaluated using the following equation:

$$\varepsilon_u = \frac{\sigma_u}{E} \tag{3.1}$$

where

ε_u is the ultimate tensile strain;
σ_u is the ultimate tensile stress; and
E is the tensile modulus of elasticity, in accordance with ISO 527-1/5 (1997).

Reinforcing Steel

Steel bars of grade 500 with nominal diameter, ϕ_s, of 6 mm, were used for the longitudinal reinforcement of the slabs (CEB-FIP Model Code, 1993). No shear reinforcement was used in the slabs.

Three tension coupons from the ϕ_s = 6 mm conventional reinforcing steel bars were tested to acquire their modulus of elasticity, yield stress and ultimate tensile strength. The coupons were tested in direct tension, using a DARTEC universal testing machine with a load cell of 600 kN capacity and an accuracy better than ± 2% (see ***Figure 3.16***) The samples were loaded at a constant stress rate of 18 $N/mm^2\ s^{-1}$. The bar elongation was measured using a clip-gauge of 100 mm gage length. The tensile tests were conducted according to the standard procedures found in ASTM A 370 (2002) and EN 10 002-1 (1990).

The three obtained stress-strain curves are depicted in ***Figure 3.17***. The mechanical properties of the steel reinforcing bars, evaluated from the direct tensile tests, are reported in ***Table 3.10***. The results of the three tests were almost identical, and all tests exceeded the specified yield strength of 500 MPa. All stress-strain curves showed a linear elastic behavior up to a yield stress of about 500 N/mm^2 and strain of 2.3 ‰. This tested yield strain was slightly lower the expected yield strain of 2.5 - 2.4 ‰. This results in a tested elastic modulus of 217 kN/mm^2, which is slightly greater than that typically used for steel reinforcement (200 - 210 kN/mm^2). Above the yield strain, the steel experienced strain hardening up to reach the ultimate strength. The clip-gauge was removed at a strain of approximately 50 ‰ to protect it from damage.

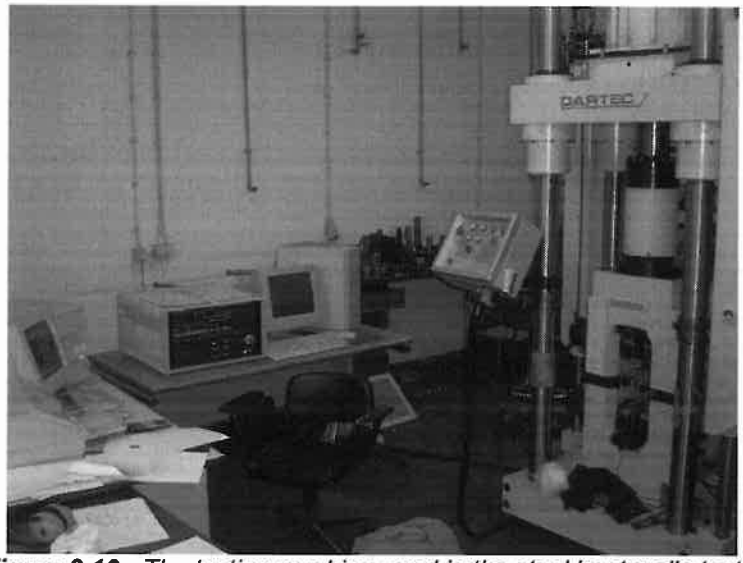

Figure 3.16 - *The testing machine used in the steel bar tensile tests.*

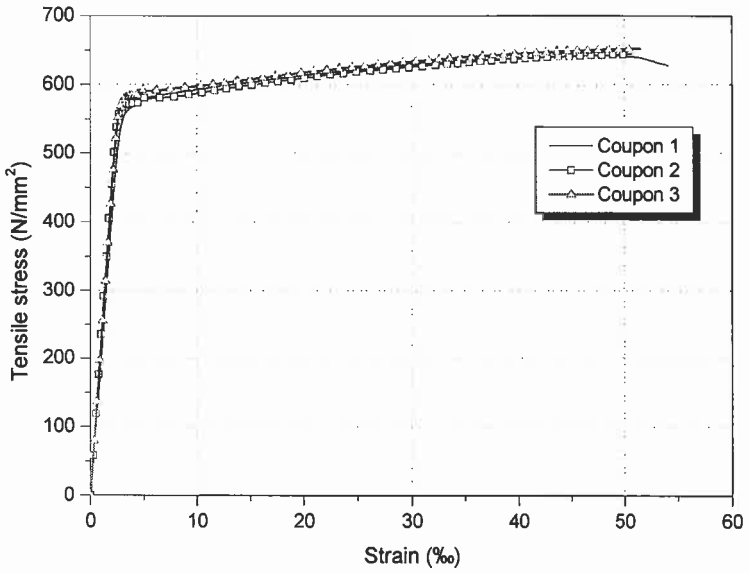

Figure 3.17 *- Stress-strain diagram of reinforcing steel.*

Table 3.10 *- Steel bars mechanical properties evaluated from the direct tensile tests.*

Sample	**Modulus of elasticity** (kN/mm^2)	**Yield strength (0.2 %)**[1] (N/mm^2)	**Strain at Yield stress**[2]	**Tensile strength** (N/mm^2)
1	202.484	540.76	0.0029	641.95
2	224.791	546.42	0.0025	645.99
3	224.644	559.38	0.0027	651.56
Average	217.306	548.85	0.0027	646.50
Std.Dev.	12.836 *(5.91%)*	9.55 *(1.74%)*	0.0002 *(6.35%)*	4.83 *(0.75%)*

[a] Yield strength determinated by the "*Offset Method*", according to ASTM 370 (2002)
[b] Strain at yield point, for the 0.2 % offset stress
(*value*) Coefficient of Variation (COV) = (Standard deviation/Average) x 100

4 Preparation of the Specimens

Eight reinforced concrete slabs strips of 300 mm x 1965 mm, with 80 mm thickness, were cast at distinct periods from different concrete mixes. For each concrete batch, four cylindrical concrete specimens, of 150 mm diameter and 300 mm depth, and three beams of 100 mm x 100 mm cross section and 850 mm length, were cast. The slabs, cylinders and beams moulds used are shown in ***Figure 4.1****(a)*. For each concrete batch, each slab, cylinder and beam specimen was cast in two layers, each one vibrated using an electrical concrete poker vibrator with a 25 mm tip and 50 Hz frequency, see ***Figure 4.1****(b)*.

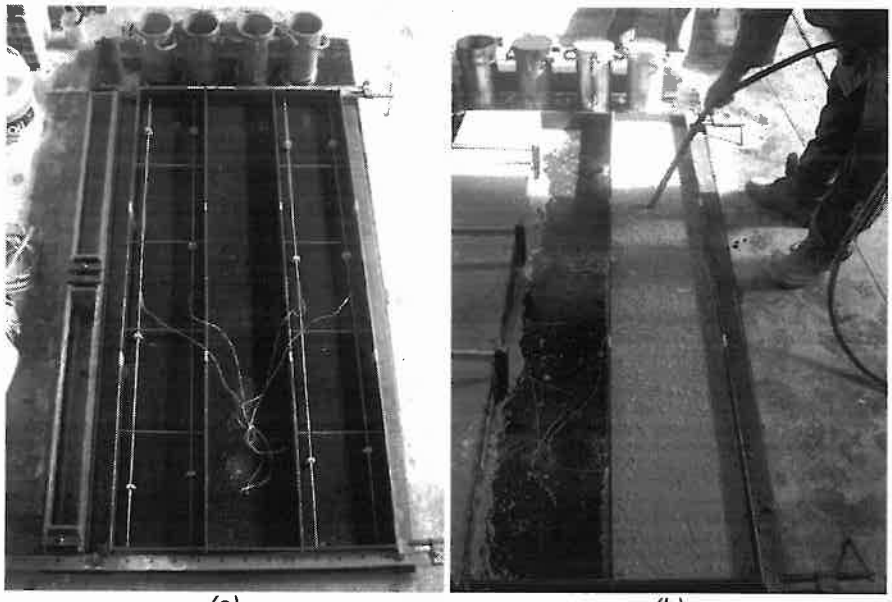

(a) *(b)*

Figure 4.1 *- Slab strips, cylinders and beam specimens: (a) formwork set up and moulds used, and (b) plain concrete consolidation.*

A detail of one strain gauge installed on a reinforcing bar, the bar plastic support used to set the bar correctly, and the constructive reinforcement ϕ3 mm is shown in ***Figure 4.2***.

After the slabs, the cylinder, and beam concrete specimens have been cast, their top surfaces were finished manually using a smooth plastic float and were covered with wet burlap sacks. The burlap sacks were monitored and kept wet for two days (see ***Figure 4.3***). After this curing period, the slabs, the cylinder and the beam specimens were removed from the moulds and maintained in natural laboratory environmental conditions up to getting 28 days.

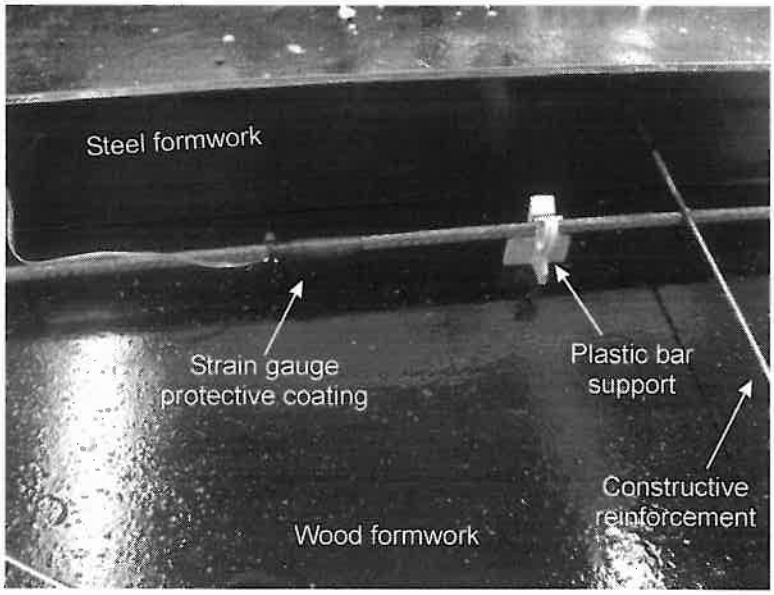

Figure 4.2 *- Detail of the strain gauge at the steel bar, bar plastic support and constructive reinforcement.*

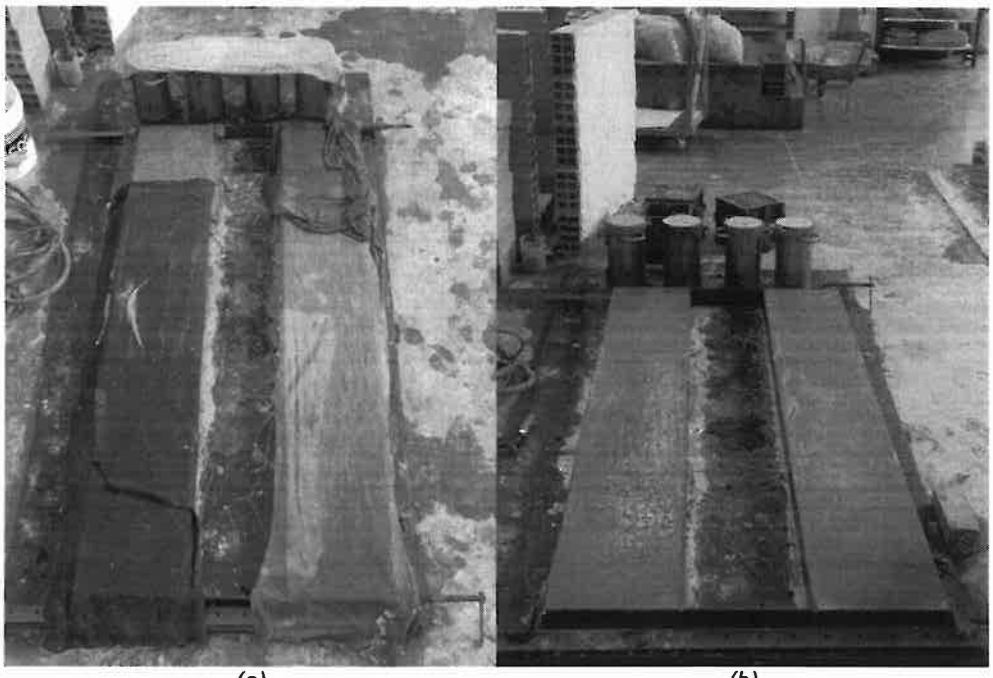

(a) *(b)*

Figure 4.3 *- Curing with water-retaining covering (a), and final aspect of the specimens (b).*

5 Strengthening Steps

The procedures of the hybrid strengthening technique are described in this chapter.

NSM Strengthening Technique

When the concrete slabs attained approximately 28 days of age, the slab specimens to be strengthened were placed outside the laboratory and the grooves were made using a Hilti diamond saw cutter machine, model DC 230-S (HILTI, 2004), see ***Figure 5.1***. The slits had about 4.5 mm width and 15 mm depth on the concrete cover of the slab's surface that will be in tension.

(a) (b)

Figure 5.1 *- Making the slits (a), and diamond saw cutter machine detail (b).*

In order to eliminate the dust resultant from the sawing process, the slits were cleaned with compressed air before bonding the laminate strips to the concrete into to slits (***Figure 5.2***). The CFRP laminates were cleaned with acetone to remove eventual dirt.

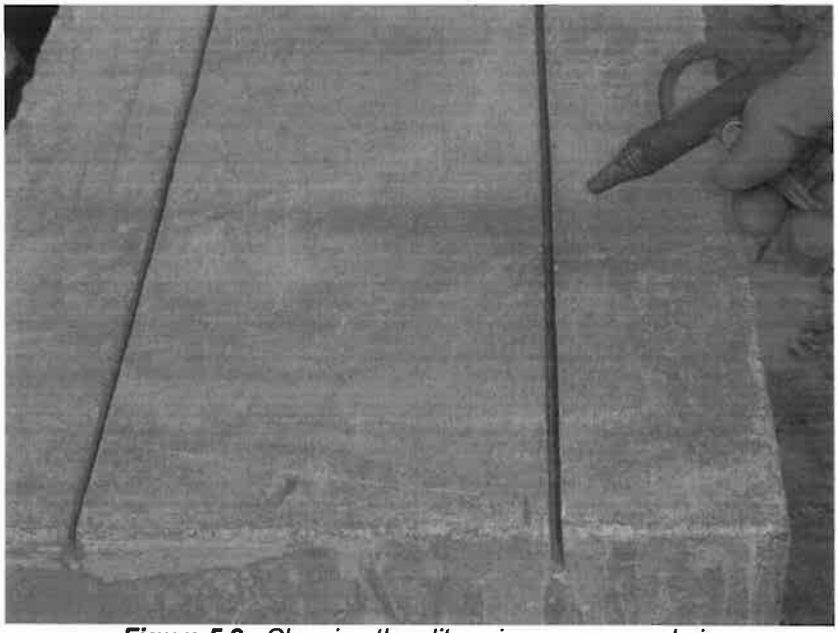

Figure 5.2 *- Cleaning the slits using compressed air.*

Figure 5.3 shows an overview before installing the CFRP laminates into the slits. The laminate strips were fixed to the concrete slits using the aforementioned epoxy adhesive (Section "CFRP-Concrete Bond Product"). The slits were filled with the epoxy adhesive using a spatula, and the CFRP laminates were then introduced into the slits (***Figure 5.4***).

Figure 5.3 *- A specimen before to be strengthened; the adhesive compound recipients; the acetone bottle; the CFRP laminate strips; and the tools used to mix and to apply the epoxy adhesive into the slits.*

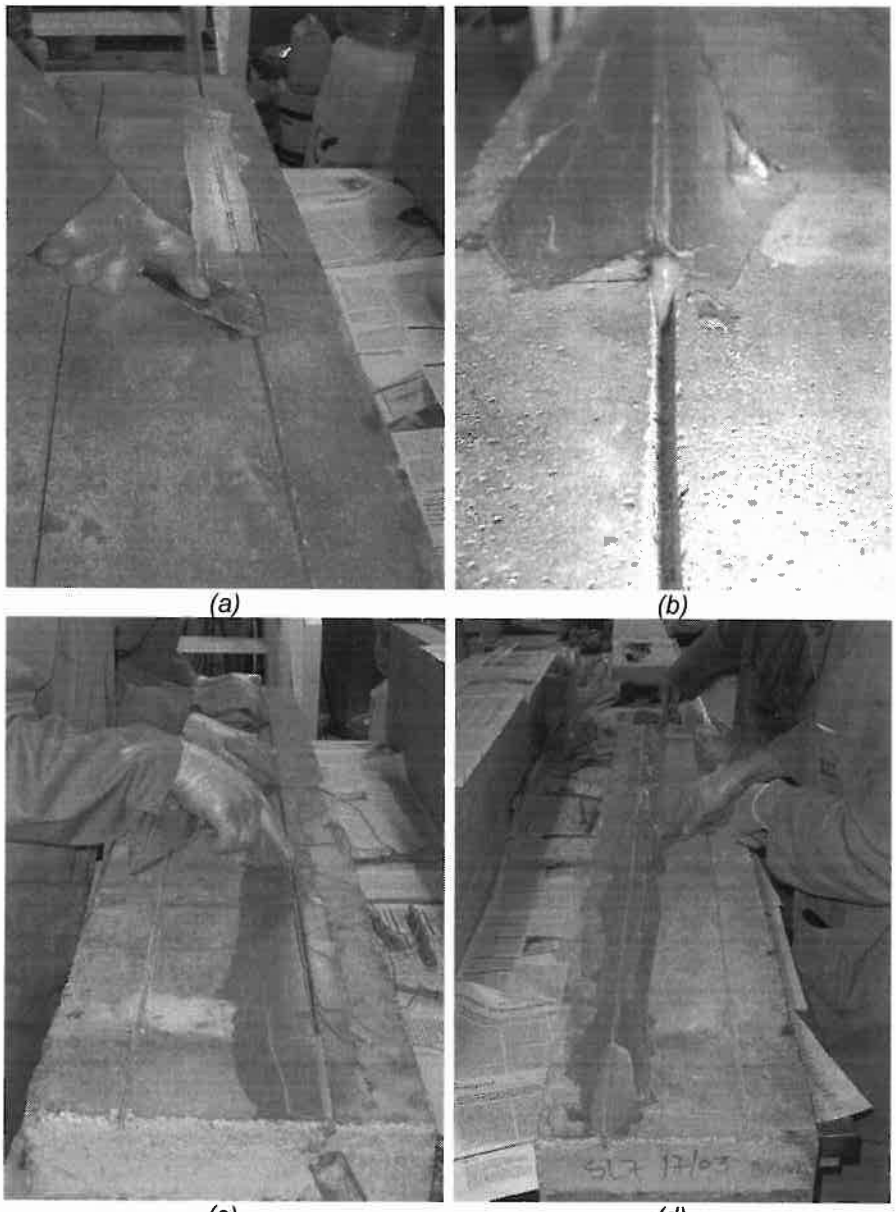

Figure 5.4 - Filling the slit with epoxy (a), slit totally filled (b), placing the CFRP laminate (c), and finishing the CFRP laminate placing procedure (d).

SFRC Overlay Strengthening

The slab specimens to be overlaid were placed outside of the laboratory and the top surface was sandblasted, see ***Figure 5.5***. To ensure good adhesion between new concrete overlay and the old concrete, a fast layer should be removed up to get aggregates uncovered. Therefore, the surface preparation technique of sandblasting the old concrete was employed.

To eliminate the dust resultant from the sandblasting process, before applying the bond product, the top surface of the specimen was cleaned with compressed air (***Figure 5.6***).

***Figure 5.5** - Sandblasting the top surface specimen.*

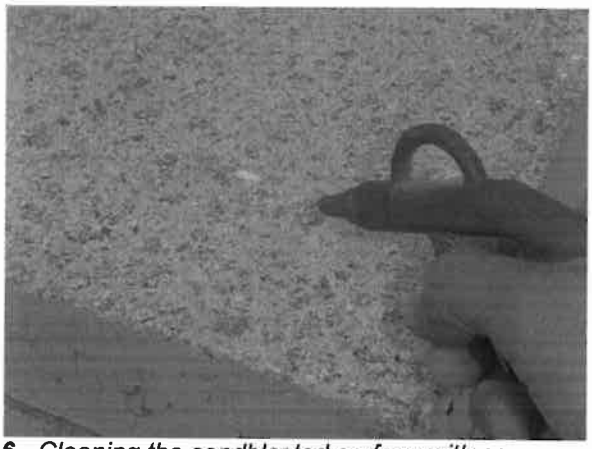

***Figure 5.6** - Cleaning the sandblasted surface with compressed air jet.*

The SFRC overlay was bonded to the concrete slab sandblasted surface using the epoxy adhesive indicated in Section "Overlay Bond Product". The main bond steps are shown in ***Figure 5.7***. An overview before applying the bond product and the freshly SFRC is shown in ***Figure 5.7****(a)*. The bond product was spread over the substrate top surface with a spatula ***Figure 5.7****(b,c)*. The fresh concrete overlay was cast as is illustrated in ***Figure 5.7****(d)*. A mini slipform showed in ***Figure 5.8****(a,b)* was used to consolidate the thin SFRC overlay and beam SFRC specimens. The mini slipform intends to simulate the real conditions of compaction of a thin SFRC overlay. The SFRC beam specimens were cast in three layers (about 50 mm thickness) and each one was consolidated using the mini slipform. The SFRC cylinder specimens were cast in two layers, each one consolidated using a vibratory compaction table during about 5 seconds.

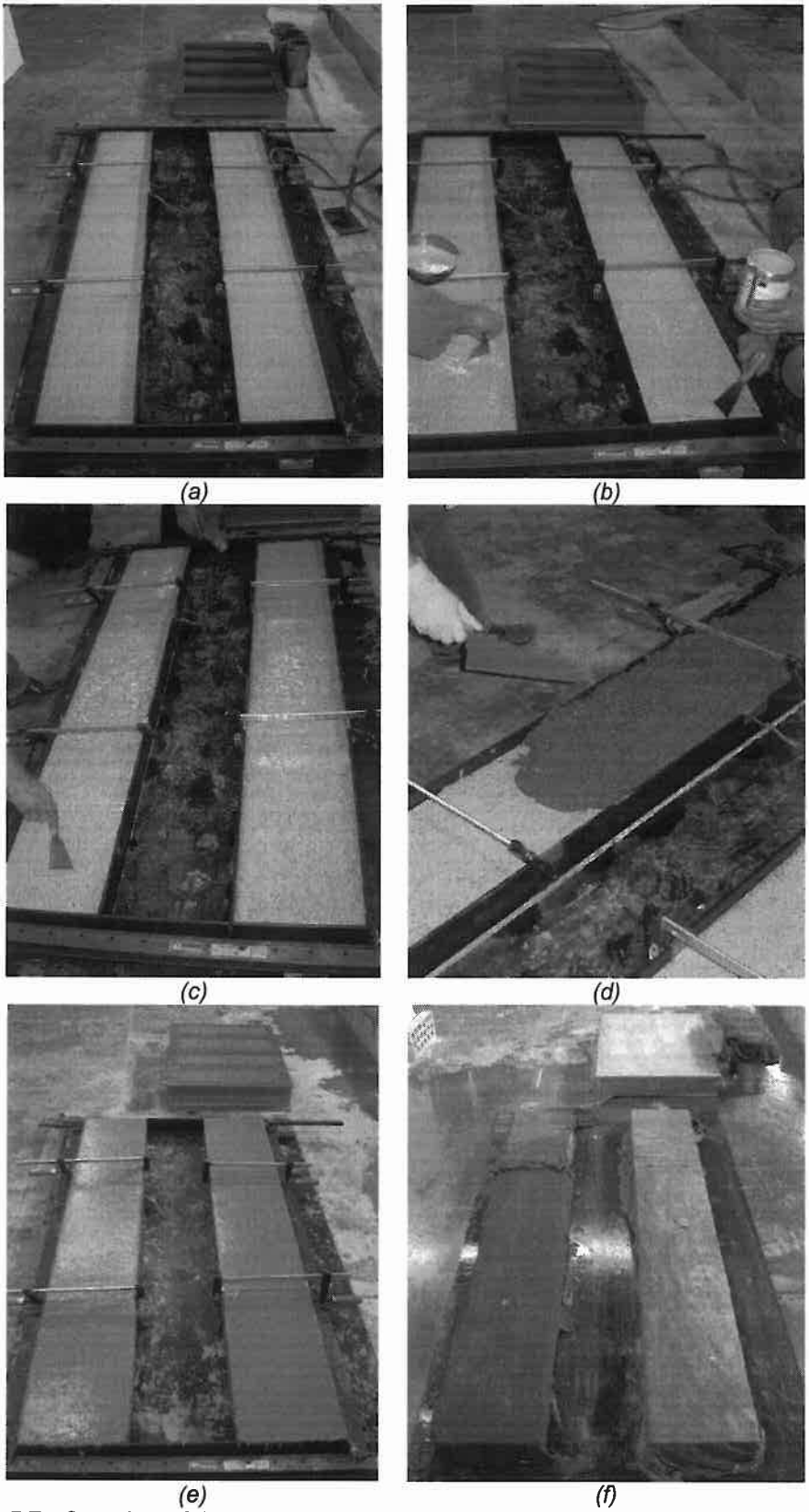

***Figure 5.7** - Overview of the specimens and the moulds before applying the SFRC overlay.*

The work of bonding the fresh SFRC overlay to the hardened concrete followed the manufactures specifications (SIKA, 2002) and the ACI guidelines (ACI 503.2-92,

ACI 503.5R-92 and ACI 503.6R-97). In the present experimental program, an overlay thickness of approximately 30 mm of SFRC layer was adopted.

For each SFRC batch, three cylinder concrete specimens (150mm x 300mm) and four beams (150 mm x 150 mm, with 600 mm length) were cast and tested at the testing age of the slab. The curing process adopted for the plain concrete was also used for the thin bonded SFRC overlay, cylinder and beam SFRC specimens (see ***Figure 5.7****(f)*).

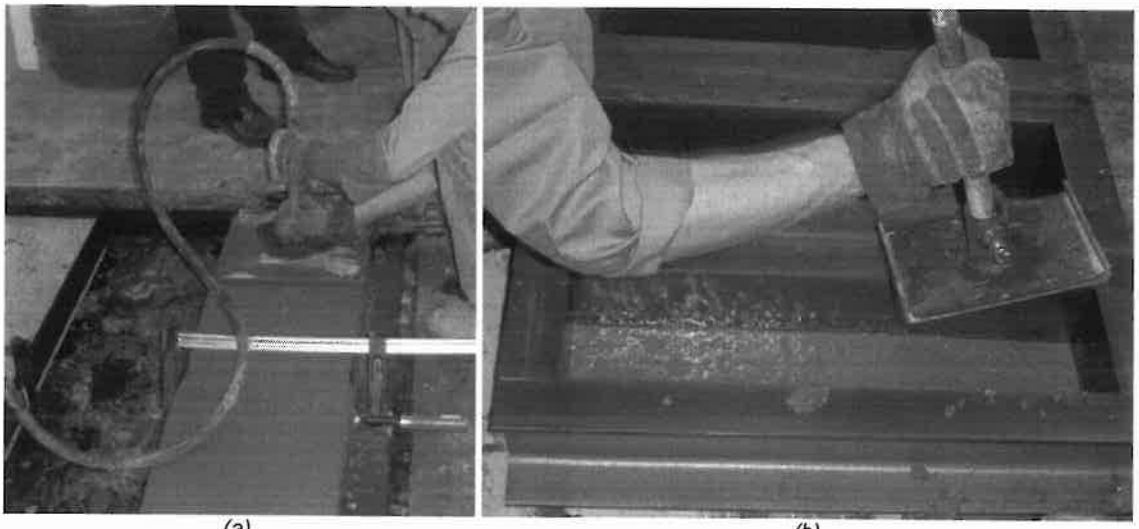

(a) (b)

Figure 5.8 *- SFRC consolidation with a mini slipform: (a) SFRC overlay, and (b) beam specimens.*

6 Results

The notation adopted to identify each slab specimen is: **SLxxSOy**, where:

SL = slab strip base;
xx = slab specimen number (01 to 08);
S = strengthened with CRFP laminates (if it is the case);
O = slab overlaid with SFRC layer (if it is the case), and
y = identification of the SFRC overlay mix batch (1 or 2, see ***Table 3.1***).

Therefore, SL02SO1 refers to the slab specimen number 02, strengthened with CFRP laminates in the tensile zone and overlaid with SFRC of mix number 1 in the compressive zone.

Reference Slabs

- The SL01 unstrengthened slab strip is shown in ***Figures 6.1***, before and after have been tested. The mid-span deflection, steel reinforcement strain and concrete strain are shown in ***Figures 6.2***, ***6.3*** and ***6.4***, respectively.

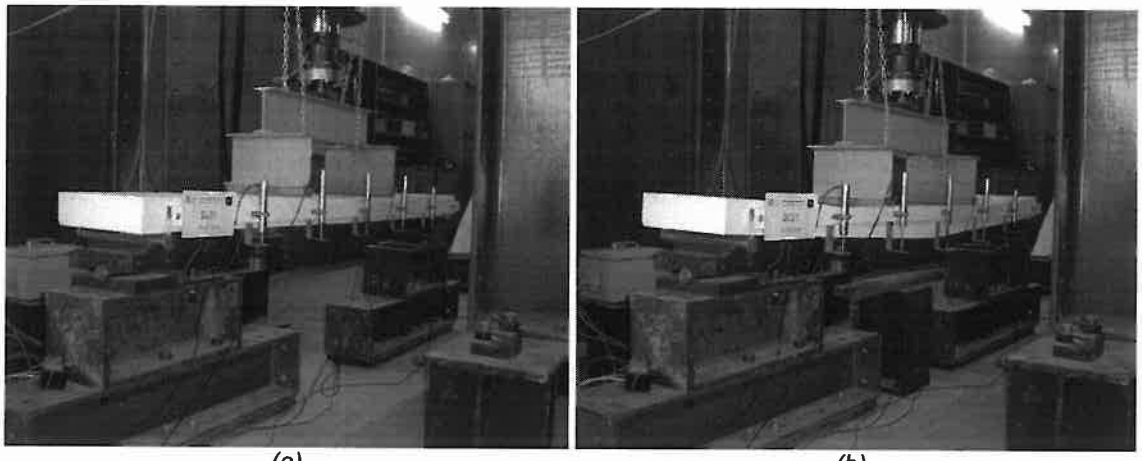

(a) (b)

Figure 6.1 - *Specimen SL01 before (a), and after have been tested (b).*

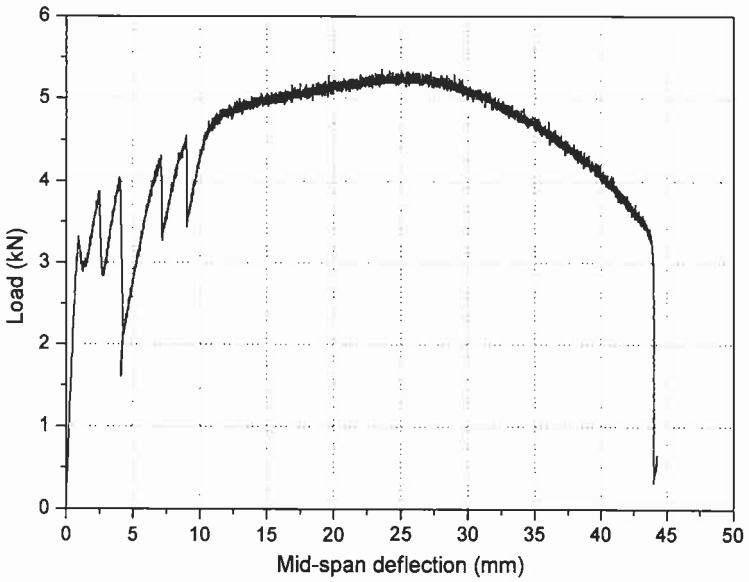

Figure 6.2 *- Relationship between applied load and deflection at mid-span of the slab SL01.*

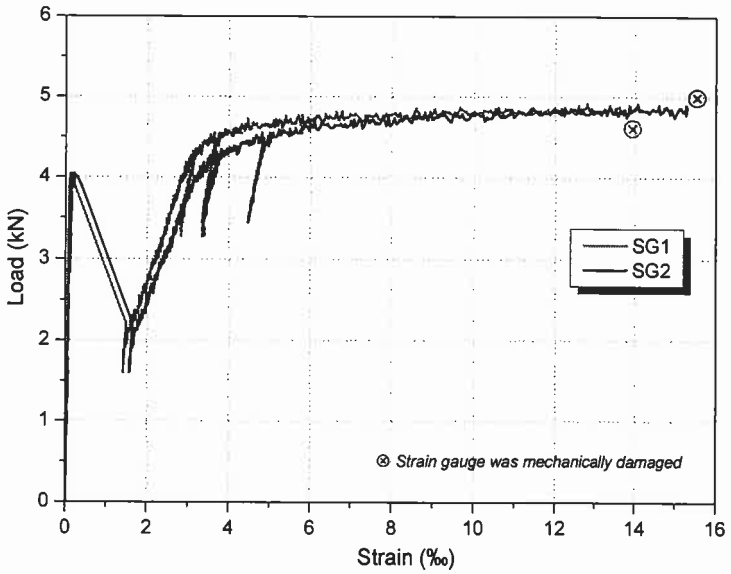

Figure 6.3 *- Relationship between applied load and tensile strain of the steel reinforcement for the slab SL01 (refer to* ***Figure 2.2****(c)).*

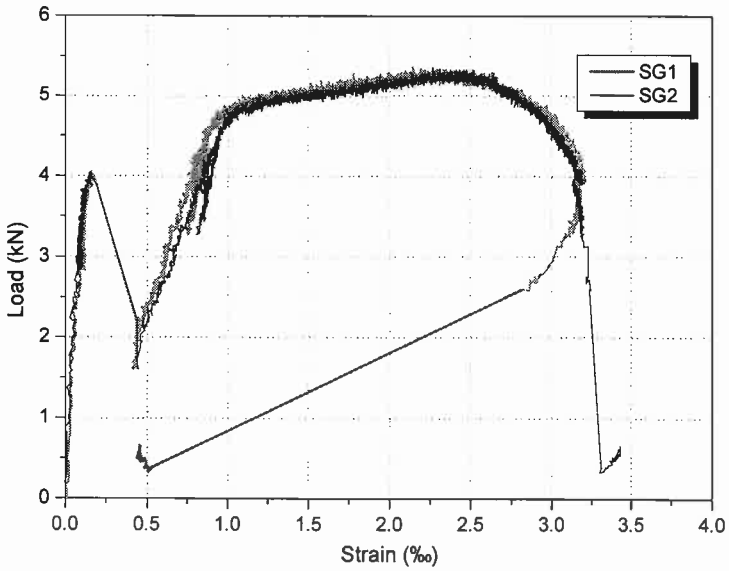

Figure 6.4 *- Relationship between applied load and compressive strain of the concrete at top surface for the slab SL01 (refer to* ***Figure 2.2****(d)).*

- The SL06 unstrengthened slab strip is shown in ***Figures 6.5***, before and after have been tested. The mid-span deflection, steel reinforcement strain and concrete strain are shown in ***Figures 6.6***, ***6.7*** and ***6.8***, respectively.

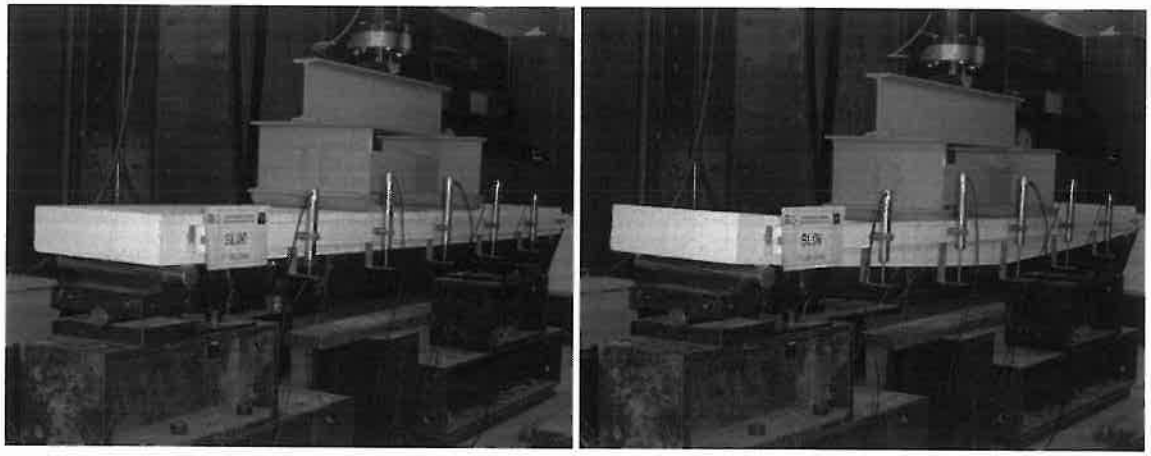

(a) *(b)*

Figure 6.5 *- Specimen SL06 before (a), and after have been tested (b).*

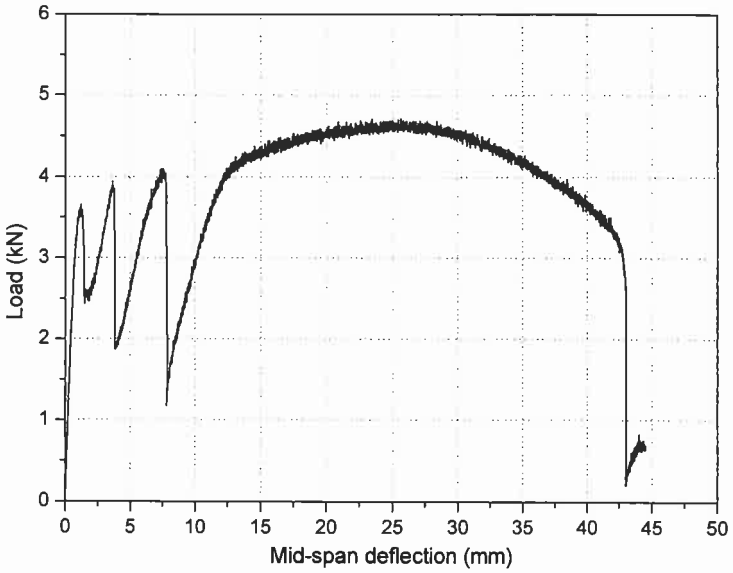

Figure 6.6 *- Relationship between applied load and deflection at mid-span of the slab SL06.*

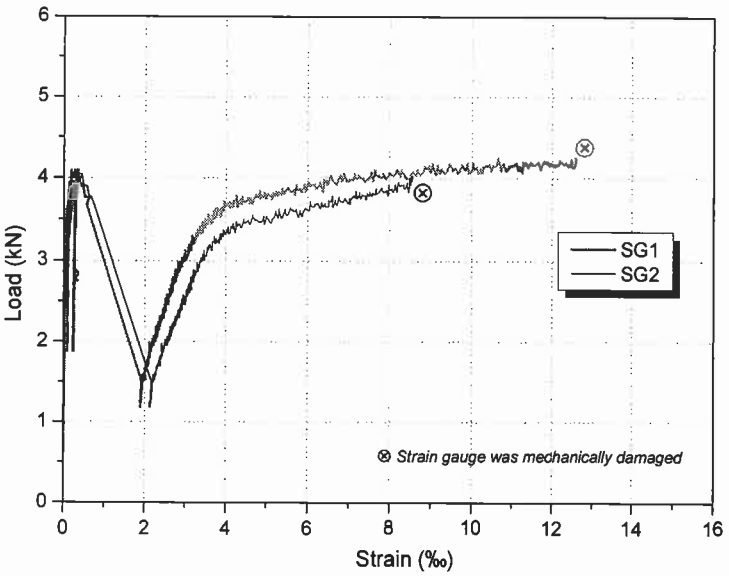

Figure 6.7 *- Relationship between applied load and tensile strain of the steel reinforcement for the slab SL06 (refer to* ***Figure 2.2****(c)).*

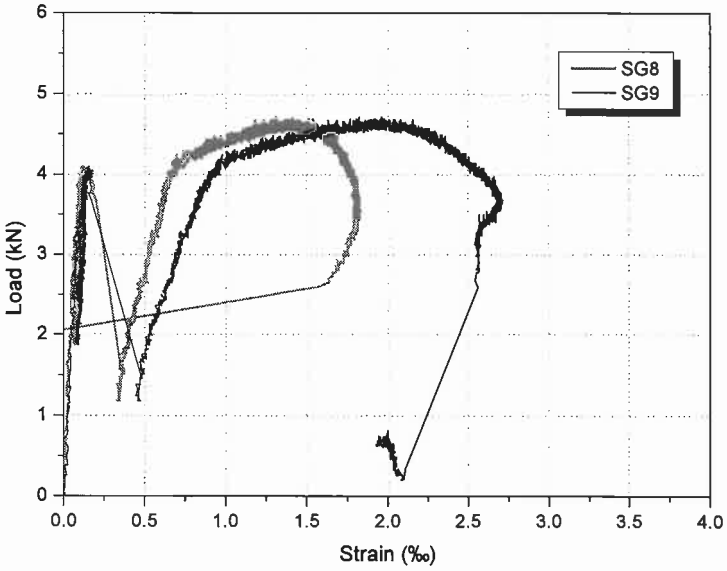

Figure 6.8 *- Relationship between applied load and compressive strain of the concrete at top surface for the slab SL06 (refer to* ***Figure 2.2****(d)).*

The bottom appearance of the unstrengthened slabs after have been tested is shown in ***Figure 6.9***.

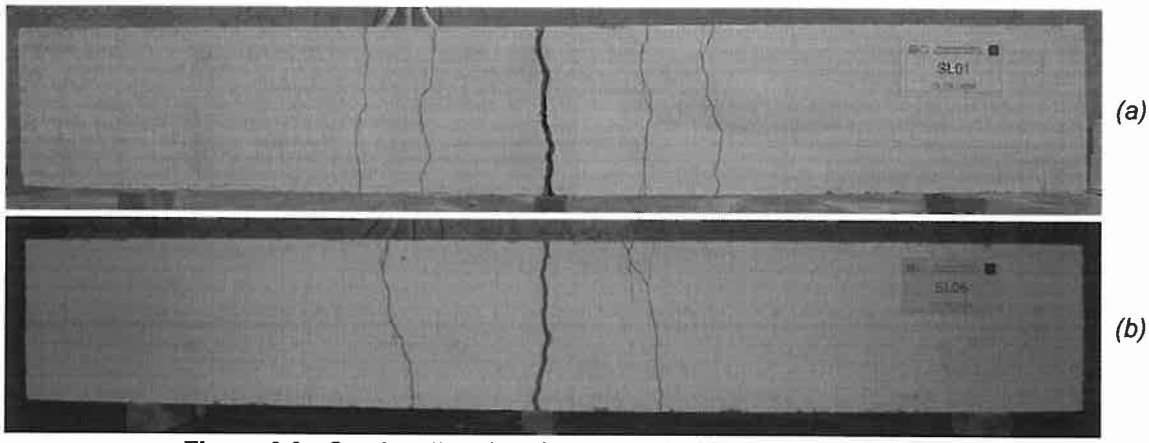

Figure 6.9 *- Crack pattern in reference slabs: (a) SL01, and (b) SL06.*

Slabs Strengthened with CFRP Laminate

- ***Figure 6.10*** shows the NSM CFRP strengthened SL03S slab strip before and after have been tested. The mid-span deflection, steel reinforcement strain, concrete strain and CFRP laminate strain are shown in ***Figures 6.11***, ***6.12***, ***6.13*** and ***6.14***, respectively.

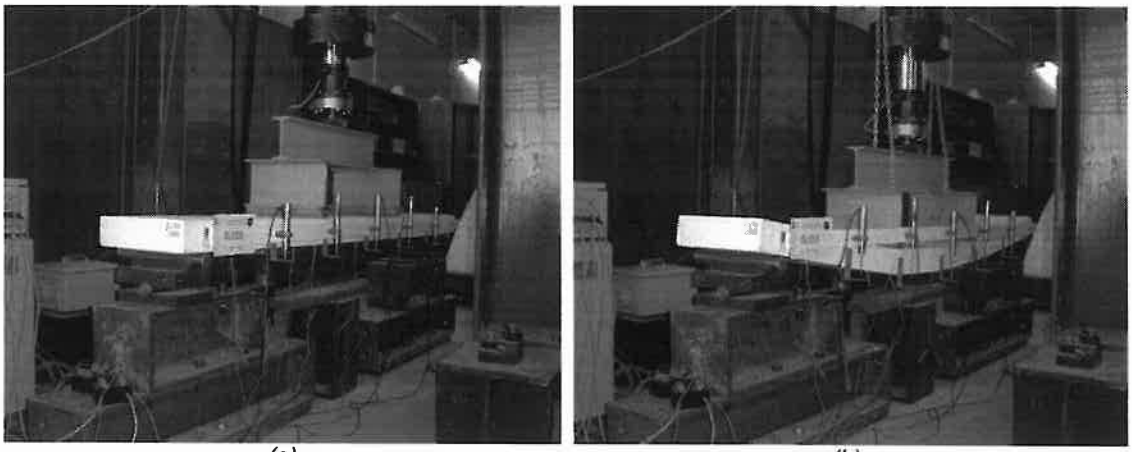

(a) (b)

Figure 6.10 *- Specimen SL03S before (a), and after have been tested (b).*

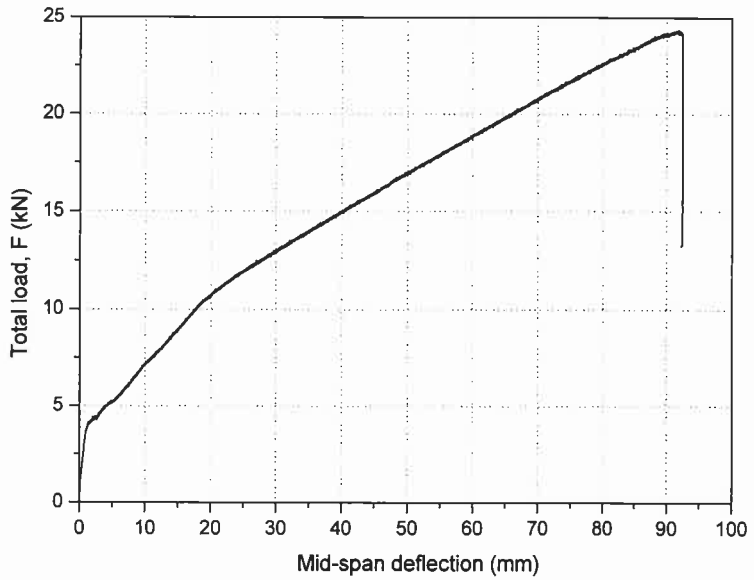

Figure 6.11 *- Relationship between applied load and deflection at mid-span of the slab SL03S.*

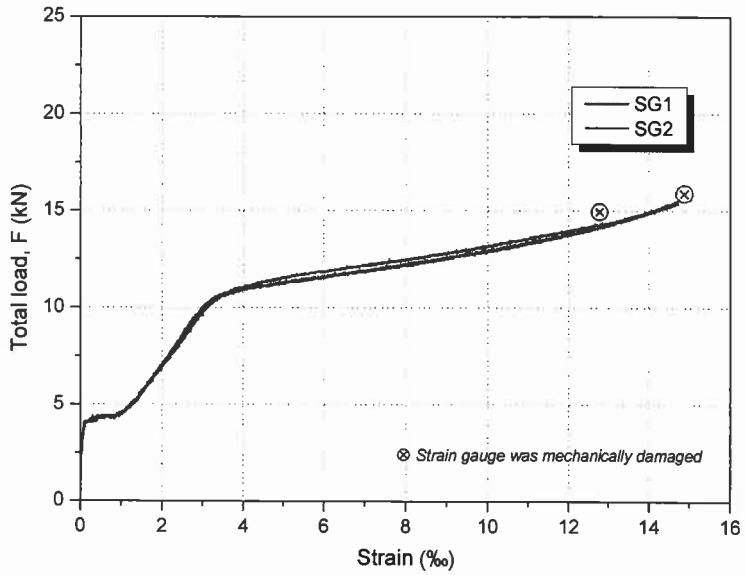

Figure 6.12 *- Relationship between applied load and tensile strain of the steel reinforcement for the slab SL03S (refer to* ***Figure 2.2****(c)).*

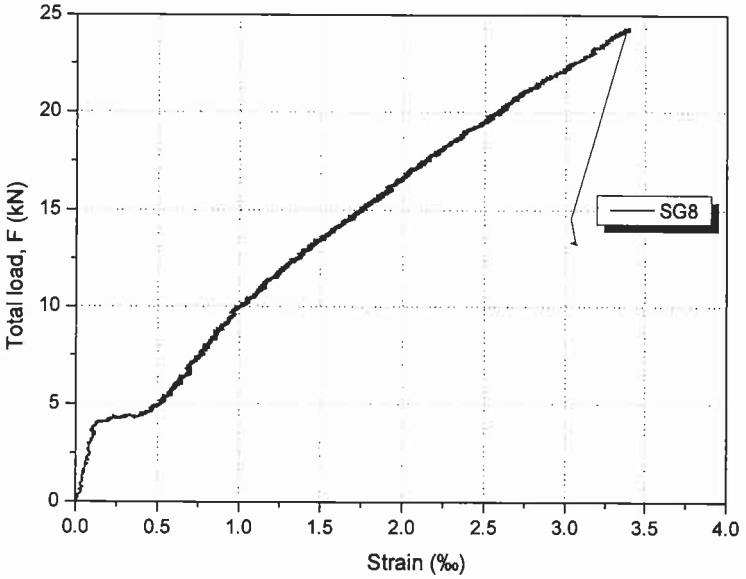

Figure 6.13 *- Relationship between applied load and compressive strain of the concrete at top surface for the slab SL03S (refer to* ***Figure 2.2****(d)).*

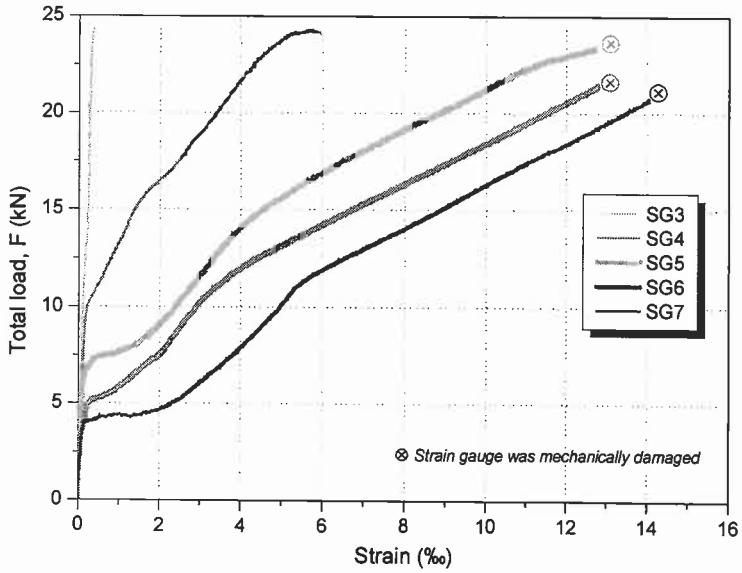

Figure 6.14 *- Relationship between applied load and tensile strain of the CFRP laminate for the slab SL03S (refer to* ***Figure 2.2****(b,c)).*

- ***Figure 6.11*** shows the NSM CFRP strengthened SL04S slab strip before and after have been tested. The mid-span deflection is shown in ***Figures 6.16***[§].

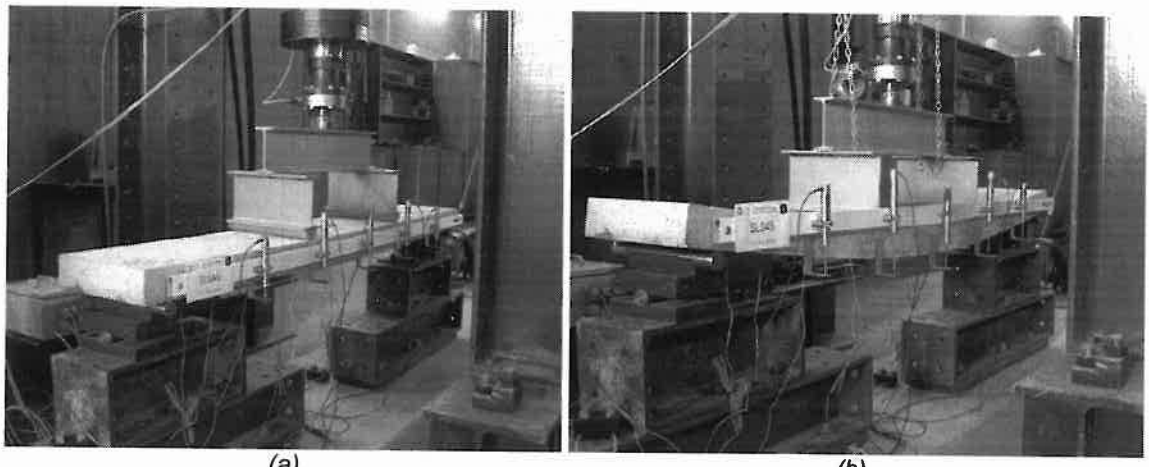

(a) *(b)*

Figure 6.15 *- Specimen SL04S before (a), and after have been tested (b).*

[§] **It was not possible to record the data of the strain gauge instrumentation for the slab strip SL04S**

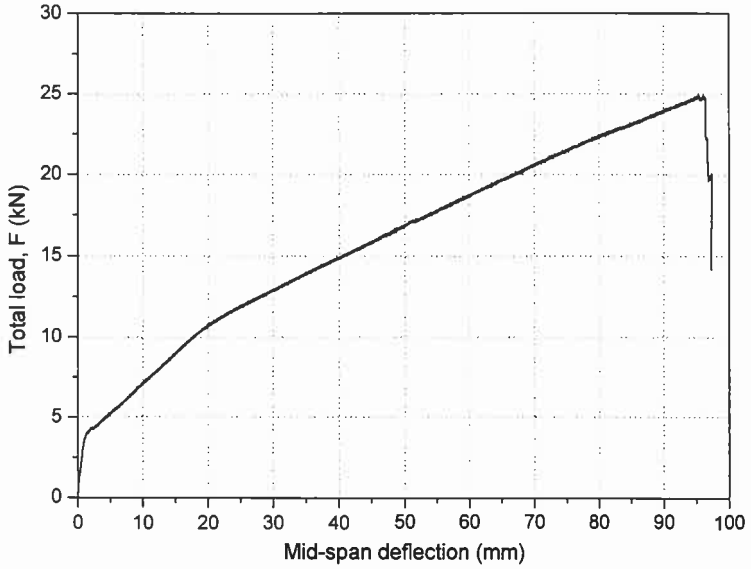

Figure 6.16 *- Relationship between applied load and deflection at mid-span of the slab SL04S.*

- ***Figure 6.17*** shows the NSM CFRP strengthened SL08S slab strip before and after have been tested. The mid-span deflection, steel reinforcement strain, concrete strain and CFRP laminate strain are shown in ***Figures 6.18***, ***6.19***, ***6.20*** and ***6.21***, respectively.

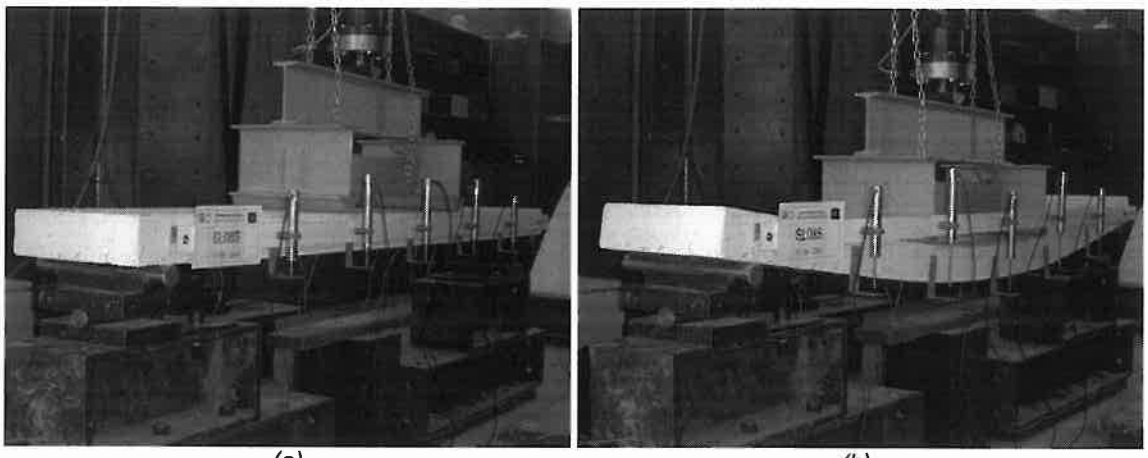

(a) *(b)*

Figure 6.17 *- Specimen SL08S before (a), and after have been tested (b).*

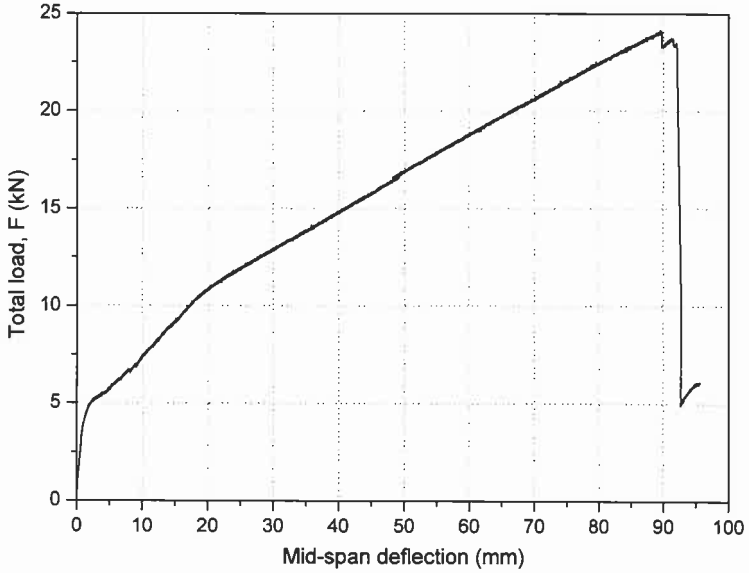

Figure 6.18 *- Relationship between applied load and deflection at mid-span of the slab SL08S.*

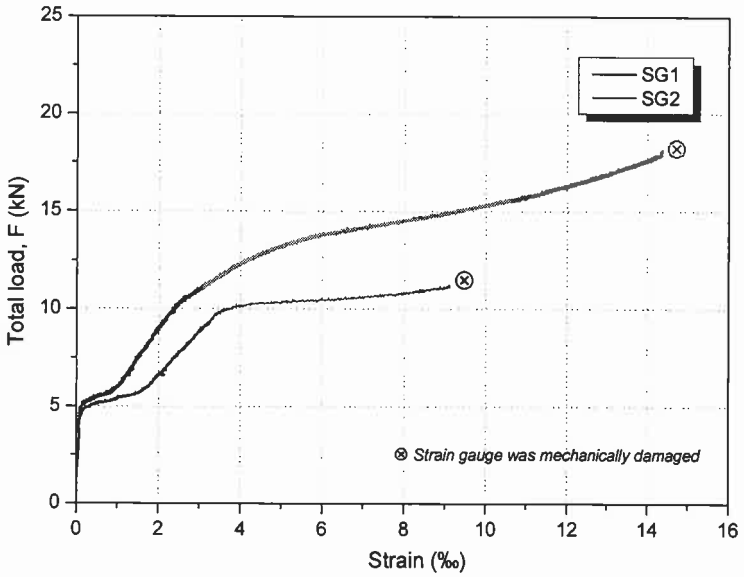

Figure 6.19 *- Relationship between applied load and tensile strain of the steel reinforcement for the slab SL08S (refer to* ***Figure 2.2****(c)).*

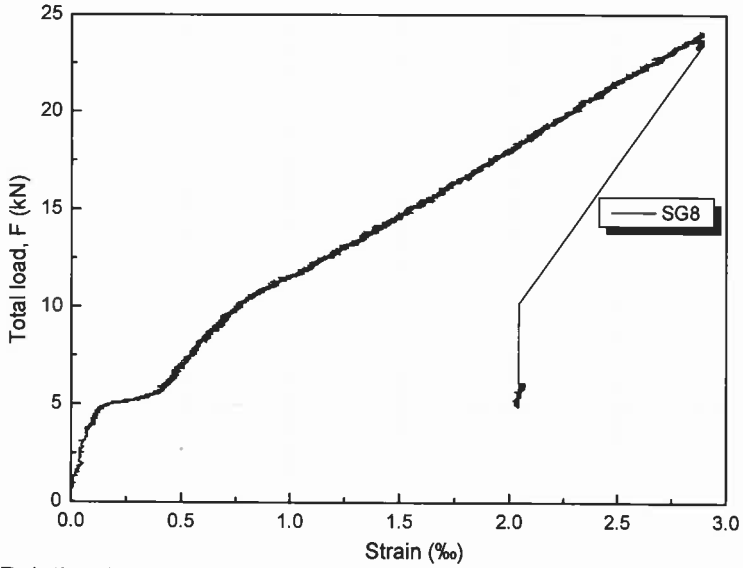

Figure 6.20 *- Relationship between applied load and compressive strain of the concrete at top surface for the slab SL08S (refer to* ***Figure 2.2****(d)).*

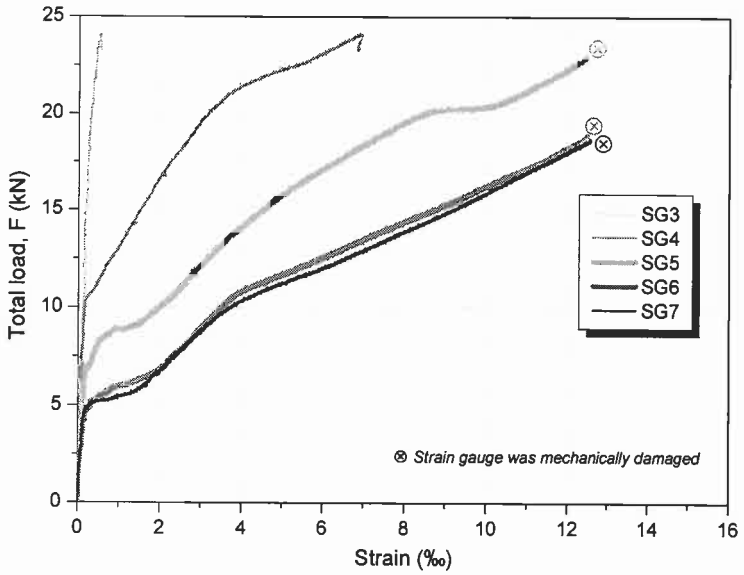

Figure 6.21 *- Relationship between applied load and tensile strain of the CFRP laminate for the slab SL08S (refer to* ***Figure 2.2****(b,c)).*

The bottom appearance of the slabs strengthened with CFRP laminates after have been tested is shown in ***Figure 6.22***.

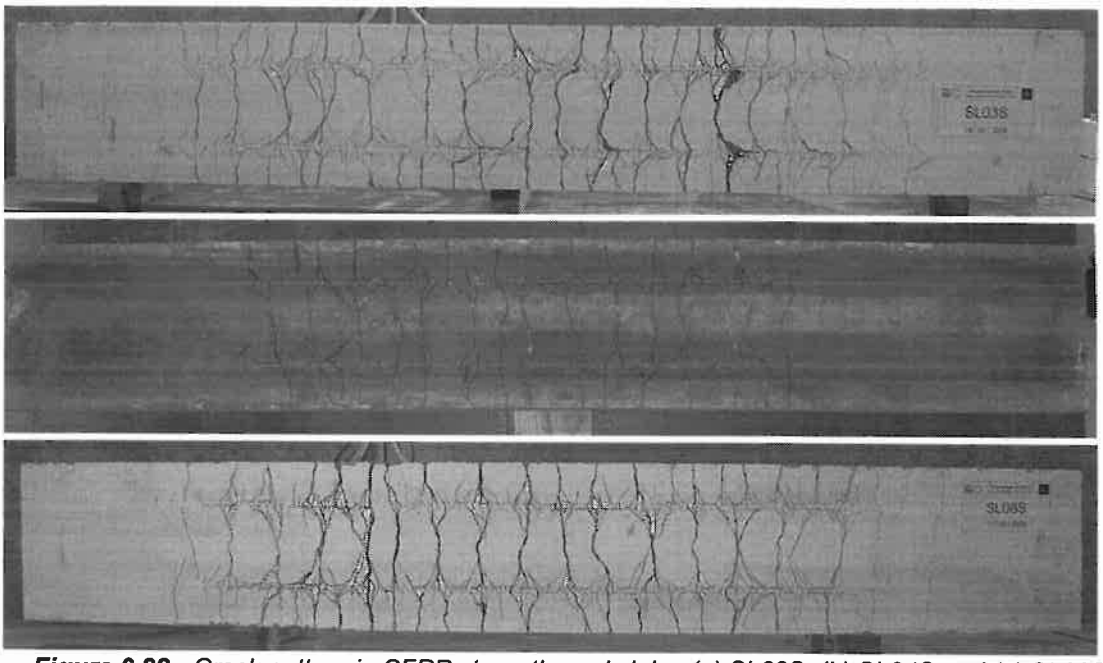

Figure 6.22 *- Crack pattern in CFRP strengthened slabs: (a) SL03S, (b) SL04S and (c) SL08S.*

Slabs Strengthened with CFRP Laminate and SFRC Overlay

- SL02SO1 is a slab strip strengthened by combining CFRP laminates, applied according to the NSM technique, and a SFRC compression overlay. ***Figures 6.23*** shows the SL02SO1 slab strip before and after have been tested The mid-span deflection, steel reinforcement strain, concrete strain and CFRP laminate strain are shown in ***Figures 6.24***, ***6.25***, ***6.26*** and ***6.27***, respectively.

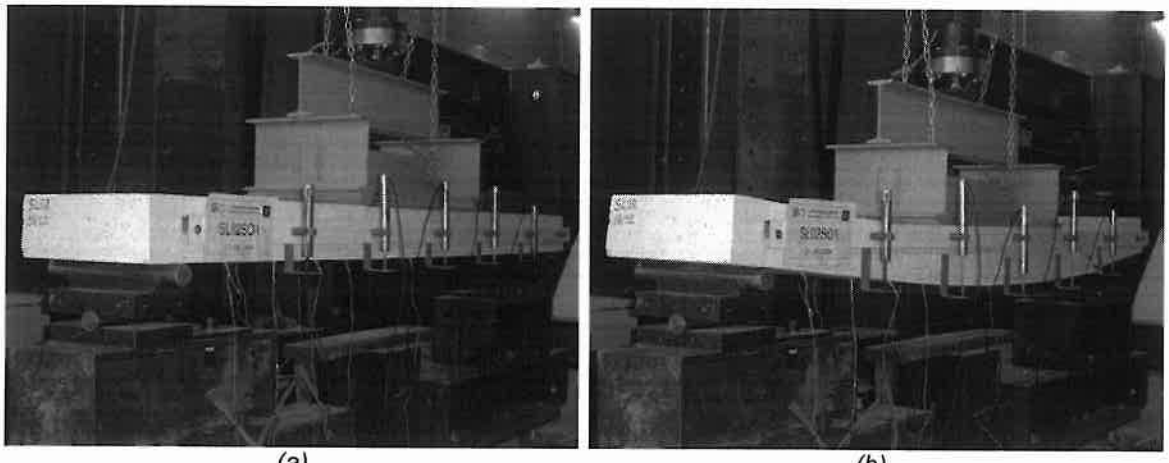

(a) (b)

Figure 6.23 *- Specimen SL02SO1 before (a), and after have been tested (b).*

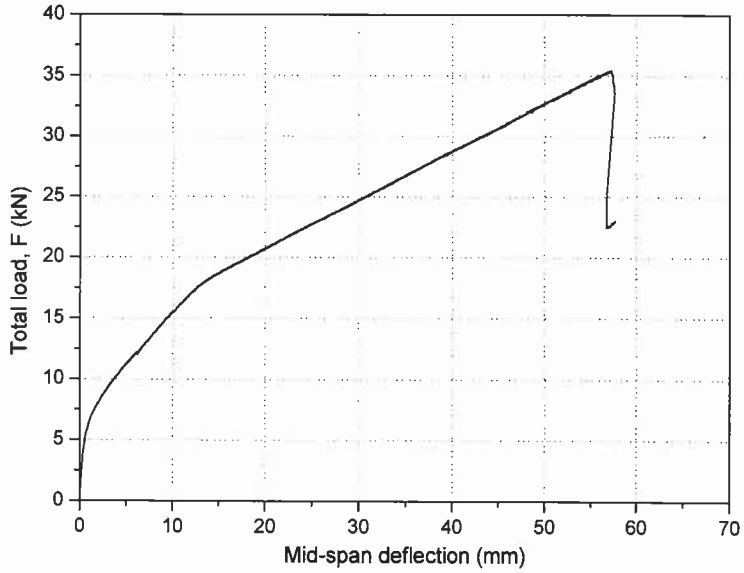

Figure 6.24 *- Relationship between applied load and deflection at mid-span of the slab SL02SO1.*

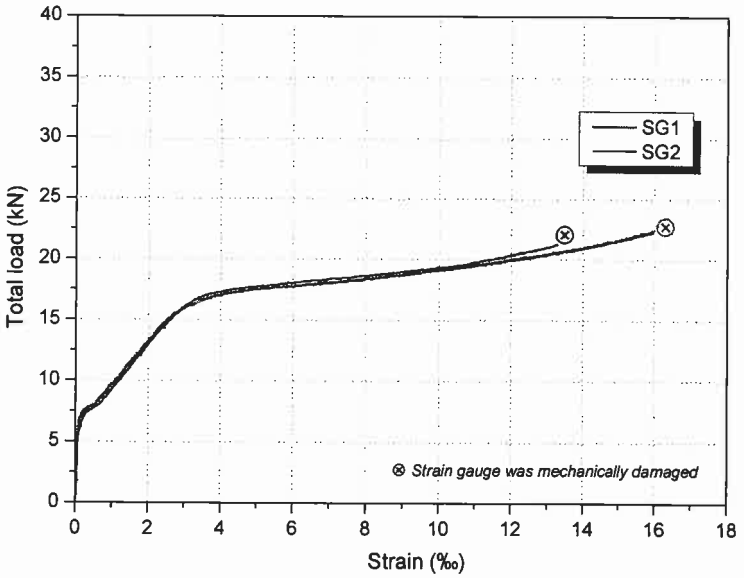

Figure 6.25 *- Relationship between applied load and tensile strain of the steel reinforcement for the slab SL02SO1 (refer to* ***Figure 2.2****(c)).*

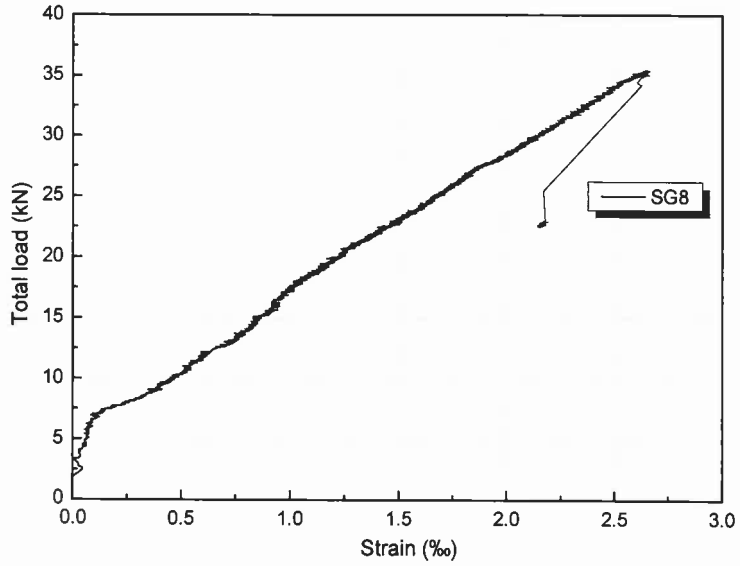

Figure 6.26 *- Relationship between applied load and compressive strain of the concrete at top surface for the slab SL02SO1 (refer to* ***Figure 2.2****(d)).*

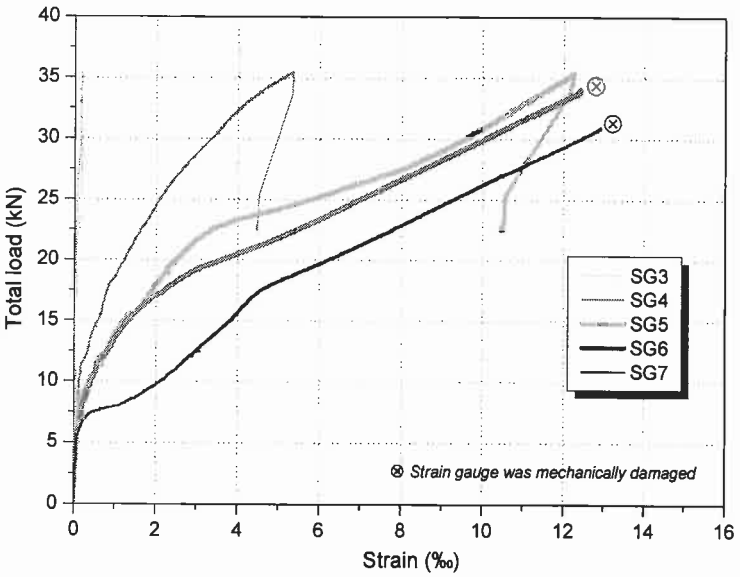

Figure 6.27 *- Relationship between applied load and tensile strain of the CFRP laminate for the slab SL02SO1 (refer to* ***Figure 2.2****(b,c)).*

- SL05SO1 is a slab strip strengthened by combining CFRP laminates, applied according to the NSM technique, and a SFRC compression overlay. ***Figures 6.28*** shows the SL02SO1 slab strip before and after have been tested The mid-span deflection, steel reinforcement strain, concrete strain and CFRP laminate strain are shown in ***Figures 6.29***, ***6.30***, ***6.31*** and ***6.32***, respectively.

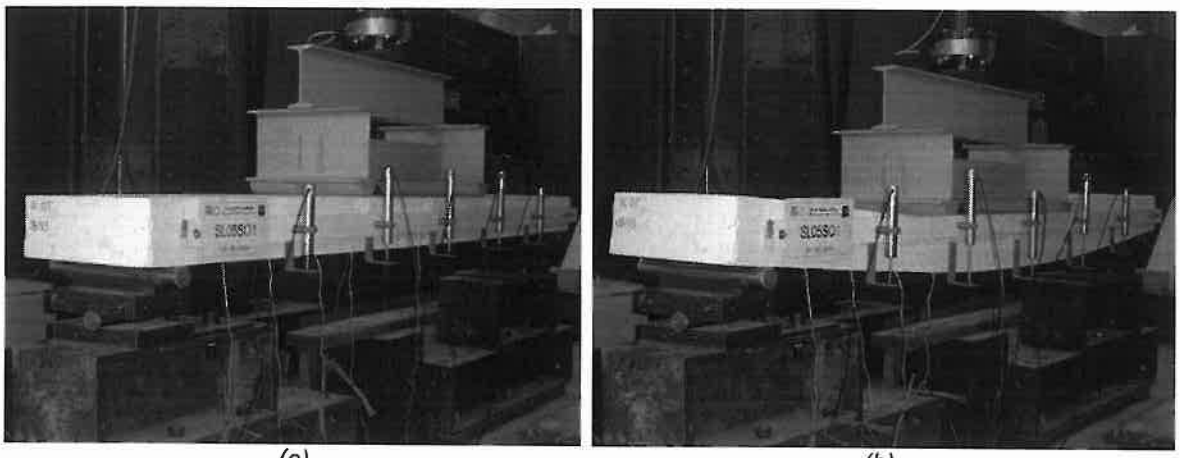

(a) (b)

Figure 6.28 *- Specimen SL05SO1 before (a), and after have been tested (b).*

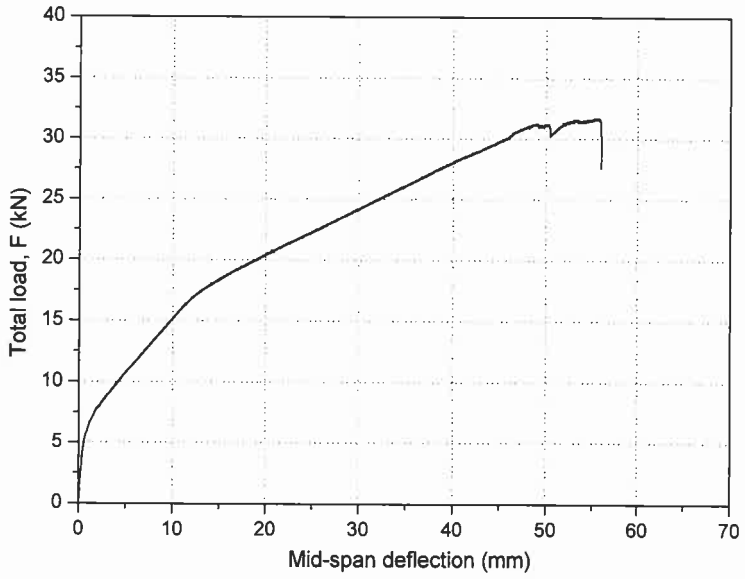

Figure 6.29 *- Relationship between applied load and deflection at mid-span of the slab SL05SO1.*

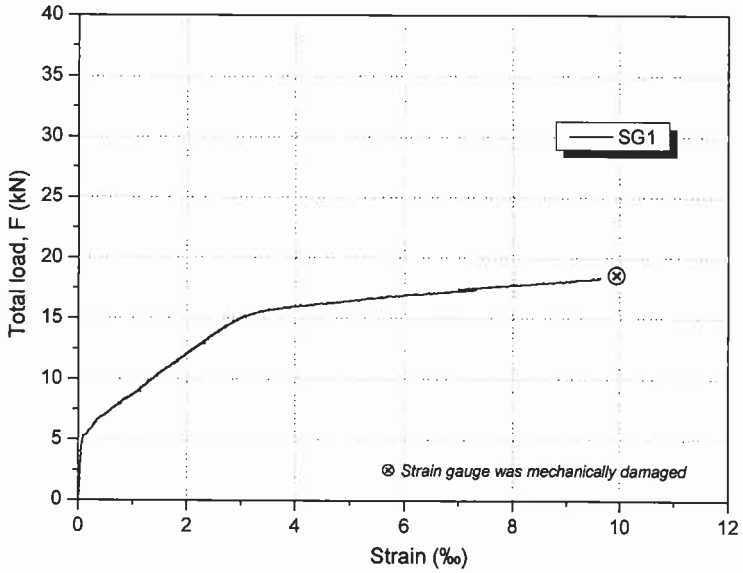

Figure 6.30 *- Relationship between applied load and tensile strain of the steel reinforcement for the slab SL05SO1[§] (refer to* ***Figure 2.2****(c)).*

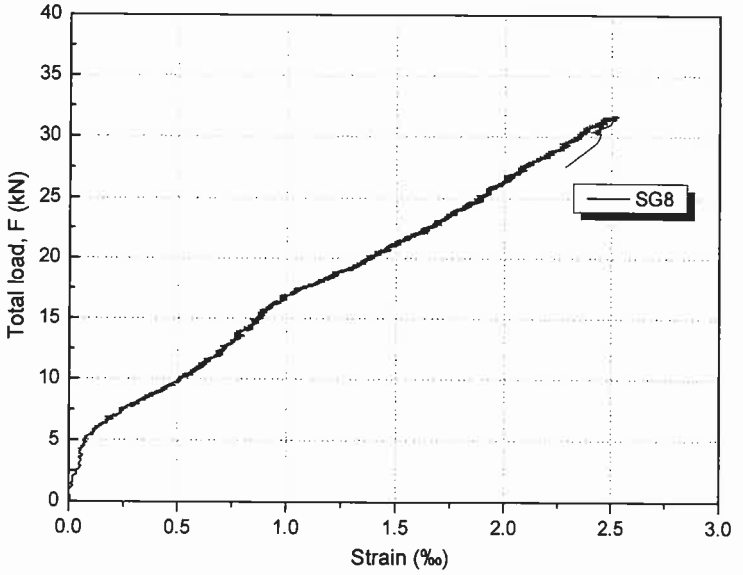

Figure 6.31 *- Relationship between applied load and compressive strain of the concrete at top surface for the slab SL05SO1 (refer to* ***Figure 2.2****(d)).*

[§] **It was not possible to record the data of the SG2**

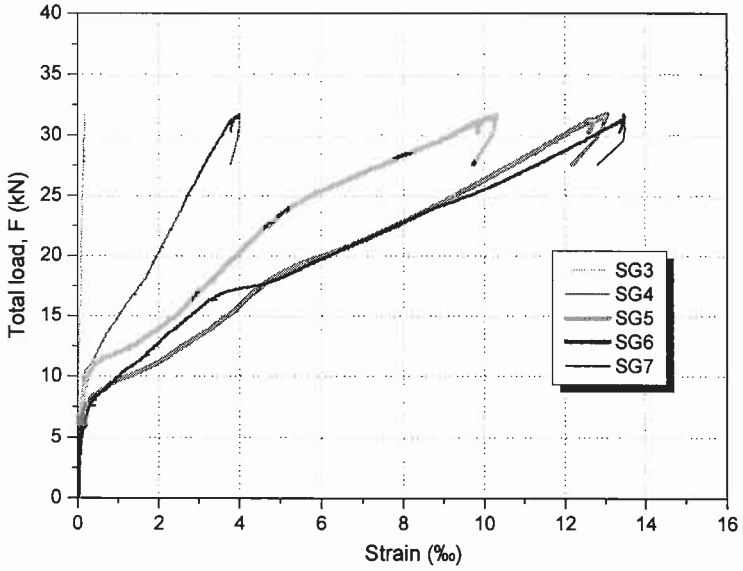

Figure 6.32 *- Relationship between applied load and tensile strain of the CFRP laminate for the slab SL05SO1 (refer to* ***Figure 2.2****(b,c)).*

- SL07SO2 is a slab strip strengthened by combining CFRP laminates, applied according to the NSM technique, and a SFRC compression overlay. ***Figures 6.33*** shows the SL02SO1 slab strip before and after have been tested The mid-span deflection, steel reinforcement strain and CFRP laminate strain are shown in ***Figures 6.34***, ***6.35***, and ***6.36***, respectively[§].

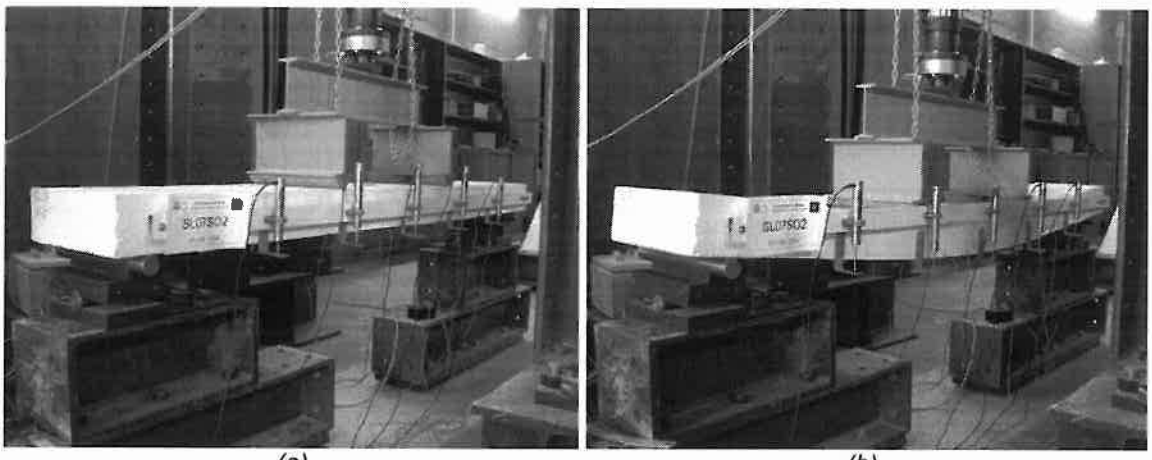

(a) *(b)*

Figure 6.33 *- Specimen SL07SO2 before (a), and after have been tested (b).*

[§] **It was not possible to record the data of the external concrete SG8 for the slab strip SL07SO2**

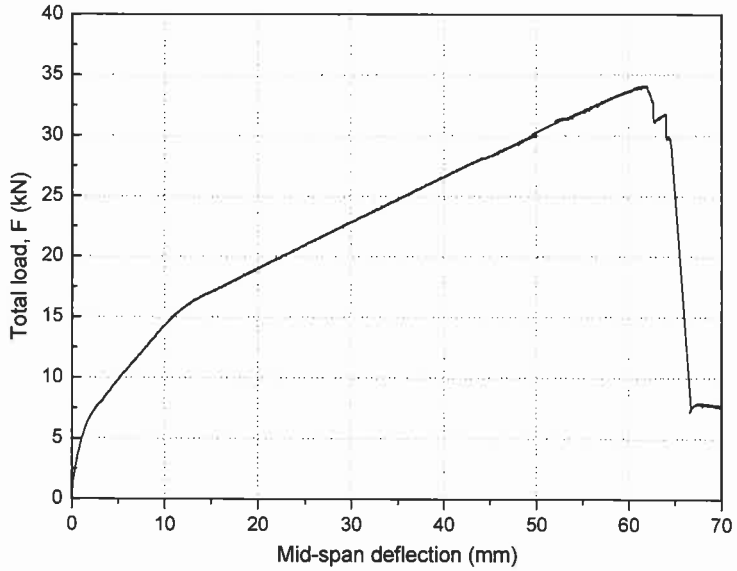

Figure 6.34 *- Relationship between applied load and deflection at mid-span of the slab SL07SO2.*

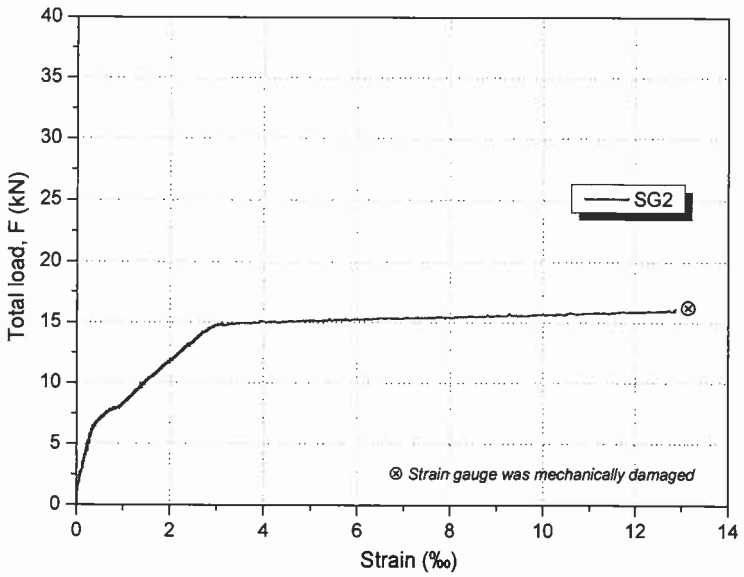

Figure 6.35 *- Relationship between applied load and tensile strain behaviour of the steel reinforcement for the slab SL07SO2[§] (refer to* ***Figure 2.2****(c)).*

[§] It was not possible to record the data of the SG1

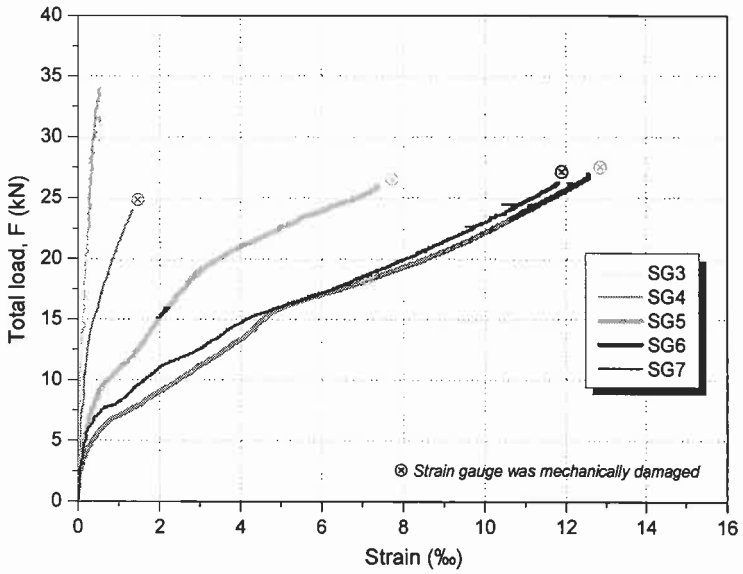

Figure 6.36 *- Relationship between applied load and tensile strain of the CFRP laminate for the slab SL07SO2 (refer to* ***Figure 2.2****(b,c))..*

The bottom appearance of the slabs strengthened with CFRP laminate and SFRC overlay after have been tested is shown in ***Figure 6.37***.

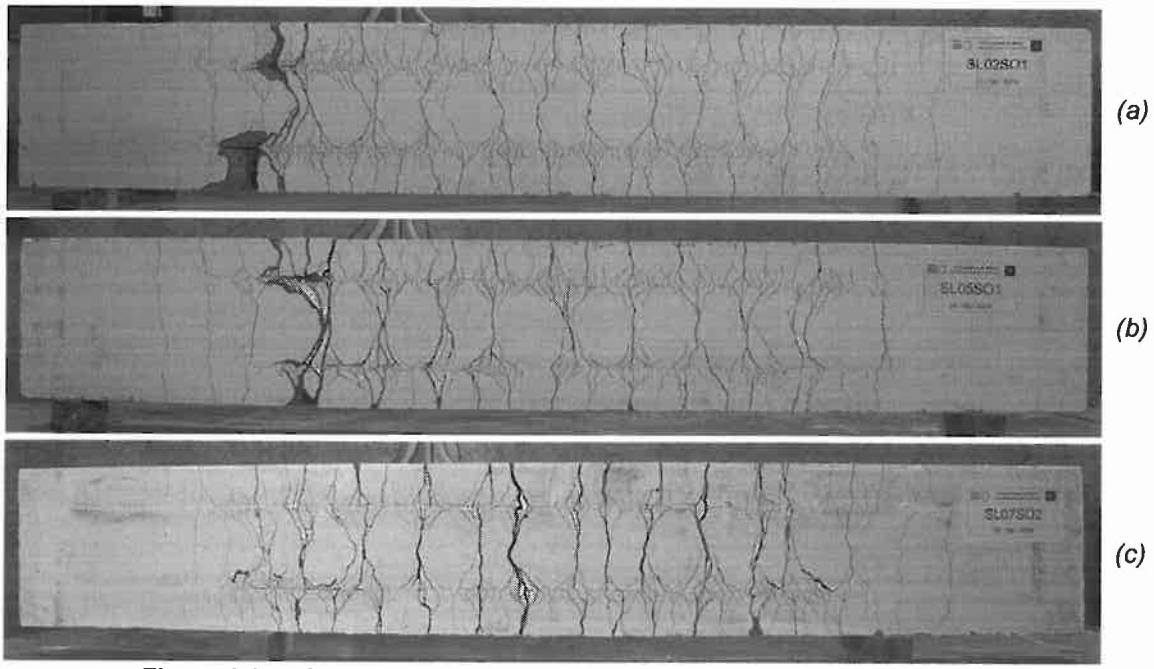

Figure 6.37 *- Crack pattern in CFRP strengthened and SFRC overlaid slabs: (a) SL02SO1, (b) SL05SO1 and (c) SL07SO2.*

7 Analyses of Results

The analysis of the results of the eight tested slabs is presented in this chapter. Their behavior regarding load-displacement response, ultimate strength and mode of failure, bond stress along the laminate strips, crack spacing and ductility of the slab specimens tested, is described.

Load-displacement Response

The load-mid span deflection curves from the tests are presented in ***Figure 7.1***. The relationship between the displacements recorded in the other LVDTs and load are included in **Annex F**. It can clearly be noticed in ***Figure 7.1*** that the experimental load-displacement curves for the strengthened specimens coincide in a typical trilinear diagram, defined by the three singular ranges: the uncracked elastic stage, the crack propagation phase with steel bars in elastic stage and the steel reinforcement post-yielding stage. Due to the reduced steel reinforcement ratio ($\rho_s = 0.24\%$), the unstrengthened slabs had an unstable crack propagation phase.

The cracking, yielding and maximum loads, and the strength increasing ratio are given in ***Table 7.1***. The strength increasing ratio, in ***Table 7.1***, was calculated using the following expressions:

- *CFRP strengthened slabs:* $\frac{F_{UL}^{CFRP} - F_{UL}^{U}}{F_{UL}^{U}}$, (7.1)

and

- *CFRP & SFRC strengthened slabs:* $\frac{F_{UL}^{CFRP\&SFRC} - F_{UL}^{U}}{F_{UL}^{U}}$ and $\frac{F_{UL}^{CFRP\&SFRC} - F_{UL}^{CFRP}}{F_{UL}^{CFRP}}$ (7.2) and (7.3)

where

F_{UL}^{CFRP} - is the average maximum load of CFRP strengthened slabs;

F_{UL}^{U} - is the average maximum load of unstrengthened slabs, and

$F_{UL}^{CFRP\&SFRC}$ - is the average maximum load of CFRP and SFRC overlay strengthened slabs.

The monitored strains at the mid-span, in the concrete top surface, steel bar and CFRP laminates are listed in ***Table 7.2***.

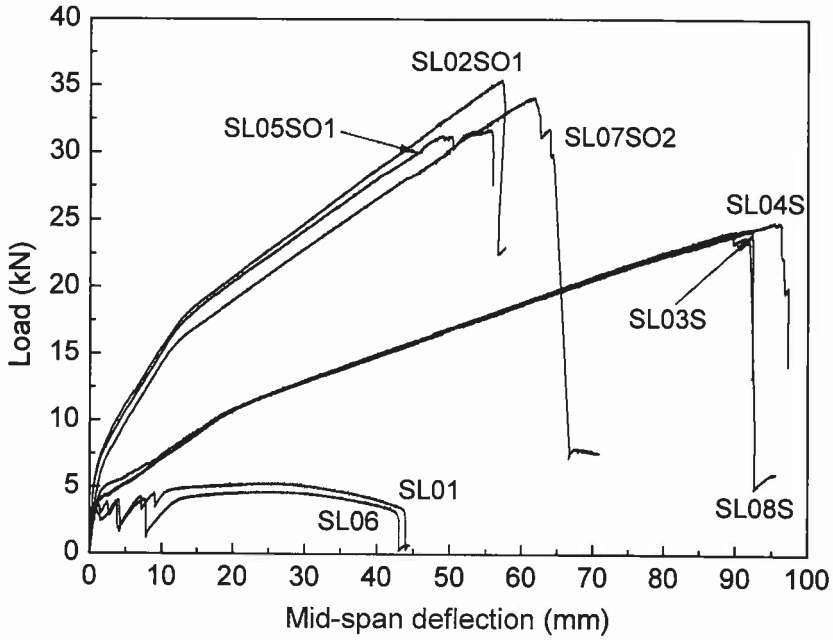

Figure 7.1 *- Load-deflection behaviour at mid-span of all slabs.*

Table 7.1 *- Summary of the results in terms of loads.*

Strengthening	Slab designation	Cracking Load[a] (kN)	Yielding Load[b] (kN)	Maximum load (kN)	Average ultimate load (kN)	Strength increasing ratio (%)
Reference	SL01	3.28	2.50	5.35	5.03 (*9.00%*)	NA
	SL06	3.28	3.78	4.71		
CFRP laminate strengthening	SL03S	3.62	9.10	24.38	24.48 (*1.59%*)	386.68
	SL04S	3.41	9.28	24.91		
	SL08S	3.72	9.34	24.15		
CFRP + SFRC overlay strengthening	SL02SO1	4.78	15.21	35.47	33.79 (*5.56%*)	571.77[c] 38.03[d]
	SL05SO1	4.00	14.25	31.76		
	SL07SO2	4.34	14.20	34.13		

(*value*) Coefficient of Variation (COV) = (Standard deviation/Average) x 100

[a] In an experimental test, the cracking load is normally reported at a load step when cracking is detected for the first time. However, the cracking load is considered here as the load at which a significant change in the slope of the total load-deflection relationship is observed

[b] The yield load is defined herein as the load which leads to an elongation on steel reinforcement corresponding to the yield point from tension test in coupons. A significant change in the slop of the total load-deflection curve is also observed in the vicinity of yield load.

[c] With respect to the reference

[d] With respect to the CFRP laminate strengthening

NA: not applicable

Table 7.2 - *Summary of the monitored strains.*

Strengthening	Slab	Concrete compression strain[a] (‰)	Steel strain[b] (‰)	CFRP laminate strain[c] (‰)
Reference	SL01	2.26[*5.35*][d]	15.30[*4.90*]	NA
	SL06	1.96[*4.71*]	12.60[*4.20*]	NA
CFRP laminate strengthening	SL03S	3.40[*24.24*]	14.71[*15.60*]	14.10[*23.13*]
	SL04S	NE	NE	NE
	SL08S	2.90[*24.00*]	14.36[*18.10*]	12.70[*18.70*]
CFRP + SFRC overlay strengthening	SL02SO1	2.66[*35.42*]	15.95[*22.35*]	12.95[*34.42*]
	SL05SO1	2.53[*31.66*]	9.64[*18.39*]	13.50[*31.50*]
	SL07SO2	NE	12.87[*16.06*]	12.58[*26.84*]

[*value*] Corresponding load in brackets
[a] Maximum value of SG8 and SG9 for unstrengthened slabs, and SG8 for strengthened slabs.
[b] Maximum value of SG1 or SG2
[c] Maximum value recorded in SG7
[d] The load in bracket is the maximum load
NA: not applicable; NE: not evaluated

Strength and Failure Mode

Figure 7.2 illustrates the internal strain and stress distribution for the CFRP strengthened sections under flexure at the ultimate limit state. If the type of failure that can occur is assumed to be failure in the composite material with steel yielding, the nominal bending capacity can then be expressed as:

$$M = A_s \cdot f_s \cdot \left(d_s - \frac{\beta_1}{2} \cdot c \right) + A_f \cdot \varepsilon_f \cdot E_f \cdot \left(h - h_f - \frac{\beta_1}{2} \cdot c \right) \tag{7.3}$$

the horizontal equilibrium equation for the section in ***Figure 7.2****(d)* gives:

$$\beta_1 \cdot \alpha \cdot f_c \cdot b \cdot c = A_s \cdot f_s + A_f \cdot \varepsilon_f \cdot E_f \tag{7.4}$$

and solving for c (the neutral axis depth):

$$c = \frac{A_s \cdot f_s + A_f \cdot \varepsilon_f \cdot E_f}{\beta_1 \cdot \alpha \cdot f_c \cdot b} \tag{7.5}$$

The assumptions aforesaid can be also used to determine the nominal flexural strength of the hybrid strengthened section, CFRP and SFRC overlay strengthening, since the depth of the equivalent rectangular stress block does not extend beyond the bond line. Tabulated following in ***Table 7.3*** are the theoretical calculations of the load capacity, experimental loads at failure, ultimate deflections and the modes of failure of the slabs tested. In the calculations were taken:

- the rectangular stress block factors:

α = is the ratio of the average concrete stress to the concrete strength (is taken equal to 0.85, according to ACI 318-02), and

β_1 = is the ratio of the depth of the equivalent rectangular stress block to the depth of the neutral axis (According to ACI 318-02, factor β_1 is 0.85 for concrete strength, f_c, up to and including 27.6 N/mm^2. For strengths above 27.6 N/mm^2, β_1 is reduced continuously at a rate of 0.05 for each 6.9 N/mm2 of strength in excess of 27.6 N/mm^2, but β_1 shall not be taken less than 0.65. Therefore herein β_1 is taken equal to 0.72).

- material properties:

f_c = value corresponding to each slab (refer to ***Table 3.1***);

f_s = 550 N/mm^2 (refer to ***Table 3.10***);

ε_f = 18.45‰ (refer to ***Table 3.9***), and

E_f = 156.10 kN/mm^2 (refer to ***Table 3.9***).

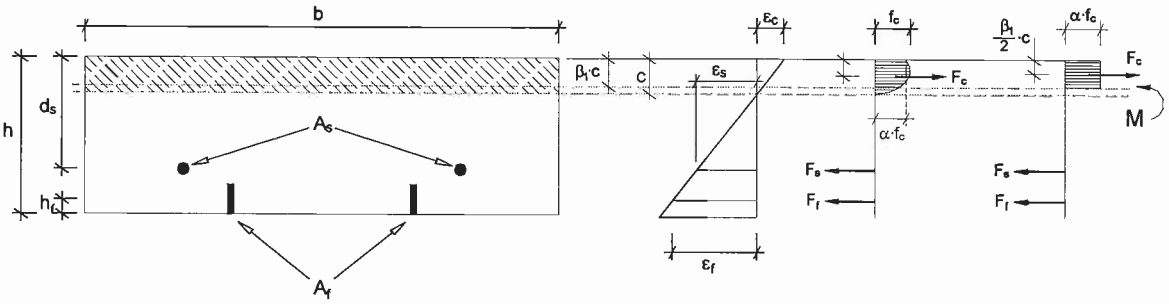

(a) cross section *(b) stress diagram* *(c) stress diagram* *(d) forces*

Figure 7.2 *- Internal strain and stress distribution for the strengthened section under flexure at ultimate stage.*

Table 7.3 *- Theoretical calculations compared with loads at failure, ultimate deflection and mode of failure.*

Strengthening	Slab	Calculated load (kN)	Maximum load (kN)	Maximum/ calculated	Ultimate deflection[a] (mm)	Type of failure
Reference	SL01	5.87	5.35	0.91	43.91	Flexure
	SL06	5.89	4.71	0.80	42.75	Flexure
CFRP laminate strengthening	SL03S	22.66	24.38	1.08	91.79	Flexo-shear[b]
	SL04S	22.09	24.91	1.13	95.39	Flexure
	SL08S	22.88	24.15	1.06	89.50	Flexure
CFRP + SFRC overlay strengthening	SL02SO1	33.71	35.47	1.05	57.18	Flexo-shear
	SL05SO1	33.19	31.76	0.96	55.20	Flexo-shear
	SL07SO2	33.71	34.13	1.01	61.70	Flexure

[a] Deflection registered at ultimate load in strengthened slabs

[b] Flexo-shear failure mode is considered here as steel yielding and shear failure was observed after significant deflections

Bond Stress Between CFRP Laminate Strips and Concrete

Using the strains recorded in the strain gauges installed to the laminate strips, the average CFRP-concrete bond stresses developed along the CFRP laminate strips can be evaluated. Therefore, the average bond stress (τ_{bm}^{RL}) in the CFRP laminate strips, in-between the strain gauges position, SG^L (left) and SG^R (right), was determined according to the following equations (refer to ***Figure 7.3***):

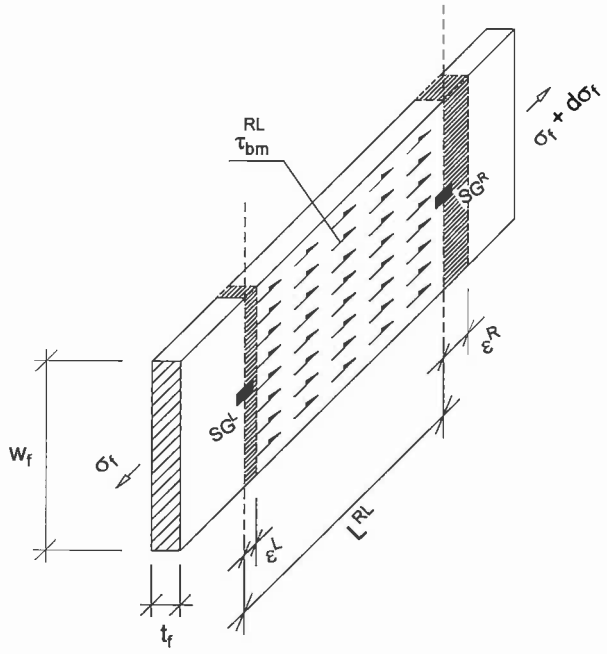

Figure 7.3 *- Average bond stress (τ_{bm}^{RL}) in-between two consecutive strain gauges installed to the CFRP laminate.*

$$\tau_{bm}^{RL} = \frac{\Delta F^{RL}}{A_b^{RL}} \tag{7.6}$$

where

ΔF^{RL} is the difference in axial force in the laminate, between the two strain gauges ($= E_{CFRP} \cdot \Delta\varepsilon^{RL} \cdot A_{CFRP}$)

A_b^{RL} is the laminate-adhesive involving area, in-between strain gauges position ($= p \cdot L^{RL}$)

E_{CFRP} is the Young's modulus

$\Delta\varepsilon^{RL}$ is the difference in axial strain between the strain gauges positioned at right and left sections ($= \left|\varepsilon_{SG}^R - \varepsilon_{SG}^L\right|$)

A_{CFRP} is the laminate cross sectional area

p is the perimeter of the contact surface between CFRP laminate and epoxy adhesive (considered here equals to $2 \cdot (W_f)$

L^{RL} is the distance between two consecutive strain gauges

ε_{SG}^R is the axial strain registered experimentally in the *right* strain gauge

ε_{SG}^L is the axial strain registered experimentally in the *left* strain gauge

hence (7.6) takes the form:

$$\tau_{bm}^{RL} = \frac{E_{CFRP} \cdot A_{CFRP} \cdot \Delta\varepsilon^{RL}}{2 \cdot W_f \cdot L^{RL}} \ (N/mm^2) \qquad (7.7)$$

In this treatment, it is assumed an average bond stress in-between the strain gauges SG^L and SG^R. This situation is illustrated in ***Figure 7.3***. The variation of the τ_{bm}^{RL} during the applied load is shown in ***Figures 7.4*** and ***7.5***, for the slab specimens strengthened with NSM technique.

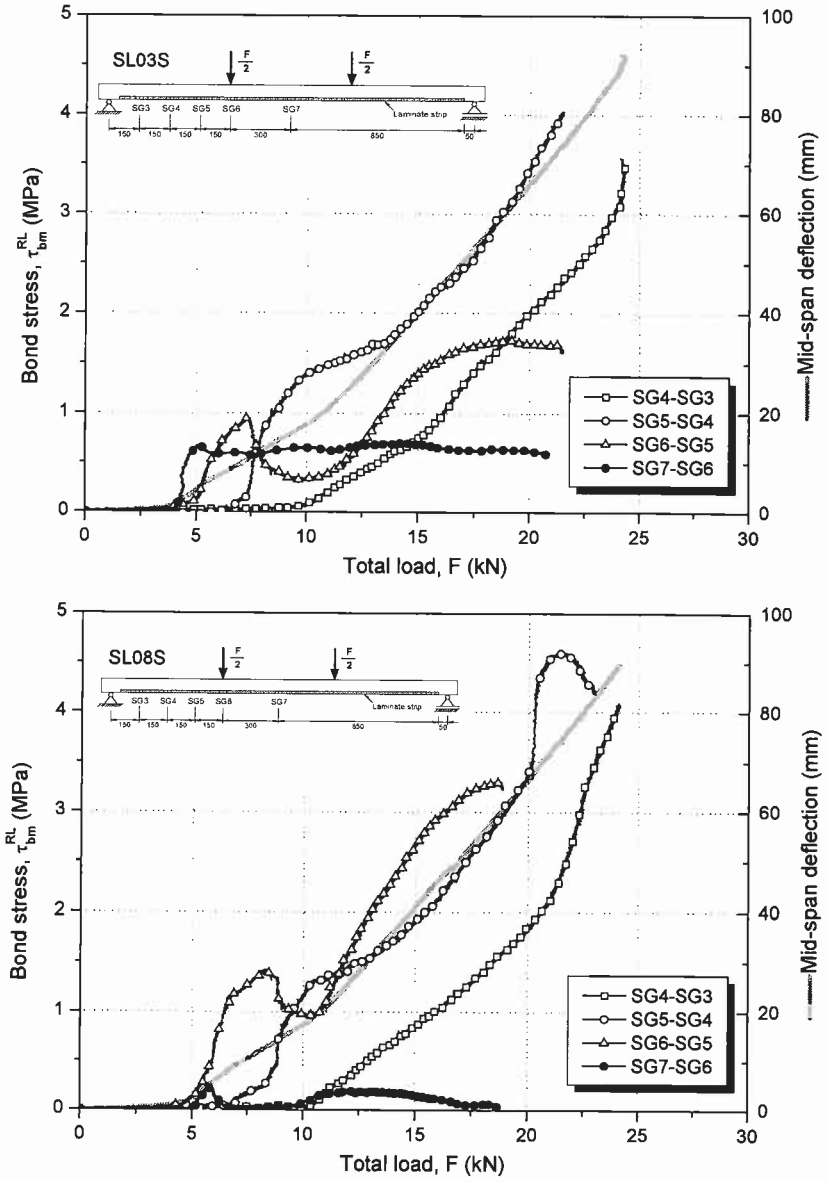

Figure 7.4 *- Bond stress variation for the slab strips (a) SL03S and (b) SL08S[§].*

[§] **It was not possible to record the data of the strain gauge instrumentation for the slab strip SL04S**

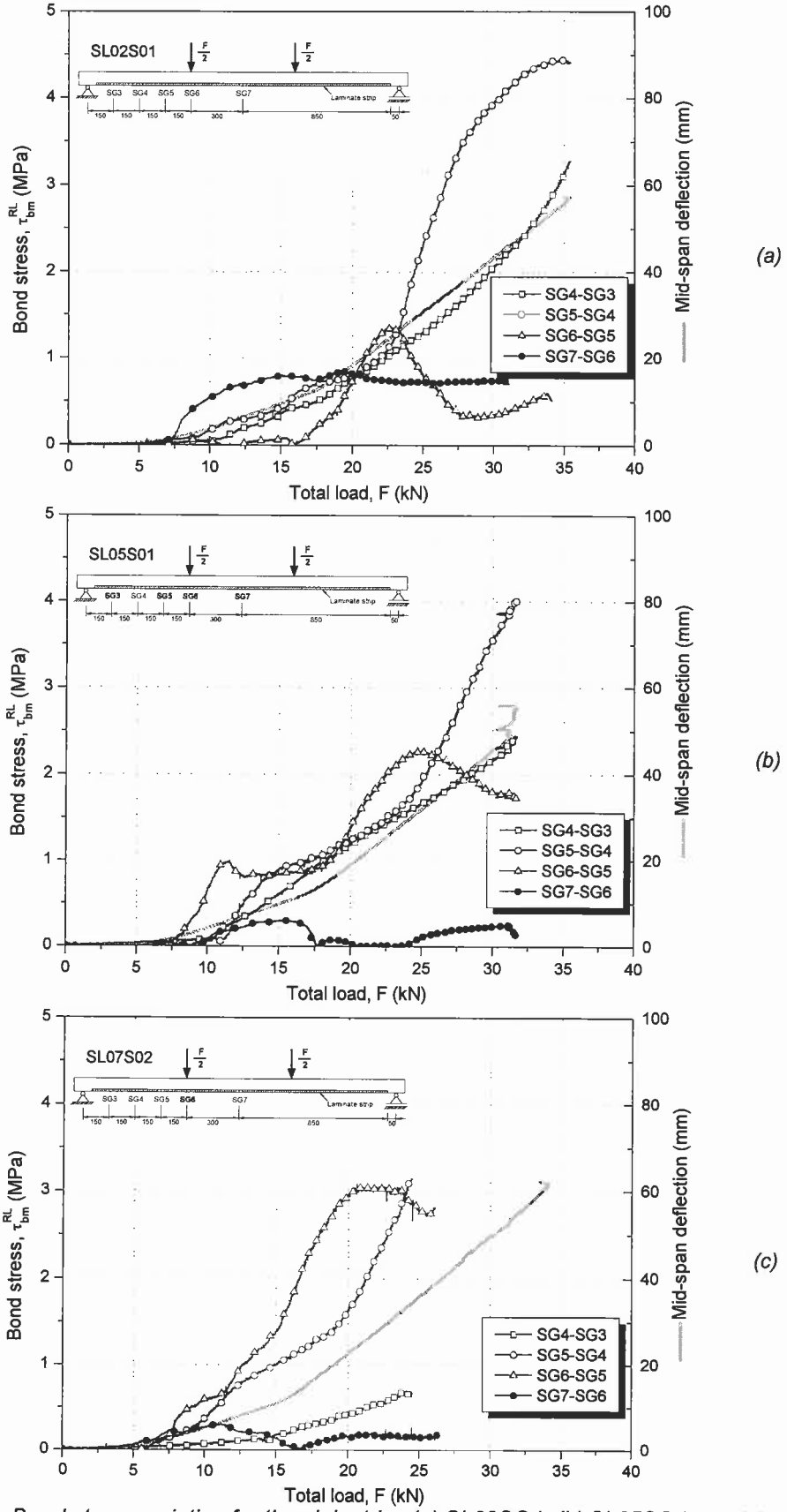

Figure 7.5 *- Bond stress variation for the slab strips (a) SL02SO1, (b) SL05SO1 and (c) SL07S02.*

It can be noticed in ***Figures 7.4*** and ***7.5*** that for loads from start up to cracking of the concrete, as the CFRP laminate strips have not been mobilized in this phase no bond stress variation is observed. In general, a very low bond stress profile is developed at the interfaces CFRP laminate-epoxy adhesive-concrete at the serviceability limit, since the average bond stress computed at the service load, corresponding to a deflection of 7.2 mm at mid-span, was below 1.0 MPa.

Despite the fact that in some strengthened slabs it was not possible to evaluate the average bond stress variation up to the ultimate load, it can be noticed, however, that the bond stress variation was below 5.0 MPa.

An extensive experimental program was conducted to investigate the bond for the near-surface mounted CFRP laminate strips (SENA-CRUZ & BARROS, 2004a and 2004b). From the pullout-bending tests a bond stress $\tau_{bm} \geq 12$ MPa was registered. The maximum average bond stress (less than 5.0 MPa) observed in the slabs herein tested is, therefore, rather lower than the bond stress limit value (12 MPa). A more extensive experimental and numerical description of bond between NSM CFRP laminate strips and concrete is given by SENA-CRUZ (2004).

In general the average bond stress was great between SG4 and SG5. For the slabs with flexo-shear failure mode, the average bond stress between SG3-SG4 and SG4-SG5 showed a tendency of increasing by increasing the load, and a tendency of decreasing between SG5-SG6 after about 18 kN for the slab SL03S and after about 23 kN for the slabs SL02S01 and SL05S. Such tendencies may be explained among others by (1) the anchorage of the CFRP laminate strips is situated in the region between SG5 and the extremity of the laminate, and (2) the wide opening of flexural cracks in the region between the SG5-SG6 which relieves the bond stress in this region.

Crack Spacing Analysis

The distinct crack feature between control slabs and slabs strengthened shown in ***Figures 6.9***, ***6.22*** and ***6.37*** clearly indicates the significant improvement in the crack behavior of the slabs strengthened with NSM technique.

The expressions from the Portuguese design code of reinforced and pre-stressing concrete structures, CEB Model Code and EUROCODE 2 were considered herein to calculate the theoretical mean spacing between cracks for the tested strip slabs. The average crack spacing, experimentally measured after the slabs have been tested, was computed as is schematically described in ***Figure 7.6***.

In the following, the analytical procedures are described and the obtained results are compared in ***Table 7.4***, to the crack spacing measured experimentally.

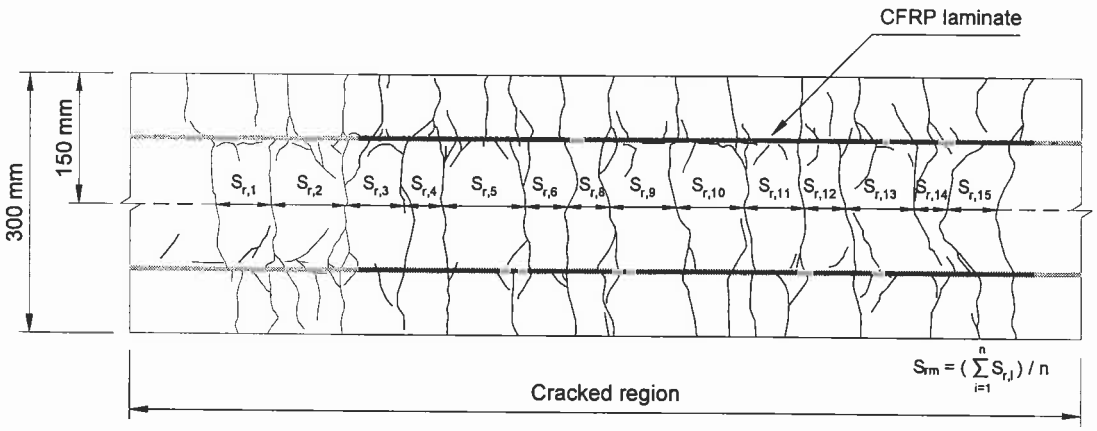

Figure 7.6 *- Determination of the average crack spacing (S_{rm}) in the tested slab strips.*

Portuguese Design Code for Reinforced and Prestressing Concrete Structures (REBAP, 1983)

According to the Portuguese design code of reinforced and pre-stressing concrete structures, the following formula can be used to estimate the average crack spacing of the stabilized crack propagation phase, for RC members.

$$s_{rm} = 2 \cdot \left(c + \frac{s}{10} \right) + \eta_1 \cdot \eta_2 \cdot \frac{\phi}{\rho_r} \tag{7.8}$$

where

c is the concrete cover to the longitudinal reinforcement

s is the rebar spacing, and $s \leq 15 \cdot \phi$

η_1 is the bond condition parameter, and $\eta_1 = \begin{cases} 0.4 & \text{high bond rebars} \\ 0.8 & \text{normal bond rebars} \end{cases}$

η_2 is the coefficient that depends on the cross section strain distribution $\left(= 0.25 \cdot \frac{\varepsilon_1 + \varepsilon_2}{2 \cdot \varepsilon_1}\right)$

ε_1 and ε_2 are the strain in the bottom and top level of the concrete surrounding the tension reinforcement, respectively (see ***Figure 7.7***).

ϕ is the steel bar diameter

ρ_r is the effective reinforcement ratio $(= A_s / A_{c,r})$

$A_{c,r}$ is the effective area of concrete in tension, the area of concrete surrounding the tension reinforcement (see ***Figure 7.7(a)***)

For the CFRP laminate strengthening members each CFRP laminate is transformed in a steel equivalent bar of cross-section, A_s^{eq}, and diameter ϕ_s^{eq} applying the following expressions:

$$A_s^{eq} = \frac{E_{CFRP}}{E_s} \cdot A_{CFRP} \tag{7.9}$$

$$\phi_s^{eq} = 2 \cdot \sqrt{\frac{A_s^{eq}}{\pi}} \tag{7.10}$$

where

A_{CFRP} is the cross-sectional area of the CFRP laminate
E_{CFRP} is the modulus of elasticity the CFRP laminate, and
E_S is the modulus of elasticity the steel reinforcement

The aforementioned parameters, therefore, can be adjusted for strengthened members:

$$s_{rm} = 2 \cdot \left(c_m + \frac{s_m}{10} \right) + \eta_1 \cdot \eta_2 \cdot \frac{\phi_m}{\rho_r} \tag{7.11}$$

c_m is the mean concrete cover (average of steel and steel equivalent bars, $= \frac{c_s + c_s^{eq}}{2}$)

s_m is the mean rebar spacing ($= \frac{s_s + s_s^{eq}}{2}$ and $s_s \le 15 \cdot \phi_s$, $s_s^{eq} \le 15 \cdot \phi_s^{eq}$)

ϕ_m is the mean bar diameter (average of steel and steel equivalent bars, $= \frac{\phi_s \cdot A_s + \phi_s^{eq} \cdot A_s^{eq}}{A_s + A_s^{eq}}$)

η_1 is the bond condition parameter, considered equal to 0.8

η_2 is the coefficient that depends on the cross section strain distribution ($= 0.25 \cdot \frac{\varepsilon_1 + \varepsilon_2}{2 \cdot \varepsilon_1}$)

ρ_r is the effective reinforcement ratio ($= \frac{A_s + A_s^{eq}}{A_{c,r}}$)

$A_{c,r}$ is the area of concrete surrounding the tension reinforcement, steel and steel equivalent bars (see ***Figure 7.7****(b)*)

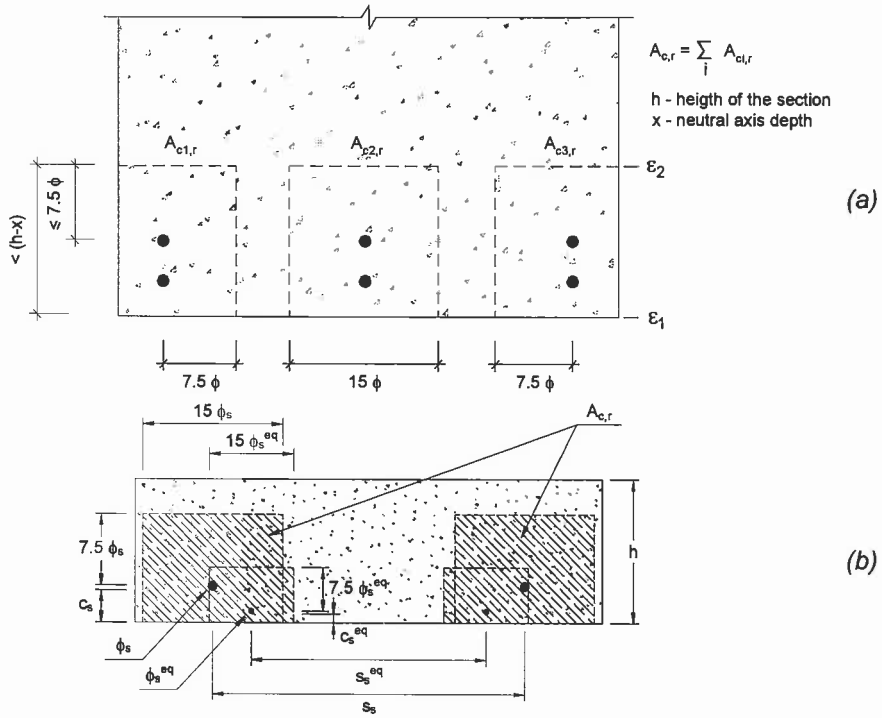

Figure 7.7 *- Effective surrounding concrete tension area: (a) REBAP (1983) and (b) adapted from REBAP for the strengthened slabs.*

CEB Model Code (1993)

Following the CEB Model Code (1993) suggestion, the average crack spacing, for stabilized cracking, may be estimated using the length over which slip between steel and concrete occurs according to (7.12).

$$s_{rm} \approx \frac{2}{3} \cdot \ell_{s,max} \tag{7.12}$$

where

$$\ell_{s,max} = \frac{\phi_s}{3.6 \cdot \rho_{s,ef}} \text{ for stabilized cracking}$$

$\ell_{s,max}$ is the length of slipping between steel and concrete

ϕ_s is the steel bar diameter

$\rho_{s,ef}$ is the effective reinforcement ratio ($= A_s / A_{c,ef}$)

$A_{c,ef}$ is the effective area of concrete in tension, the area of concrete surrounding the tension reinforcement (see ***Figure 7.8****(a)*, for slabs). Since the rebars are quite apart, the effective area was computed according to ***Figure 7.8*** *(b)*.

For the slabs strengthened with CFRP material, each laminate was converted in a equivalent steel bar (of area A_s^{eq} and diameter ϕ_s^{eq}) as described in previous sections.

The parameters, therefore, can be adjusted for strengthened members:

$$\ell_{s,max} = \frac{\phi_m}{3.6 \cdot \rho_{s,ef}} \tag{7.13}$$

where

ϕ_m is the mean bar diameter (average of steel and steel equivalent bars, $= \frac{\phi_s \cdot A_s + \phi_s^{eq} \cdot A_s^{eq}}{A_s + A_s^{eq}}$)

$\rho_{s,ef}$ is the effective reinforcement ratio ($= \frac{A_s + A_s^{eq}}{A_{c,r}}$)

$A_{c,r}$ is the area of concrete surrounding the tension reinforcement, steel and steel equivalent bars (see ***Figure 7.8*** *(c)*), and was computed using the mean concrete cover and mean bar diameter.

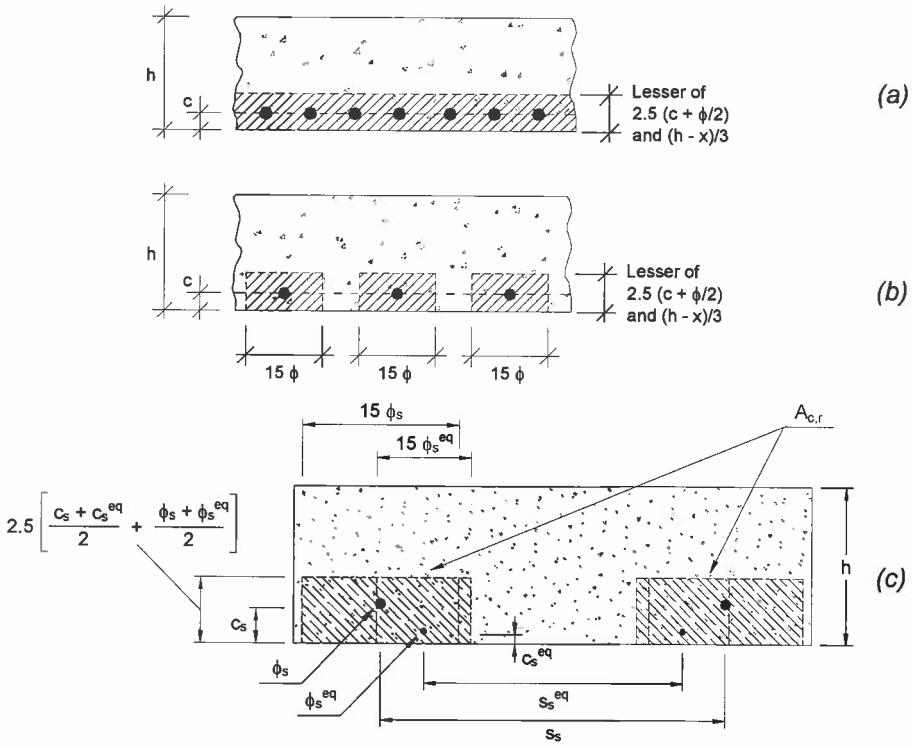

Figure 7.8 *- Effective concrete tension area in slabs: (a) CEB Model Code (1993), (b) adapted from CEB model Code for the unstrengthened slabs and (c) adapted from CEB model Code for the strengthened slabs.*

EUROCODE (2004)

For calculating flexural crack spacing in members subjected to flexure where the spacing of the reinforcing bars exceeds $5 \cdot \left(c + \phi/2 \right)$ (which is the case of the present study), EUROCODE 2 (2004) recommends the following formula to evaluate the average crack spacing in the stabilized crack phase.

$$s_{rm} = 1.3 \cdot (h - c) \tag{7.14}$$

where

h is the total height of the member
c is the neutral axis depth

Table 7.4 *- Experimental and analytical crack spacing.*

Strenthening	**Slab**	**Average crack spacing** (mm)							
		Experimental[a]		**REBAP**[b] **(1983)**		**CEB (1990)**	**EUROCODE 2**		
Reference	SL01	167	*(196)*	185	*(188)*	203	89	*(90)*	
	SL06	225		191			91		
CFRP laminate strengthening	SL03S	79		84			88		
	SL04S	63	*(73)*	83	*(84)*	95	86	*(87)*	
	SL08S	76		84			88		
CFRP + SFRC overlay strengthening	SL02SO1	87		96			120		
	SL05SO1	99	*(90)*	95	*(96)*	95	116	*(120)*	
	SL07SO2	83		97			124		

a Measures take in the mid-base on the bottom surface of the slab strip (see *Figure 7.6*)
b The cross section strain distribution was derived from the strain gauges data, for a elongation close to the first yield of the conventional reinforcement
b The neutral axis depth was derived from the strain gauges data, for a elongation close to the first yield of the conventional reinforcement
Where the strain gauge data was not recorded, a cross section analysis was carried out
(value) average value when is the case

Compared to the expressions of CEB and EUROCODE 2, the Portuguese Design Code formula lead to better results of predicted crack spacing for the unstrengthened and NSM strengthened slabs.

Ductility Analysis

Safety is the most important consideration for the design of new and strengthened structures. When minimum requirements of ductility and energy dissipation capacity are guaranteed, the structure, if overload, will exhibit stress redistribution and notable deformation, providing a set of visible warning prior to collapse, i.e. an unexpected sudden failure of the structure is prevented (DUTHINH & STARNES, 2001; KELLEY, BRAINERD & VATOVEC, 2000).

Otherwise, in strengthening of RC structures with EBR it is notable that the increase in strength and stiffness is sometimes attained at the expense of a loss in ductility, or capacity of the structures to deflect inelastically while sustaining load at the ultimate state (DUTHINH & STARNES, 2001). Since ductility is an important property for safe design of strengthening of any structural element and moreover, NSM strengthening with CFRP is a fairly new innovation, understanding the effect of this strengthening technique on the ductility of a RC member is critical. A method, based on the ductility index commonly used, is considered in this section to analyse the ductility of the composite slab specimens.

Ductility of RC members has generally been measured by a ratio called bending ductility index or factor (μ). The ductility index is usually expressed as a ratio of the rotation (θ), curvature (χ), or deflection (Δ) at the ultimate load[§] (subscript U) to the corresponding property at the yield load (superscript Y), as follows:

$$\mu_\theta = \frac{\theta_U}{\theta_Y} \qquad \mu_\chi = \frac{\chi_U}{\chi_Y} \qquad \mu_\Delta = \frac{\Delta_U}{\Delta_Y} \tag{7.15}$$

Another common way of measuring ductility consists in compute the ratio of reinforcing steel strain at failure of the element to the yield strain of the steel (KELLEY, BRAINERD & VATOVEC, 2000).

For this study, deflection was used to measure the ductility of the slab specimens tested. ***Table 7.5*** lists the ductility ratio for each of the specimens and the average ductility ratio for the unstrengthened and strengthened situations. Values for the NSM strengthened slabs were in the range from 5.82 to 6.33 and compared to 3.00 and 4.42 for the companion control slabs.

By examining the ***Table 7.5***, it can be noticed an increase of about 60% in the averaged ductile ratio of the strengthened slabs comparatively to the reference slabs. Furthermore, no significant changing in the ductility index of the slabs strengthened using NSM and SFRC overlay with respect to the NSM strengthened slabs was observed. The marginal increase verified in the ductility index can be referred to the high toughness of the SFRC overlay in the slabs strengthened with the hybrid system

[§] **The ultimate load is considered here as the maximum load reached in the test**

relatively to the NSM strengthened slabs. However, the deformability of these slabs was directly limited by the shear failure.

To understand in depth the ductility behaviour of RC flexural members strengthened with composite materials, it is important to examine and perceive the behaviour at failure prior and after strengthening. This requires over than traditional evaluation of the limits associated with the rupture of the steel or composite, or the crushing of the concrete. In other words, issues as failure mechanism of the composite-concrete substrate bond system and the ratio of strengthening area to the existing steel reinforcement area are crucial (KELLEY, BRAINERD & VATOVEC, 2000).

Table 7.5 *- Ductility ratios of the slab specimens tested.*

Strengthening	Slab	Δ_Y (mm)	Δ_U (mm)	Ductile ratio, μ_Δ (mm/mm)	Average μ_Δ (mm/mm)
Reference	SL01	5.64	24.95	4.42	3.71
	SL06	8.71	26.10	3.00	*(27.20%)*
CFRP laminate strengthening	SL03S	15.30	91.79	6.00	5.99 *(2.76%)*
	SL04S	15.50	95.39	6.15	
	SL08S	15.39	89.50	5.82	
CFRP + SFRC overlay strengthening	SL02SO1	9.61	57.18	5.95	6.14 *(3.10%)*
	SL05SO1	9.00	55.20	6.13	
	SL07SO2	9.74	61.70	6.33	

(*value*) Coefficient of Variation (COV) = (Standard deviation/Average) x 100

Accordingly, the bond mechanism of the composite reinforcement for high strengthening ratios, in flexural strengthening of RC members, not only limits the load carrying capacity, but also can results in non-safety strengthened members when EBR systems are used. Therefore, the enhanced bond condition provides a much more ductile behaviour for the NSM strengthening technique comparatively to the EBR strengthening technique and, as illustrated before in ***Figure 1.4*** (Section "Brief Background"), the bond ductility when the composite material is applied into silts is comparable to the bond ductility of embedded steel rebars.

8 Summary and Conclusions

An experimental program was conducted in order to: (a) investigate the NSM strengthening technique for reinforced concrete slabs, and (b) evaluate structural performance of the hybrid strengthening technique, CFRP laminates and SFRC overlay for concrete slabs. For this purpose a total of eight slabs were tested.

The conclusions from this experimental study are the following:

- The test program carried out demonstrated that the hybrid strengthening technique has great potential application towards flexural strengthening of RC slabs,

- A percentage of 0.12% of CFRP laminates (CFRP reinforcement to the conventional steel reinforcement ratio close to 50%) has increased in about 54% the service load of the 1.8 m RC slabs with a steel reinforcement ratio of 0.24%. However, the slabs strengthened with NSM technique and SFRC showed an increase of approximately 212% in the service load with respect to the reference slabs. Comparatively to the NSM technique, the hybrid strengthening strategy has lead to an increase of about 103% in load at the service load level;

- The hybrid strengthening system has also lead to an increase of about 570% in the RC slab maximum load carrying capacity with respect to the reference slabs and an increase of about 40% in comparison with the slabs strengthened only with NSM technique. When compared with the reference case, close to 390% of increase in the load carrying capacity was attained by the strengthening with NSM technique;

- The cracking spacing calculations and crack features observations, at the bottom of the slabs, indicate that a significant improvement in the crack behavior of RC slabs can be achieved with the NSM technique. In the results obtained, the average crack spacing of the lightly RC slabs strengthened with NSM technique measured after failure were about 63% lower than that measured in reference slabs, almost the same reduction (about 54%) in the average crack spacing was observed in the hybrid strengthened slabs;

- For the stabilized cracking phase and taking into account appropriate considerations for the NSM strengthening system, the average crack spacing of the strengthened slabs may be achieved with acceptable accuracy using the analytical expression suggested by the Portuguese Design Code;

- When compared with the bond stress limit, which was recorded in pullout-bending tests, a very low bond stress profile was observed through the interfaces CFRP laminate-epoxy adhesive-concrete along the laminate strips in slabs where NSM strengthening was applied;

- In general, for all slabs strengthened with NSM system, the average ductility indexes, based on deflections measurements, were about 60% higher when compared to the reference slabs;

- The NSM strengthening system has also provided a significant increase in the stiffness and deformability consistent with the high stress redistribution (closely spaced crack pattern) owing to the prominent composite action between the CFRP reinforcement and concrete. Otherwise, since the hybrid strengthening system has lead to substantial increase in flexural load, the shear capacity of the composite slabs has limited their deformability; however, the stiffness of the slabs has increased strongly and the ductility level maintained, and

- The SFRC overlay bonding procedures can be considered adjusted, once no slip was observed, the connection between SFRC overlay and the RC slab was able to transfer horizontal shear stress, forming consequently a monolithic flexural cross-section.

Acknowledgements

The authors acknowledge the financial support of the Portuguese Science and Technology Foundation (FCT), PhD grant number *SFRH / BD / 11232 / 2002*.

Thanks also for the companies "Companhia Geral de Cal e Cimento S.A. (SECIL)", Sika S.A., "Central do Pego", "Pedreiras Bezerras", Bekaert NV, "Degussa Construction Chemicals Portugal S.A.", S&P® Reinforcement, which generously have supplied cement; overlay bond product; fly ash; aggregates; steel fibres; superplasticizer and CFRP adhesive; and CFRP laminate, respectively.

References

ACI 318 Building Code Requirements for Structure Concrete and Commentary, Reported by committee 318, American Concrete Institute, 445 pp., 2002.

ACI 503R. Use of epoxy compounds with concrete, ACI Manual of Concrete Practice, Part 5, Reported by Committee 503, American Concrete Institute, 28 pp., 1993 (Reapproved 1998).

ACI 503.2. Standard specification for bonding plastic concrete to hardened concrete with a multi-component epoxy adhesive, ACI Manual of Concrete Practice, Part 5, Reported by Committee 503, American Concrete Institute, 5 pp., 1992 (Reapproved 1997).

ACI 503.5R. Guide for the selection of polymer adhesives with concrete, ACI Manual of Concrete Practice, Part 5, Reported by Committee 503, American Concrete Institute, 4 pp., 1997.

ACI 503.6R. Guide for the application of epoxy and latex adhesives for bonding freshly mixed and hardened concretes, ACI Manual of Concrete Practice, Part 5, Reported by Committee 503, American Concrete Institute, 16 pp., 1992 (Reapproved 1997).

ALKHRDAJI, T., NANNI, A. Surface bonded FRP reinforcement for strengthening/repair of structural reinforced concrete. In ICRI-NR Workshop. Baltimore, MD, October 30, 1999.

ASTM C 143. Standard test method for slump of hydraulic cement concrete, American Society for Testing and Materials, Annual Book of ASTM Standards, Vol. 4.02, West Conshohocken, PA 1998.

ASTM D 3039/D 3039 M. Standard test method for tensile properties of polymer matrix composite materials, American Society for Testing and Materials, Annual Book of ASTM Standards, Vol. 15.03, pp. 118-127, West Conshohocken, PA 1993.

ASTM A370. Standard test methods and definitions for mechanical testing of steel products. American Society for Testing and Materials, 2002.

BALAGURU, P. N., SHAH, S. P. Fiber reinforced cement composites. McGraw-Hill International Editions, Civil Engineering Series, 530 pp., 1992.

BARROS, J. A. O. Comportamento do betão reforçado com fibras - análise experimental e simulação numérica (Behavior of fiber reinforced concrete - experimental analysis and numerical simulation). PhD Thesis, Civil Eng. Dept., Faculty of Engineering, University of Porto, Portugal, 1995. (in Portuguese)

BARROS, J. A. O., FIGUEIRAS, J. A. Experimental behaviour of fibre concrete slabs on soil. Mechanics of Cohesive-frictional Materials, Vol. 3, No. 03, pp. 277-290, July 1998.

BARROS, J. A. O., SENA-CRUZ, J. M. Strengthening a prestressed concrete slab by epoxy - bonded FRP composites and SFRC overlayer, 7th Internacional Conference on Inspection Appraisal Repairs & Maintenance of Buildings & Structures, Nottingham Trent University, UK, 11-13 September, 2001.

BARROS, J. A. O., DIAS, S. J. E. Shear strengthening of reinforced concrete beams with laminate strips of CFRP, International Conference Composites in Constructions - CCC2003, Cosenza, Italy, pp. 289-294, 16-19 September, 2003.

BARROS, J. A. O., CUNHA, V. M. C. F., RIBEIRO, A. F., ANTUNES, J. A. B. Post-cracking behaviour of steel fibre reinforced Concrete, Materials and Structures, Vol. 38, No. 275, pp. 47-56, January 2004.

BARROS, J. A. O., FORTES, A. S. Flexural strengthening of concrete beams with CFRP laminates bonded into slits, Cement and Concrete Composites, Vol. 27, No. 4, pp. 471-480, April 2005.

BONALDO, E., BARROS, J. O., LOURENÇO, P. B. Bond characterization between concrete base and repairing SFRC by pull-off tests, Report 04-DEC/E-13, May 2004.

BETTOR MBT. MBrace Laminate, Technical sheet, Rio de Mouro, Portugal, 2 pp. 2003.

BETTOR MBT - Degussa Construction Chemical Portugal, S.A., http://www.bettormbt.pt/MBTPortugal/Home/default.htm, Portugal, 2004. (available on September 24, 2004)

BETTOR MBT. MBrace Resin 220, Technical sheet, http://www.degussa-cc.es, Spain, 3 pp., 2005. (available on January 25, 2005)

BLASCHKO, M., ZILCH, K. Rehabilitation of concrete structures with CFRP strips glued into slits, In Proceeding of the 12th International Conference on Composites Materials. Paris, 5-9 July, 1999.

CEB-FIP Model Code. Design code. Comité Euro-International du Béton, Bulletin d'Information No. 213/214, Lausanne, Switzerland, 1993.

CAROLIN, A. Strengthening of concrete structures with CFRP - Shear strengthening and full-scale applications. Licentiate Thesis, Division of Structural Engineering, Luleå University of Technology, Luleå, Sweden, pp. 120, June 2001. ISBN: 91-89580-01-X, ISSN: 1402-1757.

CAROLIN, A. Carbon fibre reinforced polymers for strengthening of structural elements. Doctoral Thesis, Division of Structural Engineering, Luleå University of Technology, Luleå, Sweden, pp. 190, June 2003. ISBN: 91-89580-04-4, ISSN: 1402-1544.

COMYN, J. Adhesion Science, The Royal Society of Chemistry, Cambridge, UK, 149 pp., 1997.

COUTINHO, A. S. Manufacturing and properties of concrete, National Civil Engineering Laboratory, 3 volumes, Lisbon, Portugal, 1988. (in Portuguese)

DE LORENZIS, L., NANNI, A. Shear strengthening of reinforced concrete beams with near-surface mounted reinforced polymer rods. ACI Structural Journal, Vol. 98, No. 01, January-February 2001a.

DE LORENZIS, L., NANNI, A. Characterization of FRP rods as near-surface mounted reinforcement. Journal of Composites for Construction, Vol. 05, No. 02, May 2001b.

DORELL, J., NORDBERG, E. Begränsning av krypsprickor vid pågjutningar med fiberbetong. Master of Science Thesis, Division of Structural Engineering, Luleå University of Technology, Luleå, Sweden, December 1993.

DRAMIX: product data sheet, N. V. Bekaert S.A., 1998.

DUTHINH, D., STARNES, M. Strength and ductility of concrete beams reinforced with carbon FRP and steel, National Institute of Standards and Technology Technology Administration (NIST), U.S. Department of Commerce, NISTIR 6830, 33 pp., November 2001.

EN 10 002-1. Metallic materials - Tensile testing. Part 1: Method of test (at ambient temperature). European Standard, CEN, Bruxelas, 35 pp., November 1990.

ENV 1992-1-1, Eurocode 2: Design of concrete structures - Part 1-1: General rules and rules for buildings, CEN, Bruxelas, 225 pp., 2004.

FIB. Externally bonded FRP reinforcement for RC structures - Technical report on the "Design and use of externally bonded fibre reinforced polymer reinforcement (FRP EBR) for reinforced concrete structures", by 'EBR' working party of fib TG 9.3, 138 pp., July 2001, ISBN 2-88394-054-1.

FISCHER, G., LI, V. C. Deformation behavior of fiber-reinforced polymer reinforced engineered cementitious composite (ECC) flexural members under reversed cyclic loading conditions. ACI Structural Journal, Vol. 100, No. 01, pp. 25-35, January-February 2003.

GRZYBOWSKI, M. Determination of crack arresting properties of fiber reinforced cementitious composites, Publication TRITA-BRO-8908, ISSN 1100-648X, Royal Institute of Technology, Stockholm, Sweden, 190 pp., June 1989.

GRZYBOWSKI, M., and SHAH, S. P. Shrinkage cracking of fiber reinforced concrete, ACI Material Journal, Vol. 87, No. 02, pp. 138-148, March-April 1990.

HILTI - Hilti Corporation, www.hilti.com, 2004. (available on December 28, 2004)

ISO 527-1. Plastics - Determination of tensile properties - Part 1: General principles, International Organization for Standardization, Genèva, Switzerland, 9 pp., 1993.

ISO 527-2. Plastics - Determination of tensile properties - Part 2: Test conditions for moulding and extrusion plastics, International Organization for Standardization, Genèva, Switzerland 5 pp., 1993.

ISO 527-5. Plastics - Determination of tensile properties - Part 1: Test conditions for unidirectional fibre-reinforced plastic composites, International Organization for Standardization, Genèva, Switzerland, 9 pp., 1993.

KELLEY, P. L., BRAINERD, M. L., VATOVEC, M. Design philosophy for structural strengthening with FRP, Concrete International, Vol. 22, No. 2, pp. 77-82, February 2000.

KOTYNIA, R. Strengthening of reinforced concrete structures with near surface mounted FRP reinforcement, 5th International Conference - Analytical models and new concepts in concrete and masonry structures AMCM 2005, 8 pp., Gliwice - Ustroń, 12-14 June, 2005.

MAYS, G. C., HUTCHINSON, A. R. Adhesives in Civil Engineering, Cambridge University Press, New York, USA, 333 pp., 1992.

REBAP. Regulamento de estruturas de betão armado e pré-esforçado (Portuguese design code for reinforced and prestressing concrete structures), 191 pp., Porto Press, 1983. (in Portuguese)

RILEM. FMC1 - Determination of the fracture energy of mortar and concrete by means of three-point bend tests on notched beams, Materials and Structures, Vol. 18, No. 106, pp. 285-290, July-August 1985.

RILEM. Technical Committee 162-TDF - Test and design methods for steel fibre reinforced concrete. Recommendation for bending test (Chairlady L. Vandewalle), Materials and Structures, Vol. 33, No. 225, pp. 3-5, January-February 2000.

RILEM. Technical Committee 162-TDF - Test and design methods for steel fibre reinforced concrete. Final Recommendation, Materials and Structures, Vol. 35, pp. 579-582, November 2002.

RDP. LVDTs calibration certificates, RDP Group, October1995.

SENA-CRUZ, J. M., BARROS, J. A. O., Modeling of bond between near-surface mounted CFRP laminate strips and concrete, Computers and Structures, Vol. 82, No. 17-19, pp. 1513-1521, July 2004a.

SENA-CRUZ, J. M., BARROS, J. A. O., Bond between near-surface mounted CFRP laminate strips and concrete in structural strengthening, Journal of Composites for Construction, Vol. 8, No. 6, pp. 519-527, November-December 2004b.

SENA-CRUZ, J. M., Strengthening of concrete structures with near-surface mounted CFRP laminate strips. PhD Thesis, Department of Civil Engineering, University of Minho, 198 pp., 2004.

SIKA, Technical data sheet - construction, Sika - Chemical Industry, S.A., Edition No. 5, 434 pp., 2002. (in Portuguese)

S&P - Clever Reinforcement Company, http://www.sp-reinforcement.ch, Switzerland, 2004. (available on September 24, 2004)

TÄLJSTEN, B., CAROLIN, A. Concrete Beams strengthened with near surface mounted CFRP laminates. 5th International Conference on Fibre Reinforced Plastics for Reinforced Concrete Structures - FRPRCS-5 (Edited by Chris Burgoyne), Cambridge, UK, Vol. 01, pp. 107-116, 16-18 July, 2001.

TML - Tokyo Sokki Kenkyujo Co., Ltd., http://www.tokyosokki.co.jp/e/index.html, Japan, 2004. (available on September 24, 2004)

ANNEXES

Annex A - Physical properties of the aggregates

Annex B - Particle sizing of the aggregates

Annex C - Data of the compressive strength of the substrate concrete and of the SFRC overlay

Annex D - Flexural tensile behavior of the plain concrete and SFRC overlay

Annex E - Epoxy adhesive dosages adopted and respective proportions

Annex F - Load-deflection curves of the lateral LVDTs

Annex G - Side view of the slabs after test

Annex A - Physical properties of the aggregates

Table A1 *- Specific gravity and water absorption of fine aggregate 4/11.*

P_1	WEIGHT OF THE SAMPLE DRIED IN AIR	4795.2 g
P_2	WEIGHT OF THE SATURATED SAMPLE IN THE AIR WITH DRY SURFACE	4857.6 g
P_3	WEIGHT OF THE SATURATED SAMPLE IN WATER	3023.0 g
G_a	SPECIFIC GRAVITY OF THE WATER AT TEST TEMPERATURE	1000.0 kg/m^3
$\frac{P_1}{P_2-P_3}\times G_a$	SPECIFIC GRAVITY OF THE DRY PARTICLES	2613.8 kg/m^3
$\frac{P_1}{P_1-P_3}\times G_a$	SPECIFIC GRAVITY OF THE IMPERMEABLE MATERIAL OF PARTICLES	2705.8 kg/m^3
$\frac{P_2}{P_2-P_3}\times G_a$	SPECIFIC GRAVITY OF SATURATED PARTICLES WITH DRY SURFACE	2647.8 kg/m^3
$\frac{P_2-P_1}{P_1}\times 100$	ABSORPTION	1,3 %

Table A2 *- Specific gravity and water absorption of coarse aggregate 11/16.*

P_1	WEIGHT OF THE SAMPLE DRIED IN AIR	5324,0 g
P_2	WEIGHT OF THE SATURATED SAMPLE IN THE AIR WITH THE DRY SURFACE	5378,0 g
P_3	WEIGHT, IN WATER, OF THE SATURATED SAMPLE	3359,2 g
G_a	SPECIFIC GRAVITY OF THE WATER AT TEST TEMPERATURE	1000,0 kg/m^3
$\frac{P_1}{P_2-P_3}\times G_a$	SPECIFIC GRAVITY OF THE DRY PARTICLES	2637.2 kg/m^3
$\frac{P_1}{P_1-P_3}\times G_a$	SPECIFIC GRAVITY OF THE IMPERMEABLE MATERIAL OF PARTICLES	2709.7 kg/m^3
$\frac{P_2}{P_2-P_3}\times G_a$	SPECIFIC GRAVITY OF SATURATED PARTICLES WITH DRY SURFACE	2664.0 kg/m^3
$\frac{P_2-P_1}{P_1}\times 100$	ABSORPTION	1,0 %

Table A3 - *Specific gravity and water absorption of fine river sand.*

P_1	WEIGHT OF THE SATURATED SAMPLE WITH DRY SURFACE	500.1 g
P_2	WEIGHT OF THE FULL WATER BOTTLE	709.6 g
P_3	WEIGHT OF THE FULL BOTTLE WITH SATURATED SAMPLE AND WATER	1014.33 g
P_4	WEIGHT OF THE DRY SAMPLE	494.7 g
G_a	SPECIFIC GRAVITY OF THE WATER AT TEST TEMPERATURE	1000.0 kg/m^3
$\frac{P_4}{P_1+P_2-P_3}\times G_a$	SPECIFIC GRAVITY OF THE DRY PARTICLES	2532.6 kg/m^3
$\frac{P_4}{P_4+P_2-P_3}\times G_a$	SPECIFIC GRAVITY OF THE IMPERMEABLE MATERIAL OF PARTICLES	2604.3 kg/m^3
$\frac{P_1}{P_1+P_2-P_3}\times G_a$	SPECIFIC GRAVITY OF SATURATED PARTICLES WITH DRY SURFACE	2560.1 kg/m^3
$\frac{P_1-P_4}{P_4}\times 100$	ABSORPTION	1,1 %

Table A4 - *Specific gravity and water absorption of coarse river sand.*

P_1	WEIGHT OF THE SATURATED SAMPLE WITH DRY SURFACE	500.0g
P_2	WEIGHT OF THE FULL WATER BOTTLE	709.6 g
P_3	WEIGHT OF THE FULL BOTTLE WITH THE SATURATED SAMPLE AND WATER	1006.6 g
P_4	WEIGHT OF THE DRY SAMPLE	491.3 g
G_a	SPECIFIC GRAVITY OF THE WATER AT TEST TEMPERATURE	1000.0 kg/m^3
$\frac{P_4}{P_1+P_2-P_3}\times G_a$	SPECIFIC GRAVITY OF DRY PARTICLES	2420.3 kg/m^3
$\frac{P_4}{P_4+P_2-P_3}\times G_a$	SPECIFIC GRAVITY OF THE IMPERMEABLE MATERIAL OF PARTICLES	2528.3 kg/m^3
$\frac{P_1}{P_1+P_2-P_3}\times G_a$	SPECIFIC GRAVITY OF SATURATED PARTICLES WITH DRY SURFACE	2463.1 kg/m^3
$\frac{P_1-P_4}{P_4}\times 100$	ABSORPTION	1,8 %

Annex B - Particle sizing of the aggregates

Table B1 - Sieve analysis of the fine river sand.

Sieve		Weight retained	% Retained	% Accumulated retained	% Pass
nº	(mm)				
1″	25.400				
¾″	19.100				
½″	12.700				
⅜″	9.520				
4″	4.760				
8″	2.380				100
16″	1.190	16.46	1.55	1.55	98.45
30″	0.595	81.47	7.66	9.21	90.79
50″	0.297	516.96	48.60	57.80	42.20
100″	0.149	283.82	26.68	84.48	15.52
200″	0.074	109.50	10.29	94.77	5.23
RESIDUE		55.61	5.23	100	0
TOTAL		1063.81		100	

D_{max} = 1.31 mm, according to COUTINHO (1988)

Table B2 - Sieve analysis of the coarse river sand.

Sieve		Weight retained	% Retained	% Accumulated retained	% Pass
nº	(mm)				
1″	25.400				
¾″	19.100				
½″	12.700				
⅜″	9.520				100
4″	4.760	18.80	1.88	1.88	98.12
8″	2.380	130.70	13.06	14.94	85.06
16″	1.190	259.50	25.94	40.88	59.12
30″	0.595	279.70	27.96	68.84	31.16
50″	0.297	205.90	20.58	89.42	10.58
100″	0.149	100.20	10.01	99.43	0.57
200″	0.074	5.30	0.53	99.96	0.04
RESIDUE		0.40	0.04	100	0
TOTAL		1000.50		100	

D_{max} = 5.10 mm, according to COUTINHO (1988)

Table B3 - Sieve analysis of the fine aggregate 4/11.

Sieve nº	Sieve (mm)	Weight retained	% Retained	% Accumulated retained	% Pass
1″	25.400				
¾″	19.100				
½″	12.700				100
⅜″	9.520	64.30	2.14	2.14	97.86
4″	4.760	1977.00	65.92	68.07	31.93
8″	2.380	802.80	26.77	94.83	5.17
16″	1.190	61.40	2.05	96.88	3.12
30″	0.595	22.10	0.74	97.62	2.38
50″	0.297	15.50	0.52	98.14	1.86
100″	0.149	17.20	0.57	98.71	1.29
200″	0.074	30.40	1.01	99.72	0.28
RESIDUE		8.30	0.28	100	0
TOTAL		2999.00	100		

D_{max} = 9.60 mm, according to COUTINHO (1988)

Table B4 - Sieve analysis of the coarse aggregate 11/16.

Sieve nº	Sieve (mm)	Weight retained	% Retained	% Accumulated retained	% Pass
1″	25.400				
¾″	19.100				100
½″	12.700	495.16	14.16	14.16	85.84
⅜″	9.520	1855.12	53.05	67.21	32.79
4″	4.760	1080.73	30.91	98.12	1.88
8″	2.380	21.20	0.61	98.72	1.28
16″	1.190	3.60	0.10	98.83	1.17
30″	0.595	2.63	0.08	98.90	1.10
50″	0.297	4.11	0.12	99.02	0.98
100″	0.149	7.95	0.23	99.25	0.75
200″	0.074	11.18	0.32	99.57	0.43
RESIDUE		15.19	0.43	100	0
TOTAL		3496.87	100		

D_{max} = 14.35 mm, according to COUTINHO (1988)

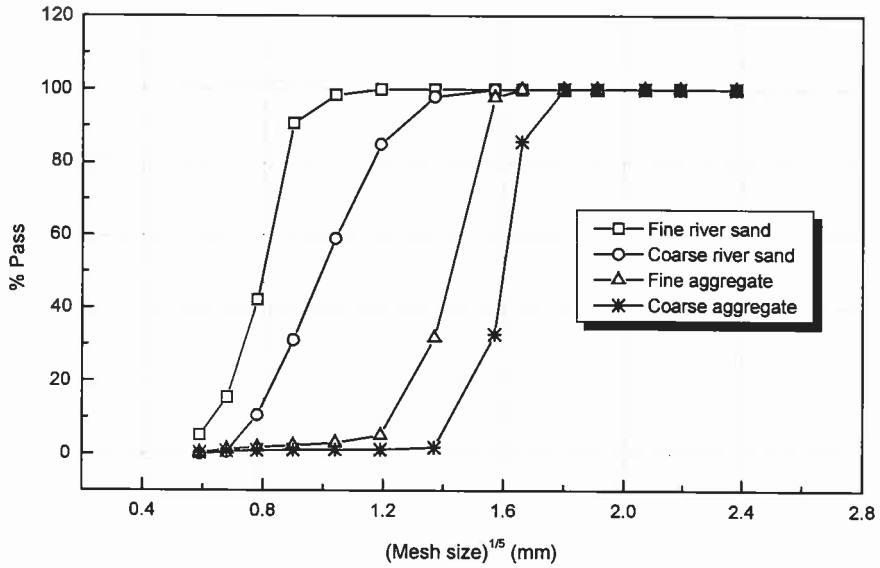

Figure B1 *- Sieve analysis of the aggregates.*

Annex C - Data of the compressive strength of the substrate concrete and of the SFRC overlay

Table C1 *- Compressive strength of concrete substrate at slab testing age.*

Designation	Age at testing (days)	Test	f_c (N/mm^2)	f_{cm} (N/mm^2)	Std. dev. (N/mm^2)	COV (%)
SL01	125	1	48.17	45.65	2.19	4.80
		2	44.25			
		3	44.52			
SL02	124	1	49.60	47.76	1.63	3.41
		2	47.20			
		3	46.49			
SL03	114	1	42.70	43.13	0.52	1.21
		2	43.71			
		3	42.97			
SL04	48	1	33.68	32.41	2.02	6.23
		2	33.46			
		3	30.08			
SL05	102	1	48.24	49.56	1.14	2.31
		2	50.31			
		3	50.12			
SL06	101	1	47.70	49.39	2.38	4.83
		2	49,24			
		3	51.07			
SL07	77	1	47.52	47.80	1.37	2.87
		2	46.59			
		3	49.29			
SL08	92	1	48.43	49.35	0.84	1.70
		2	50.07			
		3	49.55			

Note: Coefficient of Variation (COV) = (Standard deviation/Average) x 100

Table C2 *- Compressive strength of SFRC Overlay at slab testing age.*

Designation	Age at testing (days)	Test	f_c (N/mm^2)	f_{cm} (N/mm^2)	Std. dev. (N/mm^2)	COV (%)
O1	63	1	34.07	38.93	4.49	11.52
		2	42.91			
		3	39.81			
O2	33	1	54.85	53.10	1.64	3.10
		2	51.11			
		3	53.95			
		4	52.50			

Note: Coefficient of Variation (COV) = (Standard deviation/Average) x 100

Annex D - Flexural tensile behavior of the plain concrete and SFRC overlay

Plain Concrete Slab

The recommendation FMC1, from RILEM (1985), specifies a three-point bending test to characterize mortar and concrete post-cracking behaviour (see ***Figure D1***). From FMC1 method, the flexural tensile strength and the fracture energy (G_F) can be derived.

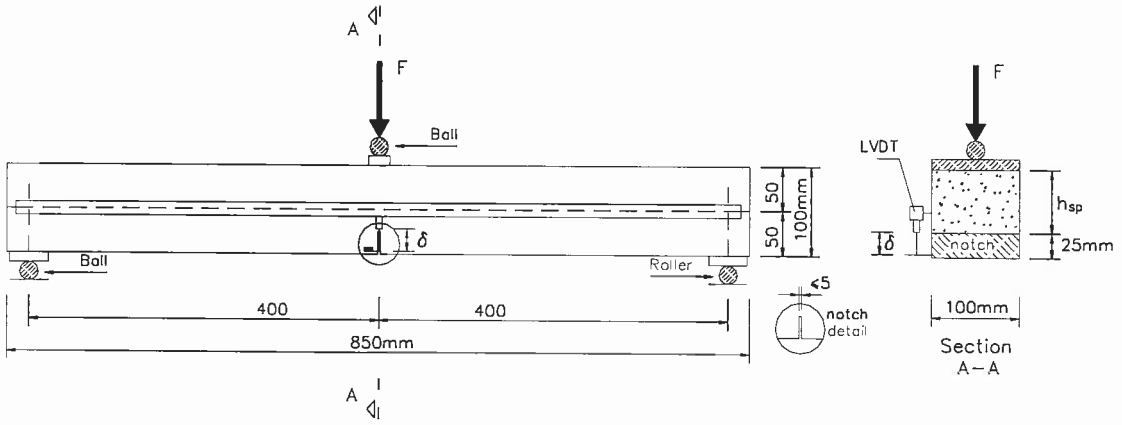

Figure D1 *- Specimen dimensions, loading and support conditions, and arrangement of the displacement transducer, according to RILEM FMC1 recommendation.*

The fracture energy is calculated from the equation:

$$G_F = \frac{(W_o + m \cdot g \cdot \delta_o)}{A_{lig}} \qquad [N/m\ (J/m^2)] \qquad (D1)$$

where

W_o = area under the load - displacement curve, ***Figure D2***, F-δ (N/mm);
m = $m_1 + 2 \cdot m_2$ (kg);
m_1 = weight of the beam between the supports, calculated as the beam weight multiplied by ℓ/L ratio (ℓ is the span and L is length of the beam, 800 mm and 850 mm, respectively, in the present case);
m_2 = weight of the part of the loading arrangement which is not attached to the machine, but follows the beam until failure;
g = gravity acceleration, 9.81 m/s^2;
δ_o = deformation at the final failure of the beam (m);
A_{lig} = area of the ligament, $h_{sp} \cdot b$ (m^2), where b is width of the beam.

To characterize the post-cracking behaviour of the plain concrete of each mix, three bending tests were carried out, in notched 100 mm x 100 mm x 850 mm beams,

according to the RILEM recommendations. The experimental set up is illustrated in ***Figure D3***. The imposed mid-span deflection, in the 3-point bending test, was measured from a LVDT yoke fixed at mid-height of the tested specimen itself (sometimes referred to as the "Japanese yoke" or "suspension yoke").

The flexural tensile strength ($f_{ct,fl}$), axial tensile strength ($f_{ct,ax}$), fracture energy (G_F) and the load-displacement responses obtained are reported in ***Table D1*** and ***Figure D4***, respectively. The value of axial tensile strength ($f_{ct,ax}$) is estimated from the flexural tensile strength, $f_{ct,fl}$, according to (D2) from CEB.

$$f_{ct,ax} = f_{ct,fl} \cdot \frac{1.5 \cdot (h_{sp}/h_o)^{0.7}}{1 + 1.5 \cdot (h_{sp}/h_o)^{0.7}} \qquad [N/mm^2] \qquad (D2)$$

where

$$f_{ct,fl} = \frac{3}{2} \cdot \frac{F_{max} \cdot \ell}{b \cdot (h_{sp})^2} \qquad [N/mm^2] \qquad (D3)$$

and

$f_{ct,fl}$ is the value of the flexural tensile strength;
h_{sp} is the depth of beam (mm), h_{sp} = 75 mm in the present case;
h_o = 100 mm;
F_{max} maximum applied load (refer to ***Figure D2***);
b is width of the beam, and
ℓ is the beam span length.

The residual flexural tensile strength ($f_{ctres,fl}$), at the final failure of the beam was determinated as follows:

$$f_{ctres,fl} = \frac{3}{2} \cdot \frac{F_{res} \cdot \ell}{b \cdot (h_{sp})^2} \qquad [N/mm^2] \qquad (D4)$$

where

F_{res} is the residual applied load at the final failure of the beam (refer to ***Figure D2***);

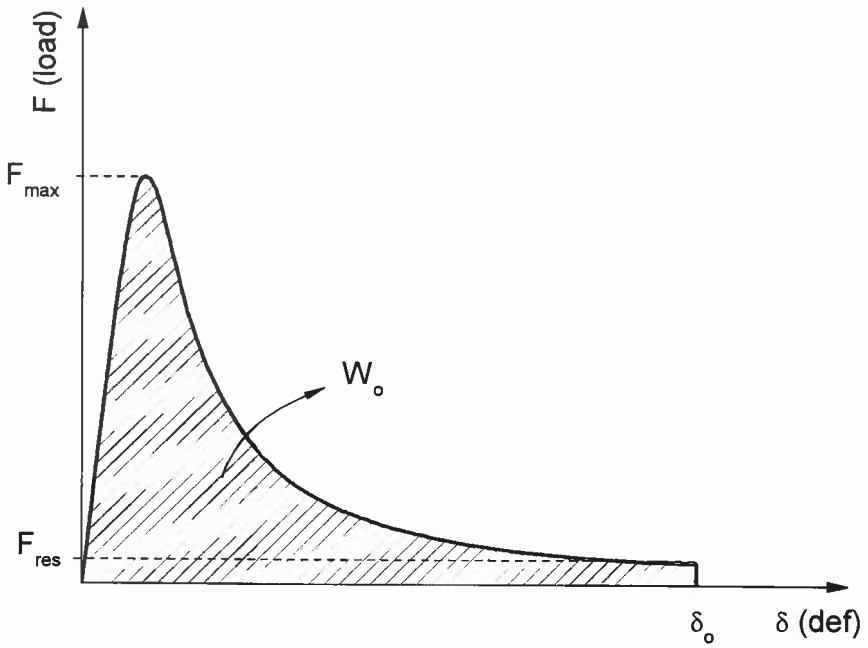

Figure D2 *- Typical load-mid span displacement curve.*

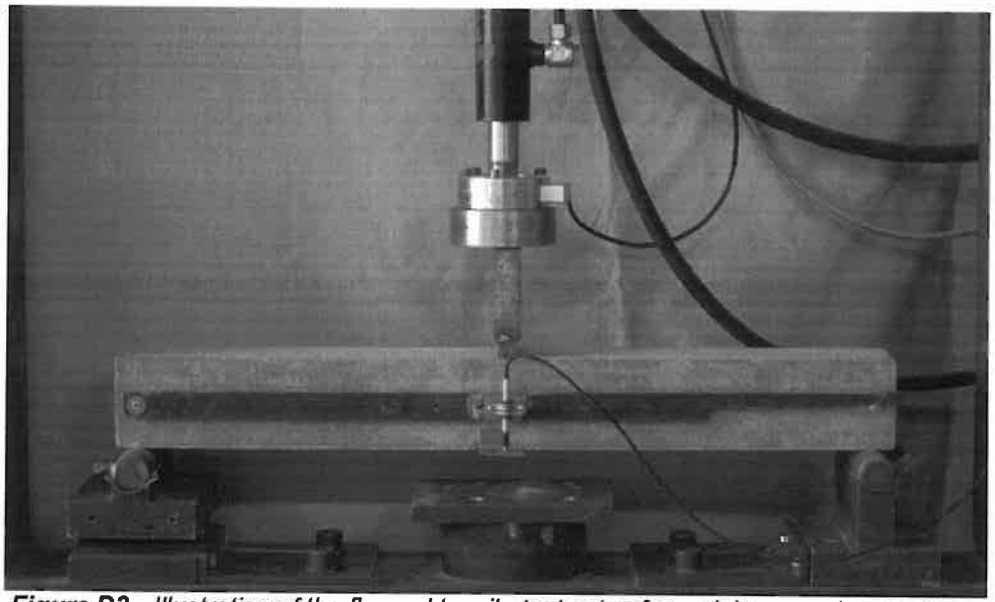

Figure D3 *- Illustration of the flexural tensile test setup for a plain concrete specimen.*

Table D1 *- Flexural tensile strength parameters of the plain concrete.*

Mix designation	Age at testing (days)	Beam	Weight (kg)	$f_{ct,fl}$ (N/mm^2)	$\delta_{fct,fl}$ (mm)	$f_{ctres,fl}$ (N/mm^2)	$f_{ct,ax}$ (N/mm^2)	G_F (N/m)
SL01	138	1	19.44	5.01	0.17	0.26	2.77	206
		2	19.48	5.02	0.16	0.26	2.77	203
		3	19.78	4.89	0.15	0.26	2.70	191
SL02	131	1	19.58	6.02	0.20	0.27	3.32	208
		2	19.80	5.41	0.15	0.25	3.00	166
		3	19.79	6.16	0.20	0.26	3.40	193
SL03	126	1	19.72	6.34	0.18	0.26	3.50	216
		2	19.84	5.92	0.16	0.25	3.27	214
		3	19.72	5.50	0.18	0.26	3.03	204
SL04	106	1	19.20	4.60	0.15	0.26	2.53	180
		2	19.28	5.37	0.18	0.26	2.96	215
		3	19.22	4.22	0.13	0.26	2.33	174
SL05	112	1	20.24	5.53	0.19	0.25	3.07	206
		2	20.06	5.17	0.19	0.25	2.86	209
		3	20.04	6.07	0.19	0.26	3.36	198
SL06	112	1	20.06	6.20	0.19	0.29	3.42	223
		2	20.10	5.96	0.19	0.26	3.30	189
		3	20.18	6.14	0.18	0.26	3.39	228
SL07	83	1	19.82	6.07	0.16	0.25	3.35	200
		2	19.75	5.96	0.18	0.25	3.29	266
SL08	103	1	20.42	6.01	0.15	0.26	3.32	192
		2	20.32	5.91	0.16	0.26	3.27	223
		3	20.16	5.48	0.17	0.25	3.04	183

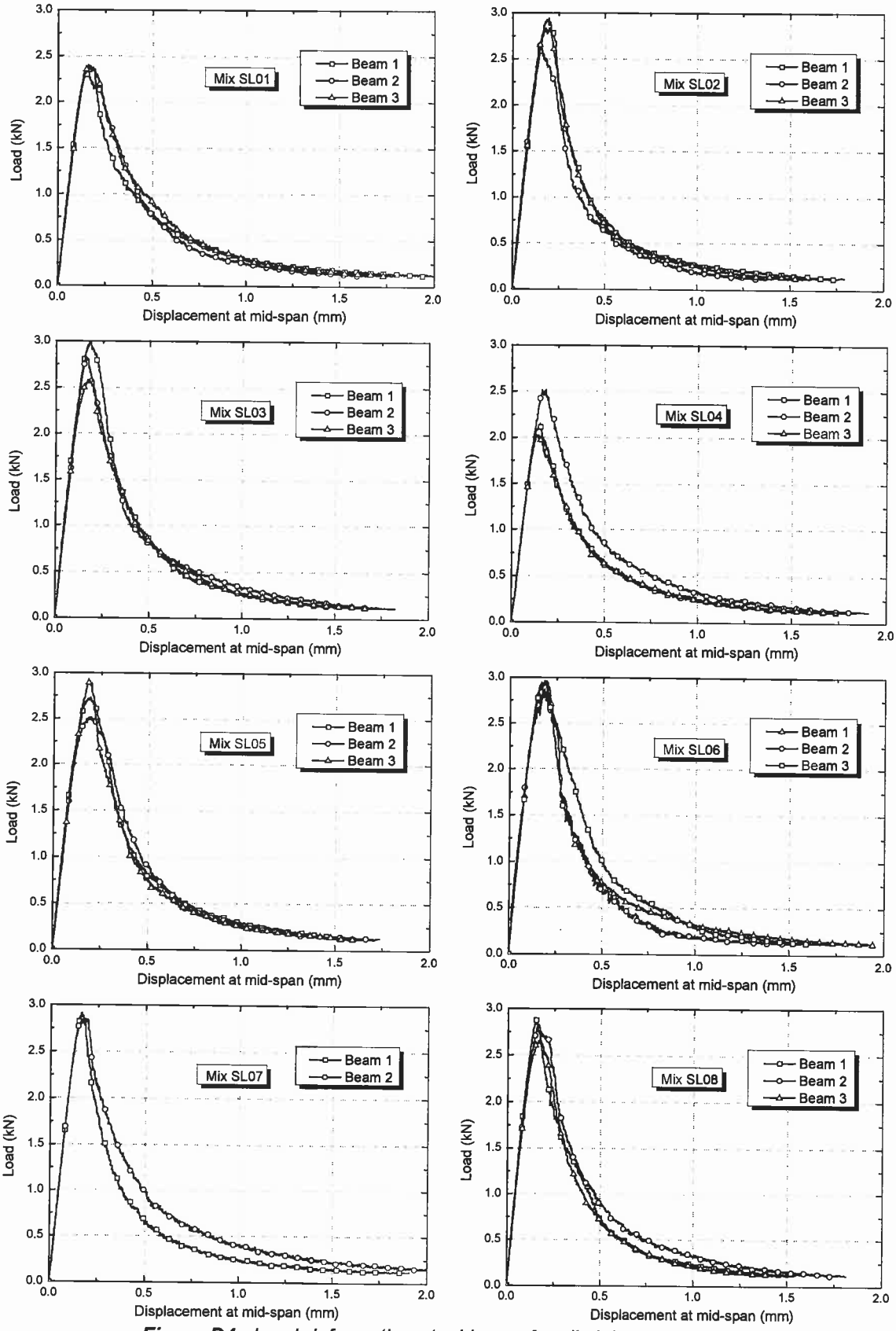

Figure D4 *- Load-deformation at mid span for all plain concrete mix.*

Concrete Overlay

RILEM TC 162-TDF Committee (RILEM, 2000 and 2002) has proposed a specimen configuration, test procedures and flexural tensile strength parameters to characterize the flexural tensile post-cracking behaviour of the SFRC.

The standard test specimen recommended by RILEM TC 162-TDF is represented ***Figure D5***. The production method for casting the specimen, the curing procedures, the position on the notch sawn into the test beam, the load and specimen support conditions, the characteristics for both the equipment and measuring devices, and the test procedures are given elsewhere RILEM (2000, 2002) documents.

From the bending test, a force-deflection relationship is obtained. From this relationship it can be evaluated the load at the limit of proportionality (F_L), the equivalent flexural tensile strength parameters ($f_{eq,2}$ and $f_{eq,3}$) and the residual flexural tensile strength parameters ($f_{R,1}$ and $f_{R,4}$). F_L is equal to the highest value of the load registered up to a deflection of 0.05 mm. The parameters $f_{eq,2}$ and $f_{eq,3}$ are related to the energy absorption capacity up to a deflection of δ_2 and δ_3 ($\delta_2 = \delta_L + 0.65$ mm, $\delta_3 = \delta_L + 2.65$ mm where δ_L is the deflection correspondent to F_L) provided by fibre reinforcement mechanisms, ($D^f_{BZ,2}$ and $D^f_{BZ,3}$), see ***Figure D6*** and ***Figure D7***. The parameters $f_{R,1}$ and $f_{R,4}$ are the stresses due to forces $F_{R,1}$ and $F_{R,4}$, respectively, corresponding to a deflection of $\delta_{R,1} = 0.46$ mm and $\delta_{R,4} = 3.0$ mm (see ***Figure D6*** and ***Figure D7***). The expressions for evaluating f_{eq} and f_R are inset on ***Figure D6*** and ***Figure D7***, where b (= 150mm), h_{sp} (~125mm) and L (= 500 mm) are the width of the specimen, the distance between the tip of the notch and the top of the cross section, and the span of the specimen, respectively. All these expressions were defined assuming a linear stress distribution on the cross section of the beam.

The experimental set up is illustrated in ***Figure D8***. For sake of test stability and measurement accuracy, the imposed mid-span deflection, in the 3-point flexural test, was measured from a reference bar leaning on the tested specimen itself (sometimes referred as "Japanese yoke" or "suspension yoke").

The load-deflection relationships obtained on the specimens reinforced with 30 kg/m³ hooked ends DRAMIX® RC-80/60-BN steel fibres are reported in ***Figure D9***. The values of the load at the limit of proportionality (F_L), equivalent flexural tensile strength ($f_{eq,2}$ and $f_{eq,3}$), residual flexural tensile strength ($f_{R,1}$ and $f_{R,4}$), and flexural modulus of elasticity (E_{cf}) are included in ***Table D2***. Three and four bending tests were carried out for the SFRC mix O1 and O2, respectively.

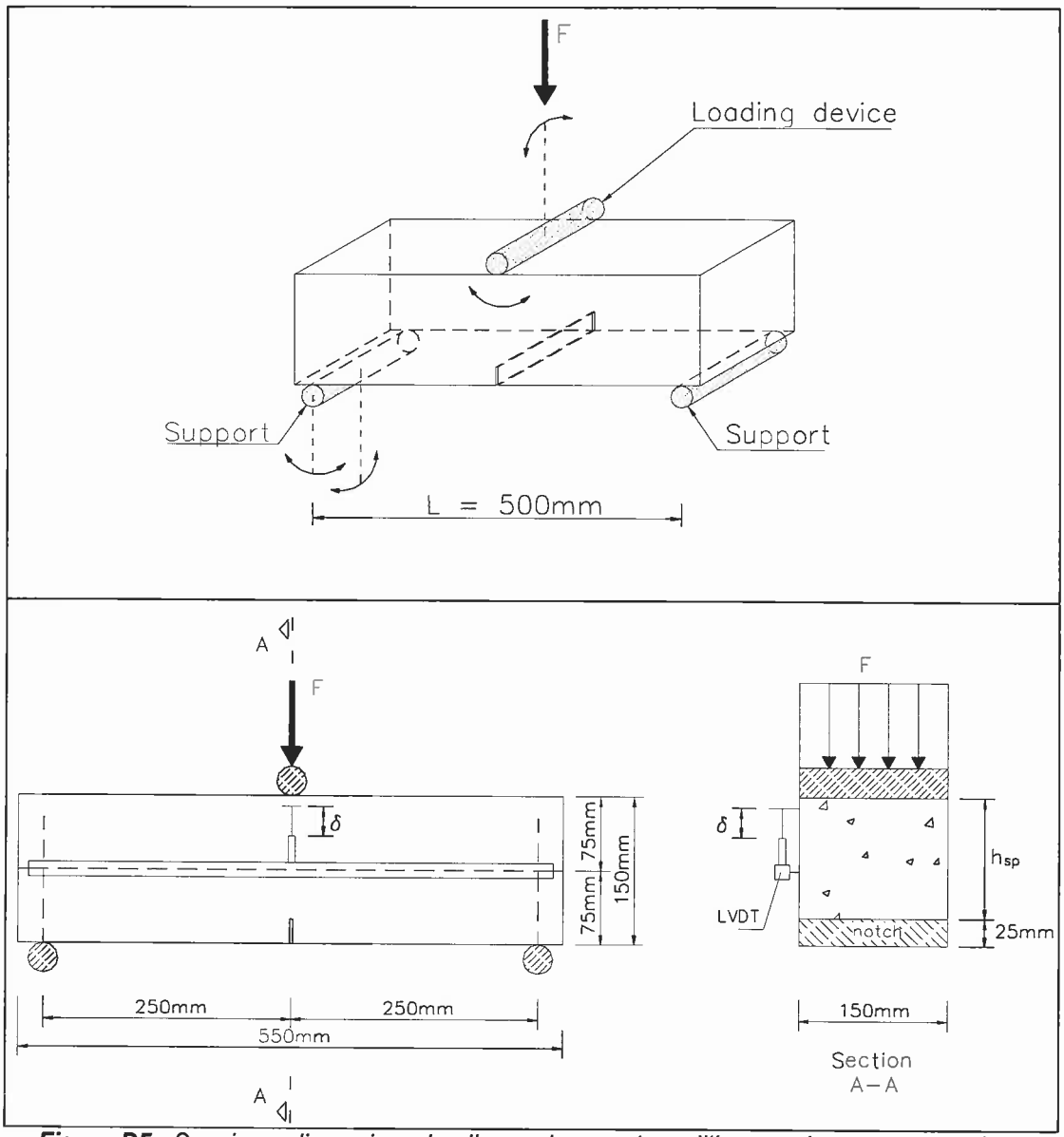

***Figure D5** - Specimen dimensions, loading and support conditions, and arrangement of the displacement transducers of the RILEM flexural tensile test.*

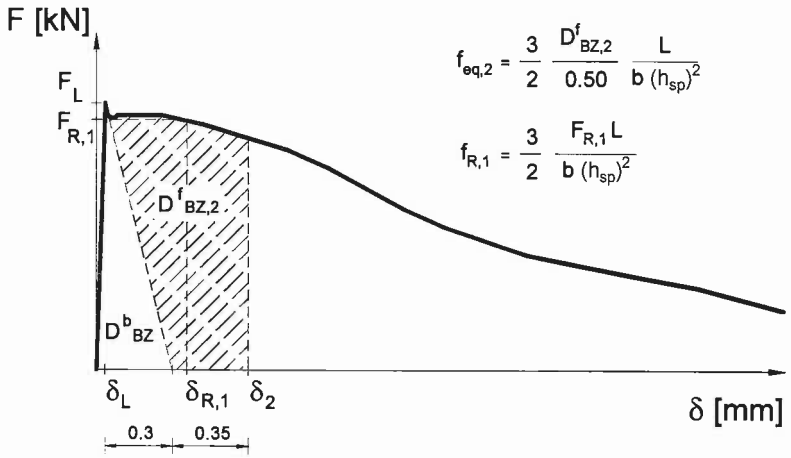

Figure D6 *- Evaluation of the equivalent two ($f_{eq,2}$) and residual one ($f_{R,1}$) flexural tensile strength parameters.*

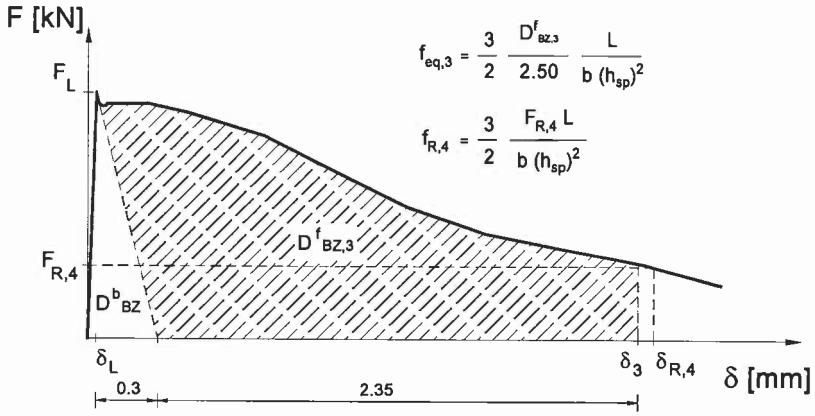

Figure D7 *- Evaluation of the equivalent three ($f_{eq,3}$) and residual four ($f_{R,4}$) flexural tensile strength parameters.*

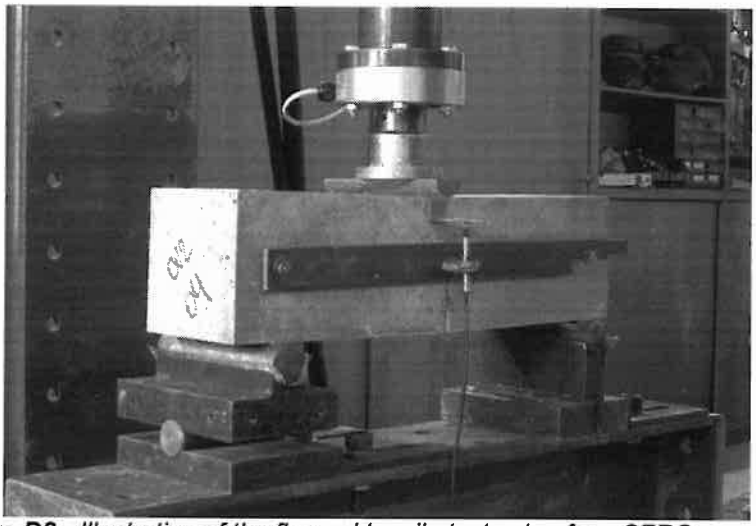

Figure D8 *- Illustration of the flexural tensile test setup for a SFRC specimen.*

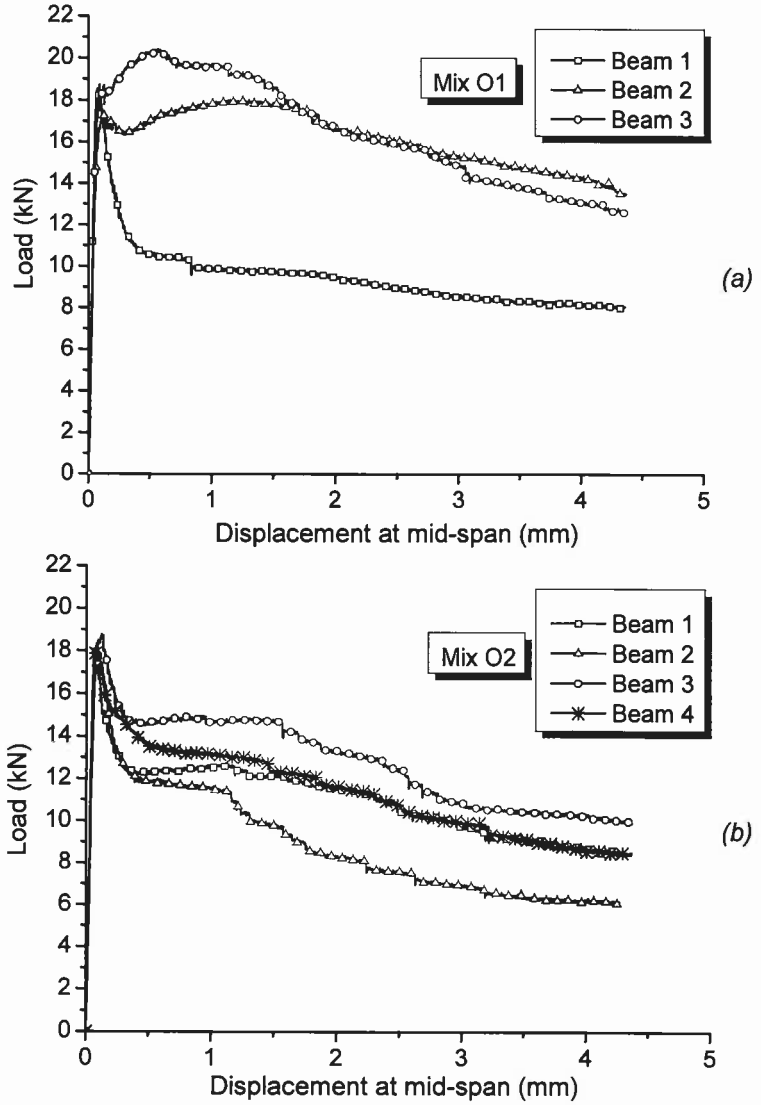

***Figure D9** - Load-deflection relationships of notched beams specimens under 3-point loading: (a) SFRC mix O1, and (b) SFRC mix O2.*

***Table D2** - Flexural tensile strength parameters of the two SFRC mix.*

SFRC mix	Age at testing (days)	Beam	F_L (kN)	$f_{eq,2}$ (N/mm^2)	$f_{eq,3}$ (N/mm^2)	$f_{R,1}$ (N/mm^2)	$f_{R,4}$ (N/mm^2)	E_{cf}[a] (kN/mm^2)
O1	68	1	15.53	3.184	3.110	3.473	2.795	35.04
		2	13.08	5.466	5.518	5.486	4.965	27.28
		3	13.97	6.351	5.864	6.510	4.828	28.11
O2	54	1	16.20	3.800	3.809	3.993	3.126	34.65
		2	18.04	3.669	3.125	3.850	2.257	34.73
		3	18.49	4.716	4.540	4.765	3.549	27.96
		4	18.34	4.280	3.976	4.493	3.210	31.94

[a] Calculated according the equation included in the reference BARROS (1993)

Annex E - Epoxy adhesive dosages adopted and respective proportions

SFRC overlay bond product **SIKADUR® 32 N**

Dosage = 0.90 kg/m^2

For each slab:

Weigth of component A = 360 g

Weight of component B = 180 g

CFRP-concrete bond product **Mbrace® RESIN 220**

Dosage = 0.13 kg per meter of slit

For each slit:

Weigth of component I = 194.06 g

Weigth of component II = 60.94 g

Annex F - Load-deflection curves of the lateral LVDTs

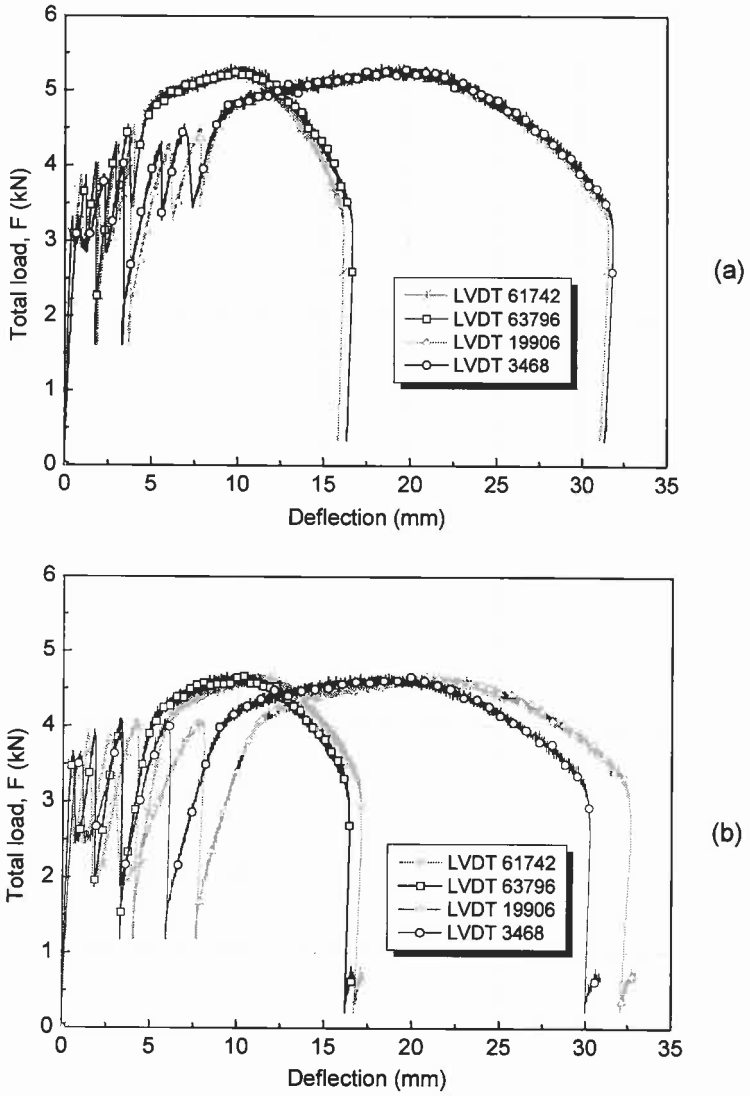

Figure F1 *- Relationship between applied load and deflection at the lateral LVDTs for the reference slabs: (a) SL01 and (b) SL06.*

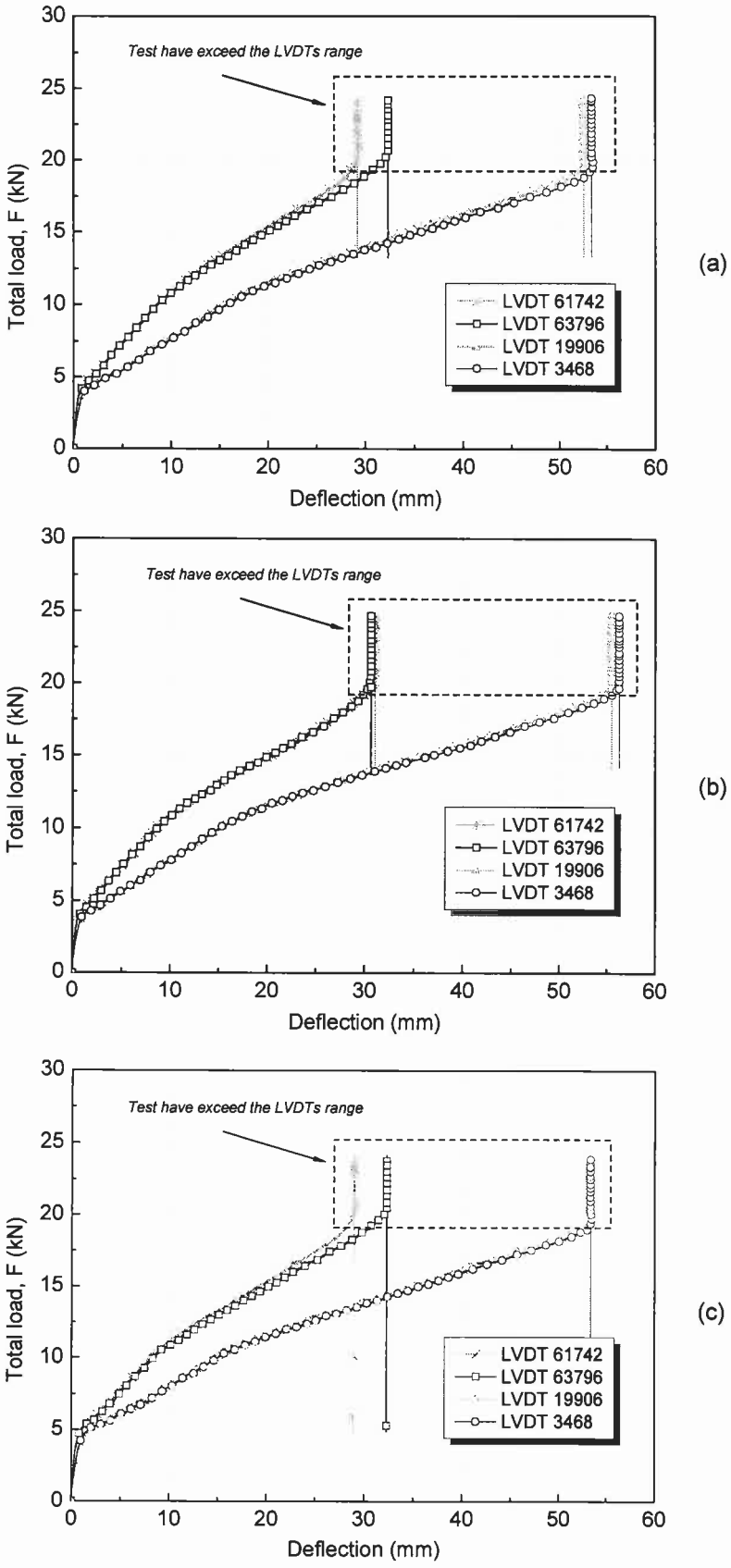

Figure F2 *- Relationship between applied load and deflection at the lateral LVDTs for the NSM CFRP strengthened: (a) SL03S, (b) SL04S and (c) SL08S.*

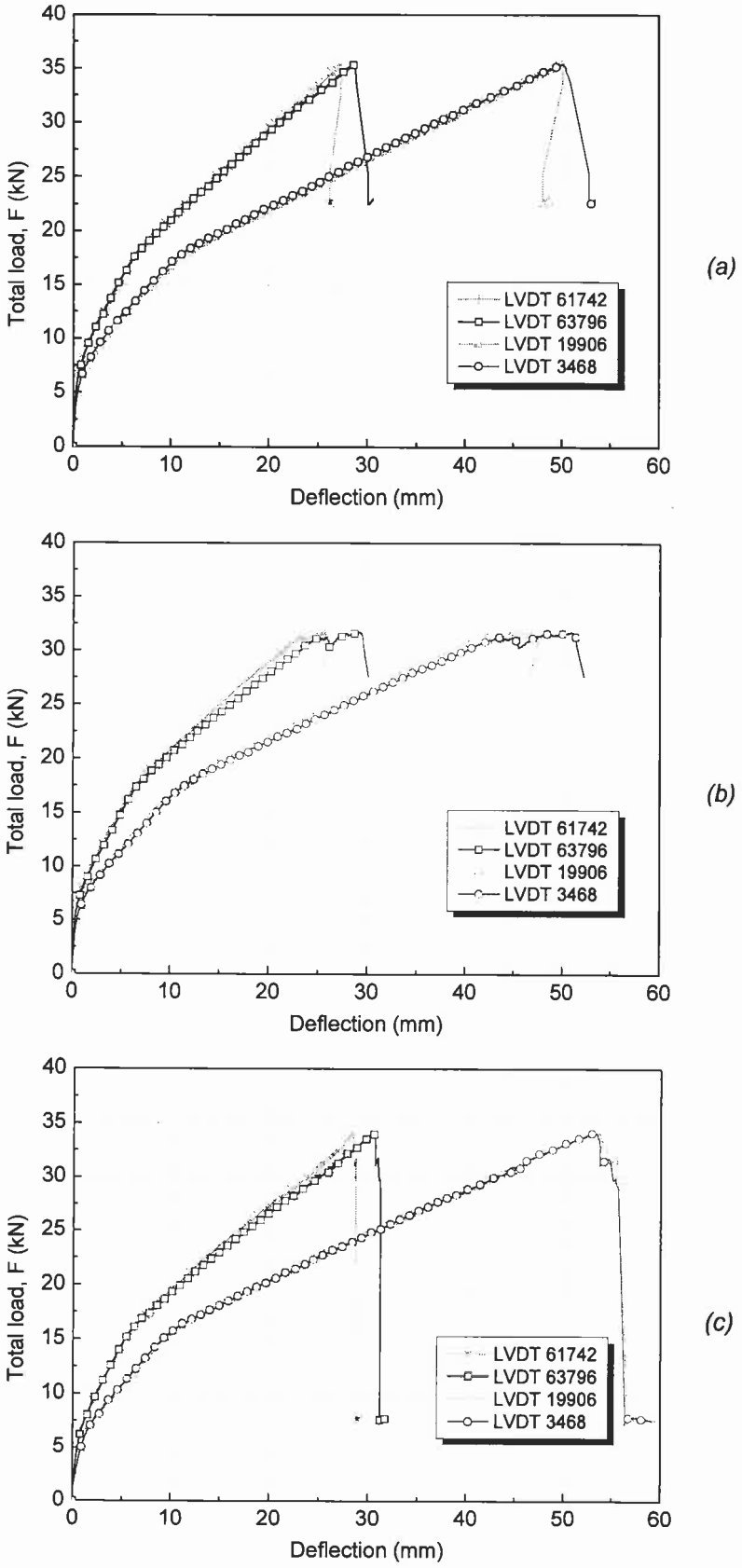

Figure F3 *- Relationship between applied load and deflection at the lateral LVDTs for the NSM CFRP strengthened: (a) SL02SO1, (b) SL05SO1 and (c) SL07SO2.*

Annex G - Side view of the slabs after test

Figure G1 *- Side view of the slabs after having been tested (the side view of the slab SL04S was not possible to be registered).*